

Washington University in St. Louis

Washington University Open Scholarship

McKelvey School of Engineering Theses & Dissertations

McKelvey School of Engineering

Summer 7-13-2023

Effect of Genetic Diversity on Cortical Bone Phenotype and Response to Mechanical Loading

Nicole Migotsky

Washington University – McKelvey School of Engineering

Follow this and additional works at: https://openscholarship.wustl.edu/eng_etds

Recommended Citation

Migotsky, Nicole, "Effect of Genetic Diversity on Cortical Bone Phenotype and Response to Mechanical Loading" (2023). *McKelvey School of Engineering Theses & Dissertations*. 943.
https://openscholarship.wustl.edu/eng_etds/943

This Dissertation is brought to you for free and open access by the McKelvey School of Engineering at Washington University Open Scholarship. It has been accepted for inclusion in McKelvey School of Engineering Theses & Dissertations by an authorized administrator of Washington University Open Scholarship. For more information, please contact digital@wumail.wustl.edu.

WASHINGTON UNIVERSITY IN ST. LOUIS

McKelvey School of Engineering
Department of Biomedical Engineering

Dissertation Examination Committee:

Matthew J. Silva, Chair

James A.J. Fitzpatrick

Michael D. Harris

Spencer P. Lake

Tim R. Peterson

Effect of Genetic Diversity on Cortical Bone Phenotype and
Response to Mechanical Loading

by

Nicole Migotsky

A dissertation presented to
the McKelvey School of Engineering
of Washington University in
partial fulfillment of the
requirements for the degree
of Doctor of Philosophy

August 2023
St. Louis, Missouri

© 2023, Nicole Migotsky

Table of Contents

List of Figures	v
List of Tables	viii
Acknowledgments.....	ix
Abstract.....	xii
Chapter 1: Overview of Bone Biology and Heritability	1
1.1 Clinical Significance and Motivation	1
1.2 Bone Components.....	2
1.3 Bone Strength.....	4
1.4 Bone Mechanobiology	7
1.5 Mouse Models of Mechanical Loading	8
1.6 Mouse Genetic Diversity	9
1.6.1 Diversity Outbred Mouse Population.....	11
1.7 Heritability of Bone Traits	12
1.8 Goals of the Dissertation.....	13
Chapter 2: Cortical Bone Relationships are Maintained Regardless of Sex and Diet in a Large Population of LGXSM Advanced Intercross Mice*	15
2.1 Abstract.....	16
2.2 Introduction.....	17
2.3 Methods and Materials.....	20
2.3.1 Mice	20
2.3.2 Phenotyping	21
2.3.3 Analysis Software	22
2.3.4 Principal Component Analysis.....	22
2.3.5 Correlation Matrix.....	22
2.3.6 Bivariate Linear Analysis.....	23
2.3.7 Multivariate Linear Regression.....	23
2.4 Results.....	24
2.4.1 Correlation of traits within each bone.....	24
2.4.2 Correlation of traits between bones	27
2.4.3 Prediction of whole-bone strength	30

2.4.4	Implications of using beam theory to predict material properties.....	31
2.5	Discussion.....	32
2.6	Supplemental Material.....	38
Chapter 3: Multi-Scale Cortical Bone Traits Vary in Two Mouse Models of Genetic Diversity		40
3.1	Abstract.....	41
3.2	Introduction.....	42
3.3	Methods.....	45
3.3.1	Mouse Populations.....	45
3.3.2	Longitudinal Measurements.....	45
3.3.3	Cortical Bone Morphology.....	46
3.3.4	Mechanical Testing.....	47
3.3.5	Osteocyte Lacunar Morphology.....	48
3.3.6	Raman Spectroscopy.....	48
3.3.7	Correlation Matrix.....	49
3.3.8	Principal Component Analysis (PCA).....	49
3.3.9	Heritability Calculations.....	50
3.3.10	Statistical Analysis.....	50
3.4	Results.....	51
3.4.1	Young-adult mice from the Inbred Founder and Diversity Outbred populations span a large range of body size and bone mass.....	51
3.4.2	Cortical morphology of three different long bones varies with mouse strain and sex.....	53
3.4.3	Cortical bone mechanical properties vary with mouse strain and sex, but material properties only vary with mouse strain.....	54
3.4.4	Within-bone correlations are similar in both mouse populations, but stronger in the Inbred Founder population.....	57
3.4.5	Inbred Founder strains separate using PCA while Diversity Outbred mice overlap many individual strains and occupy gaps between strains.....	59
3.4.6	Lacunar morphology varies between Inbred Founder strains.....	59
3.4.7	Mineral composition minimally varies between Inbred Founder mice.....	62
3.4.8	Multi-scale cortical bone traits are moderately to highly heritable in the Inbred Founder population.....	63
3.4.9	Whole-body mass significantly contributes to trait differences, but variation due to mouse strain remains significant.....	64
3.5	Discussion.....	65

3.6	Supplemental Material	72
Chapter 4: Bone Response to Mechanical Loading is Highly Heritable and Correlates with Osteocyte Lacunar Morphology in Mice		
4.1	Abstract	85
4.2	Introduction	86
4.3	Methods	88
4.3.1	Mouse Populations	88
4.3.2	Axial Tibial Loading	90
4.3.3	Calculations of Necessary Force	90
4.3.4	MicroCT (μ CT)	91
4.3.5	Dynamic Histomorphometry	92
4.3.6	Heritability Calculations	92
4.3.7	Correlations	93
4.3.8	Statistical Analysis	93
4.4	Results	94
4.4.1	Changes in bone morphology due to loading vary with mouse strain and sex	94
4.4.2	Bone formation increases and bone resorption decreases in response to loading vary with mouse strain and sex	96
4.4.3	Increases in mineralizing surface and mineral apposition rate vary with mouse strain and sex	98
4.4.4	Bone response to mechanical loading is highly heritable	100
4.4.5	Stiffer bones respond more to mechanical loading	100
4.4.6	Mouse strains with more elongated lacunae respond more to mechanical loading	103
4.5	Discussion	104
4.6	Supplemental Information	110
Chapter 5: Conclusions and Future Directions		
5.1	Conclusions	116
5.2	Future Directions	119
References		122

List of Figures

Figure 1.1: Depiction of important bone features including the three main cell types: osteoblasts, osteocytes, and osteoclasts.....	2
Figure 1.2: Overview of the osteocyte lacunocanalicular network (LCN). Osteocyte cell bodies reside in intracortical pores called lacunae and connect to each other via dendritic processes through canalicular channels that run through the mineralized bone. Adapted from Schneider et al. ³⁰	3
Figure 1.3: Schematic of three-point bending and a representative force-displacement and stress-strain curve defining all reported properties.	6
Figure 1.4: Schematic of axial, tibial loading. Adapted from Robling et al. ¹⁰⁴ and Patel et al. ⁸⁰ ..	9
Figure 1.5: Mouse family tree adapted from Petkov et al. ¹¹³ . The eight inbred strains used to found the Diversity Outbred population and used in this thesis are highlighted in red boxes.	10
Figure 2.1: Graphical abstract.....	15
Figure 2.2: PCA of morphology parameters in the femur and radius.....	25
Figure 2.3: PCA of mechanical properties in the femur and radius.....	26
Figure 2.4: Pearson’s correlation matrix for all measured bone traits in the femur and radius....	26
Figure 2.5: Morphology correlations between femur and radius.....	28
Figure 2.6: Mechanical property correlations between femur and radius	29
Figure 2.7: Material property correlations between femur and radius.....	29
Figure 2.8: Prediction of ultimate force	31
Figure 2.9: Correlation of elastic modulus with morphology parameters	32
Supplemental Figure 2.10: PCA analysis on each sex/diet group	38
Figure 3.1: Graphical abstract.....	40
Figure 3.2: Overview of the two genetic mouse models and whole-body traits.....	52
Figure 3.3: Radial morphology changes with strain in a sex dependent manner.	54
Figure 3.4: Radius mechanical and material properties vary between inbred mouse strains.	56
Figure 3.5: Within-bone correlations are maintained in outbred mice. Inbred mice cluster via mouse strain.	58
Figure 3.6: Lacunar morphology was visualized using x-ray microscopy (XRM).	61
Figure 3.7: Raman spectroscopy was used to evaluate bone mineral composition.	63

Supplemental Figure 3.8: Region of interest for Raman spectroscopy on the transverse cross-section of the femur. Bones were embedded in PMMA and polished to a smoothness of 0.05 μm . The red box shows the region where measurements were taken.	72
Supplemental Figure 3.9: Longitudinal whole-body measurements.	73
Supplemental Figure 3.10: Radial morphology changes with strain in a sex dependent manner. Additional radial traits not reported in Fig 3.3. * : $p < 0.05$ for comparison line # : F strain vs F B6 $p < 0.05$ ^ : M strain vs M B6 $p < 0.05$	74
Supplemental Figure 3.11: Radial material and mechanical properties changes with strain in a sex dependent manner. Mechanical (A-F) and material properties (G-J) not reported in Fig 3.4. * : $p < 0.05$ for comparison line # : F strain vs F B6 $p < 0.05$ ^ : M strain vs M B6 $p < 0.05$	75
Supplemental Figure 3.12: Tibial morphology changes with strain in a sex dependent manner.	76
Supplemental Figure 3.13: Femoral morphology changes with strain in a sex dependent manner. * : $p < 0.05$ for comparison line # : F strain vs F B6 $p < 0.05$ ^ : M strain vs M B6 $p < 0.05$	77
Supplemental Figure 3.14: PCA of raw and body mass adjusted data from Inbred Founder mice.	78
Supplemental Figure 3.15: Additional XRM parameters.	79
Supplemental Figure 3.16: Bivariate plot highlighting how the relationship between cortical area and ultimate force is highly conserved. The slopes and intercepts between the two linear-regression lines are not significantly different.	80
Figure 4.1: Graphical Abstract.....	84
Figure 4.2: Overview of experimental groups and timeline.	89
Figure 4.3: Changes in morphology between the pre-scan and post-scan.	95
Figure 4.4: Bone formation and resorption on the periosteal surface measured from image-registered time-lapse μCT	97
Figure 4.5: Bone formation rate on the periosteal and endocortical surfaces measured from dynamic histomorphometry.	99
Figure 4.6: Correlation between bone axial stiffness and response to loading.	101
Figure 4.7: Correlation matrix of Pearson's coefficients between starting μCT parameters (pre-loading) and all loading response outcomes.	102
Figure 4.8: Correlation matrix of Pearson's coefficients for average lacunar traits and loading outcomes in the Inbred Founder strains.	104
Supplemental Figure 4.9: Strain gauge data from the Inbred Founder strains.	110
Supplemental Figure 4.10: Force estimation error in the DO mice.	111

Supplemental Figure 4.11: Validation of image-registered time-lapse μ CT..... 112

Supplemental Figure 4.12: Loading-induced changes in bone morphology not shown in Fig 4.3.
..... 113

Supplemental Figure 4.13: Relative bone response on the endocortical surface measured from
image-registered time-lapse μ CT..... 114

Supplemental Figure 4.14: Relative dynamic histomorphometry outcomes not reported in Fig
4.5..... 115

Figure 5.1: Working model that osteocyte mechanosensitivity drives the morphology of cortical
bone..... 119

List of Tables

Table 2.1: List of phenotype variables measured for both the femur and radius.....	21
Supplemental Table 2.2: R^2 and p-values of each sex/diet group separately for correlations between the femur and radius. R^2 represents the goodness of fit while the p-value indicates if the slope is significantly non-zero.	38
Supplemental Table 2.3: Slope and intercept values of each sex/diet group separately for correlations between the femur and radius. The values for each sex/diet group are similar to the results when all four groups are pooled.	39
Table 3.1: Bones evaluated for various outcomes in both the Inbred Founders and Diversity Outbred (DO) mice.	46
Table 3.2: Broad sense heritability was calculated using data for the Inbred Founders for each trait as the fraction of total variation due to strain using the equation shown.	64
Supplemental Table 3.3: ANCOVA p-value results with body weight as a co-factor.	81
Supplemental Table 3.4: Heritability of all traits reported in main paper (left is repeated from Table 3.2) (right is body-weight adjusted).....	82
Supplemental Table 3.5: Heritability of uCT parameters from all three bones. Radial heritability values are repeated from Table 3.2. Right side shows heritability for body weight adjusted values.	83
Table 4.1: Heritability (H^2) of all relative outcomes (relative = loaded – nonloaded) measured in the Inbred Founders.	100

Acknowledgments

Before we get into the nitty, gritty science in this dissertation, there are many people that need to be thanked. To all of you, without you, this thesis would not have happened, and I would have been miserable trying.

First, thank you to the funding sources and monetary support that allowed me to accomplish all the experiments I could devise without worrying about breaking the bank (NIH / NIAMS R01 AR047867, NIH T32 DK108742, NIH T32 EB018266, NIH R21 079052I). I thank the two cores I used at WashU, the Musculoskeletal Research Center (MRC - NIH P30 AR074992) and the Center for Cellular Imaging (WUCCI- S10 OD021694). Additionally, thank you to The Jackson Labs (Jax DO Grant) that provided me 50 DO mice, giving me the opportunity to work with the outbred mice. Thank you to our collaborators, Dr. James Cheverud, Dr. Virginia Ferguson, and Dr. Charles Farber, and those that provided valuable insight and equipment (Dr. Katharine Flores, Dr. Jeffry Nyman). Finally, to the almost 400 mice that were used in this thesis, thank you for your service.

Second, thank you to my committee members Dr. James Fitzpatrick, Dr. Michael Harris, Dr. Spencer Lake, and Dr. Tim Peterson. Although we have never all been in the same room, I appreciate the support and feedback helping me to create the best thesis possible. Special thanks to my committee chair and mentor, Dr. Matthew Silva for your support before I was even a graduate student. Working in your lab as a research tech taught me how much I love research and solidified my decision to apply to grad school. I am grateful you encouraged me to rotate in other labs to gain experience with different techniques and musculoskeletal tissues, even though I came back to bone.

Third, thank you to all the previous and current members of the Silva Lab. You are the people that taught me how to love science and encouraged me every day of this journey. To Evan, Heather, Brandon, Taylor, and Pei, you were the reasons I stayed at WashU and joined Matt's lab. Without you, this thesis would probably be about tendons. To Chris, thank you for always being critical and keeping my science rigorous. Thank you for being my bike buddy up and down Clayton Road and around Illinois. Thank you to John and Surabhi for helping me BioQuant and analyze data. Thank you to Katie for always supporting me and becoming one of my closest friends. I will always follow the amazing science you are doing on your own. Thank you to the newer Silva Lab members Lisa, Nicole, Andre, and Leyi for continuing to make lab an enjoyable place, especially "other" Nicole for letting me take over a spot in the office and proving the Nicoles really do run the lab. Thank you to the unofficial Silva Lab member, Ryan; despite your best efforts I still haven't gone into industry. Finally, thank you to Michael and Jenny for running lab and basically the entire floor. Jenny, you have become my inspiration for what I want to become as a staff scientist.

Fourth, thank you to the members of the Tang Lab and the entire MRC community. To Christian, Kaitlyn, Garrett, Remy, and Sade, thank you for your friendship in and outside of lab. You are always down to picnic at the park or grab drinks after work, which made balancing life a lot easier. To the rest of the MRC, thank you for the numerous happy hours, hellos in the hallways, and examples of amazing science.

Fifth, thank you to my incoming PhD Cohort. You all do such amazing science but also know how to have a good time and just enjoy life. From camping trips to picnics on art hill, you all have made this PhD fun. Special thanks to Leanne, Molly, and Eric for always being there for me and introducing me to onsie bar crawls and the game of flong.

Fifth, thank you to my friends not in St. Louis. While I may not have gotten to see you very often, your support was felt. Thank you to Courtney and Andrew for providing me escapes from St. Louis to visit new places and hike new mountains. Thank you to Tori (and Mal) for being one of my best friends and showing legitimate interest in my research. Thank you for the many half marathons, triathlons, Mardi Gras, and many other celebrations. Thank you to your entire family for welcoming me as a Cooke and allowing me to crash weekends at the Lake, of which there will be many more.

Finally, thank you to my family. Michael and Sean, you may not always be outwardly supportive, telling me I'm going to be a "PHake" doctor, but under the jokes I feel your support and know you are proud. Thank you for welcoming me into the doctor club. Thank you to Kayla for being a supportive, kind, and caring sister-in-law and loving my brother for all his quirks. Four out of four doctor siblings is pretty good. Thank you to Dayday, even though you have very little idea what I'm doing every day I love how proud you are of me. Finally, thank you to my parents. You have always encouraged me to pursue whatever I wanted and have fully supported me along the way. You never pressured any of us to go into science or become doctors, but instead allowed us to find our passions on our own. Mom, thank you for always being curious and trying to understand my world of science and research despite my occasional short and snippy answers. Also, sorry for the tattoos.

Now, let's get back to the science.

Nicole Migotsky

Washington University in St. Louis

August 2023

ABSTRACT OF THE DISSERTATION

Effect of Genetic Diversity on Cortical Bone Phenotype and
Response to Mechanical Loading

by

Nicole Migotsky

Doctor of Philosophy in Biomedical Engineering

Washington University in St. Louis, 2023

Professor Matthew J. Silva, Chair

There is a complex interplay between genetics and bone tissue, for both bone morphology and the ability to remodel. Understanding the genetic basis of bone traits in the adult skeleton facilitates the discovery of novel genes or pathways as therapeutic targets for low bone mass. To this end, a genetically diverse mouse population has been created by The Jackson Laboratory using eight Inbred Founder strains. These eight inbred strains were cross-bred for multiple generations to produce the Diversity Outbred (DO) mice, a population with random assortments of genes more closely modeling the human population. Using all eight Inbred Founder strains and the DO mice I investigated the effect of genetic diversity on bone phenotype and the response to mechanical loading. Specifically, the goals of this dissertation were to investigate 1) the effect of genetic diversity on bone phenotype across length scales, 2) the effect of genetic diversity on bone response to loading, and 3) the correlation of phenotype to loading response in genetically diverse populations. In Aim 1, I measured bone morphology, mechanical properties, material properties, lacunar morphology, and mineral composition of mouse bones from these two populations of genetic diversity. Additionally, I compared how intra-bone relationships varied in the two populations. Multi-scale cortical bone traits vary significantly with genetic

background with heritability values ranging from 21% to 99%, indicating genetic control of bone traits across length scales. This investigation is the first to show that lacunar shape and number are highly heritable. Comparing the two populations of genetic diversity, the phenotypes of each DO mouse do not resemble that of single Inbred Founder but instead the outbred mice display hybrid phenotypes with the elimination of extreme values. Additionally, intra-bone relationships (e.g., ultimate force vs. cortical area) were mainly conserved in our two populations. In Aim 2, I mechanically loaded mice from the two populations of genetic diversity to assess the variation in bone response to loading. I showed the response to loading varies with genetic background and is highly heritable with heritability values ranging from 32% to 97%. All measurements of periosteal formation have a heritability value near or above 80%. On average, the DO population showed a more robust response to mechanical loading compared to the Inbred Founders with all DO mice having a net increase in all bone formation outcomes. In Aim 3, I combined the results from the two previous aims to explore the correlation between bone phenotype and the response to mechanical loading. Bone axial stiffness and lacunar traits correlate with the magnitude of loading outcomes. Stiffer bones and bones with more elongated lacunae respond more robustly to mechanical loading. From these correlations I developed a working model that intrinsic osteocyte mechanosensitivity – controlled at least partially by genetics – drives the morphology of bone to maintain a homeostatic mechanical strain state. The work of this thesis provides the groundwork and rationale to perform genome wide association studies (GWAS) or quantitative trait loci (QTL) analysis to identify candidate genes that regulate bone phenotype and the response to loading. Uncovering novel genes can provide new targets for therapeutics to not just stop bone loss but increase bone mass, especially in patients where weight-bearing exercise is unsafe or less feasible.

Chapter 1: Overview of Bone Biology and Heritability

1.1 Clinical Significance and Motivation

In the United States alone, over 54 million people over the age of 50 suffer from osteoporosis or low bone mass¹. This low bone mass contributes to an increase in fracture risk. For women over 55, osteoporotic fractures account for more hospitalizations than myocardial infarction (MI), stroke, or breast cancer combined². Both osteoporosis and low bone mass are moderately heritable. From studies of twins and generations of sisters, it has been shown that about 70% of variability in bone density and about 60% of variability in osteoporotic fractures is genetically based³⁻⁵. Understanding the genetic basis of bone traits can allow for the discovery of novel genes or pathways as therapeutic targets for low bone mass⁶.

Despite the large burden on the individual, increased risk of death, and economic burden of over \$17 billion annually^{5,7}, all current osteoporosis treatments have low efficacy. Since osteoporosis is characterized by reduced bone strength due to increased bone loss and decreased bone formation^{8,9}, treatments aim to re-balance bone loss and formation. Most current treatments work to decrease bone loss, leaving bone unable to repair microdamage and susceptible to fracture^{9,10}. Only two current treatments stimulate can increase in bone formation, but one is not recommended for long-term use and the other has a black-box warning due to increased risk of cardiovascular death¹¹⁻¹³, leaving doctors with limited ideal treatment options for osteoporosis. Research is needed to uncover and develop new strategies to increase the anabolic activity of bone to reduce the burden of osteoporosis and related fractures.

1.2 Bone Components

Bone consists of three main cell types – osteoblasts, osteoclasts, and osteocytes (Fig 1.1).

Osteoblasts are responsible for laying down new matrix and promoting the mineralization of bone¹⁴. Upon laying down a collagen rich matrix, osteoblasts secrete vesicles that act as seeding sites for new mineral (hydroxyapatite) crystals to form¹⁵. The major components of the mineral crystals are phosphate and carbonate¹⁴. Osteoblasts originate from the mesenchymal lineage, branching away from cartilage and fat tissue, which share common stem progenitors^{14,16,17}. To oppose the bone formation by osteoblasts, osteoclasts are responsible for resorbing existing bone. Osteoclasts originate from the hematopoietic lineage, similarly to macrophages and are much larger than osteoblasts^{14,18}. A balance between osteoblasts and osteoclasts are necessary to maintain healthy bone and properly respond to damage¹⁹. Finally, the most prominent cell type in bone is the osteocyte, composing up to 95% of cells in bone²⁰. Osteocytes are fully matured osteoblasts that have become embedded in the mineralized bone²¹. Residing deep within the bone tissue, osteocytes are the main cell type that senses and responds to mechanical loading^{22–27}, coordinating a remodeling response by osteoblasts and osteoclasts.

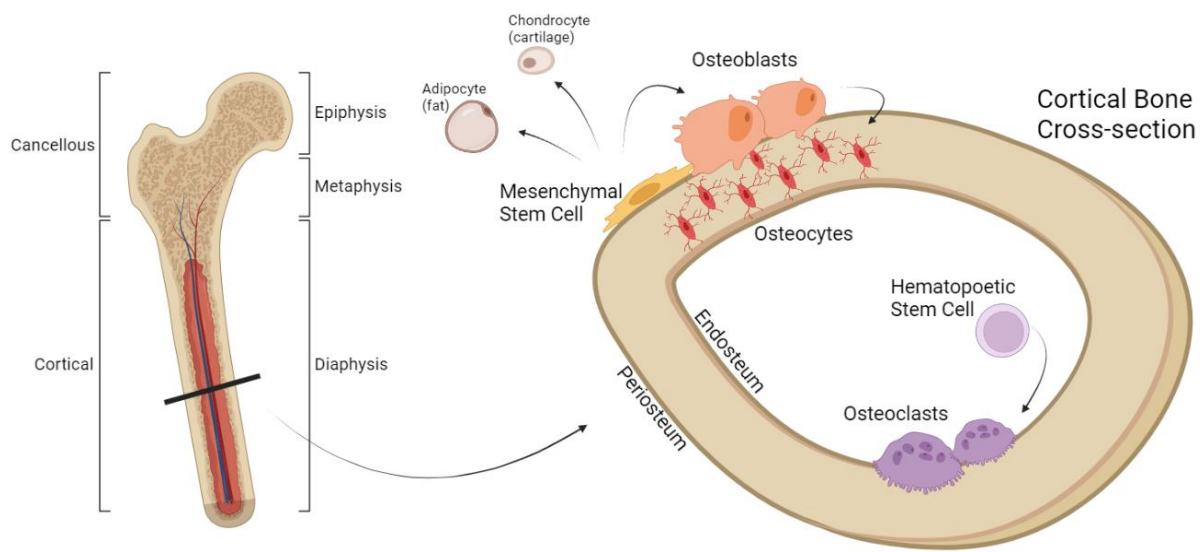


Figure 1.1: Depiction of important bone features including the three main cell types: osteoblasts, osteocytes, and osteoclasts.

Osteocytes reside in intracortical pores termed lacunae and are connected to each other via dendritic processes, which travel through microchannels termed canaliculi (Fig 1.2). Together, the lacunae and canaliculi create a microporous network filled with extracellular fluid throughout the cortical bone, which is termed the lacunocanalicular network (LCN)²⁸⁻³⁰. When external loads are applied, the whole bone only slightly deforms, yet this deformation is amplified within the small channels of the LCN and creates stress concentrations at the osteocyte cell body-dendrite interface³¹. The deformation also causes the fluid inside the LCN to pressurize and move, which further amplifies the strain on the osteocyte^{32,33}. This high level of strain triggers the osteocyte to release biochemical signals instructing the osteoblasts to increase formation and osteoclasts to decrease resorption²⁷. Alterations to the LCN will change how the strain is amplified and therefore change the signals from the osteocyte to the osteoblasts and osteoclasts^{34,35}. Changes to the cell shape may also affect how the bone responds to loading. *In vitro*, more rounded osteocytes have been shown to produce more nitric oxide in response to loading, indicating more cellular activation^{36,37}. However, with aging *in vivo*, osteocyte lacunae become more rounded and less sensitive to mechanical loading^{38,39}.

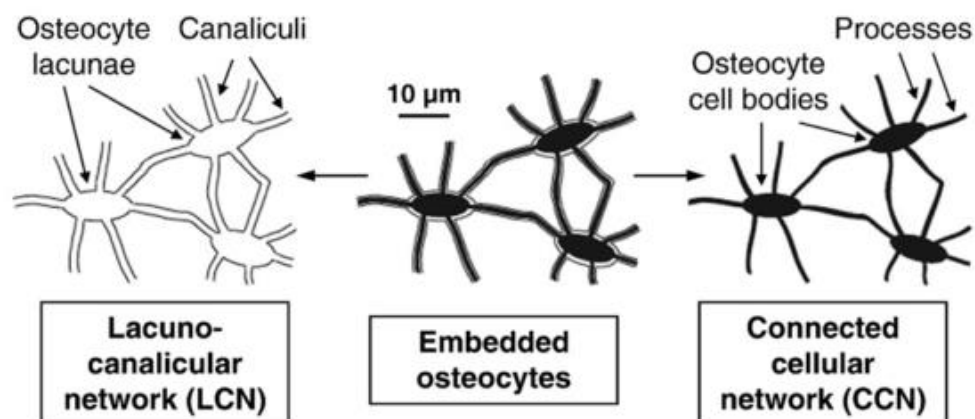


Figure 1.2: Overview of the osteocyte lacunocanalicular network (LCN). Osteocyte cell bodies reside in intracortical pores called lacunae and connect to each other via dendritic processes through canalicular channels that run through the mineralized bone. Adapted from Schneider et. al.³⁰.

To supply bone cells with nutrients, flush out waste, and transport signaling molecules, bone is highly vascularized⁴⁰. It is estimated 5-15% of cardiac output goes toward the skeleton⁴⁰⁻⁴³ and this can be vastly altered with exercise or injury^{40,42,44}. Blood vessels traverse through the thickness of bone where osteocyte dendrites can directly interact with endothelial cells lining the blood vessels^{27,45,46}. Proper vascularization is necessary for bone to remain healthy and rejuvenate after injury⁴⁰.

In long bones like the femur, tibia, and radius, there are two types of bone: cortical and cancellous (Fig 1.1). Cortical bone is dense and highly organized in ring-like lamellae^{47,48}. This type of bone is found at the center, or diaphysis of long bones, providing the bone with bending strength⁴⁸. Cancellous bone is porous and organized in rod like structures called trabeculae. This type of bone is found at the ends of long bones in the epiphysis and metaphysis⁴⁷. The more porous structure provides more surface area allowing for high metabolic exchange^{49,50}.

In addition to dividing the bone longitudinally into the diaphysis, epiphysis, and metaphysis, long bones are also divided transversely. The outer surface, called the periosteum, interacts with skeletal muscle, tendon, and ligaments⁵¹. The inner surface, call the endosteum, interacts with the marrow cavity including fat cells and immune cells⁵². These two surfaces are exposed to two different biological environments and two different mechanical environments, making it important to investigate the surfaces separately. The work in this thesis focuses only on the cortical bone but does evaluate changes on both the periosteal and endocortical surfaces individually.

1.3 Bone Strength

Clinically, osteoporosis is defined using bone mineral density (BMD) from dual-energy x-ray absorptiometry (DEXA) scans. BMD measured from DEXA accounts for 60-70% of variation in

bone strength⁵³⁻⁵⁵. However, many traits in addition to BMD contribute to bone strength and fracture risk such as morphology, mineralization, and stiffness⁵⁶. Expanding the periosteal surface to increase the diameter of bone will increase the bending resistance. The external diameter of bone predicts nearly 55% of variation in bone strength⁵⁷. More mineralized bone will lead to each unit of bone to be stronger, which, if organized in the same pattern, will lead to an overall stronger bone⁵⁸. Bone mass and fracture risk later in life depends on the peak bone mass attained as a young-adult; a 10% increase in peak bone mass reduces fracture risk in older adults by 50%⁵⁸ making it important to study what factors affect the young-adult skeleton.

There are many methods to experimentally test bone strength and the preferred method depends on the type of bone (cancellous or cortical), size of the specimen, and data desired. Cancellous bone is typically tested using a compressive test; a normal force is applied to the top and bottom surfaces to uniformly compress the specimen⁶⁰. Shear testing is also common for cancellous bone where the bottom surface is held fixed while the top surface is loaded parallel to the surface⁶¹⁻⁶³. For cortical bone, bones can be tested in tension, bending, or torsion. Large specimens are required for tensile testing, so this is typically reserved for human bones machined into a dog-bone shape⁶⁴. For mouse specimens, bending and torsion are the most common. Two different methods of bending can be used – three-point or four-point bending. For three-point bending, two support points hold the specimen in place while a third point contacts the middle of the top surface creating a bending moment (Fig 1.3). For four-point bending, the same two points hold the specimen, but instead two points spaced equally from the midpoint contact the top surface. Four-point bending requires longer specimens to ensure bending and not crushing of the bone⁶⁰. Due to this size limitation, three-point bending is used in this thesis work to determine bone strength. Finally, bones can be tested in torsion. To accomplish this, the ends of the bone

are fixed, typically in plastic, and then twisted (rotated). This testing is ideal for specimens with non-uniform geometry in the mid-section such as fracture calluses^{65,66}.

During mechanical testing, a force is applied to the specimen by displacing it at a constant rate. The reaction force and applied displacement are concurrently measured resulting in a force-displacement curve⁶⁰ (Fig 1.3). The first region will be linear where the displacement is defined as elastic – any deformation that occurs will completely return when loading is stopped. After a certain amount of displacement, the specimen will yield, and the line will become curved. After this point plastic deformation has occurred and if loading is stopped the specimen will be permanently deformed. After yielding, the specimen will hit a maximum amount of force it can maintain defined as the ultimate force. As the displacement increases, more and more damage occurs until the specimen ultimately breaks. Mechanical properties of bone are calculated from force-displacement data such as stiffness (slope of the linear region), ultimate force, yield force, post-yield displacement, and work to fracture (Fig 1.3). These properties depend on both the material and geometry of the specimen⁶⁷.

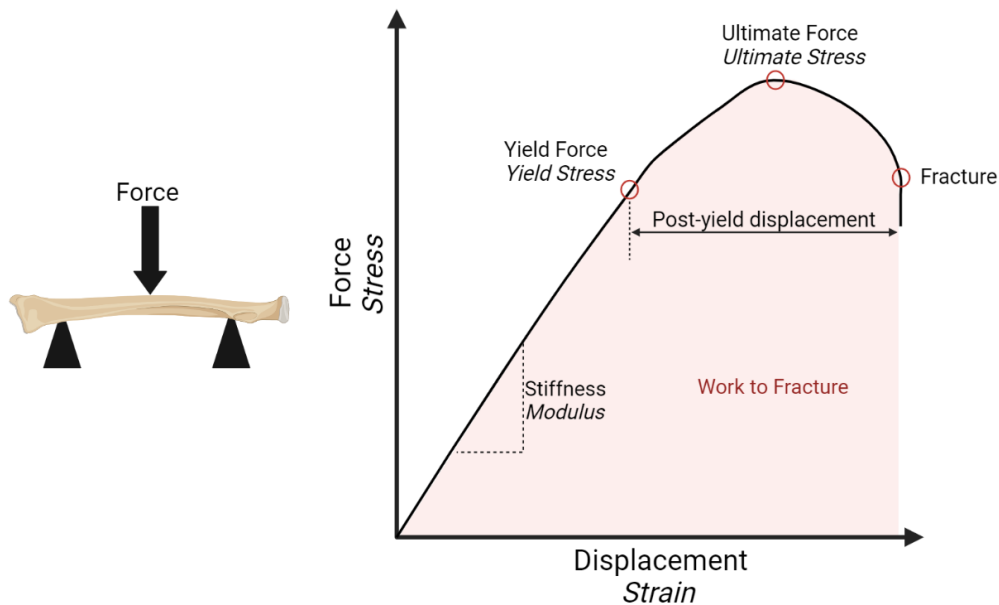


Figure 1.3: Schematic of three-point bending and a representative force-displacement and stress-strain curve defining all reported properties.

To remove dependence on geometry, forces and displacements can be normalized to create a stress-strain curve. Stress is defined as force per area the force is acting over. Strain is defined as the displacement per original length, reported as microstrain ($\mu\epsilon$) for mouse bone (1,000 $\mu\epsilon$ = 0.001 ϵ = 0.1% deformation)^{60,68}. Material properties of bone are calculated from the stress-strain data such as elastic modulus (slope of linear region), ultimate stress, and yield stress (Fig 1.3).

1.4 Bone Mechanobiology

One key feature of bone is its ability to respond and remodel in accordance with the mechanical demands placed upon it. This ability to remodel allows for the strengthening of bone in high strain regions to diminish the risk of fracture. German surgeon Julius Wolff noticed the trabecular structure in the epiphysis of the femur reminded him of the metal structures supporting cranes. The trabecular struts appeared to follow the stress lines in the bone. From these observations Dr. Wolff developed a law stating bone will adapt to meet the demands of mechanical loading placed on it⁶⁹. Specifically, an increase in loading will cause bone to strengthen and a decrease in loading will cause bone to weaken⁷⁰⁻⁷². In accordance with this law, dynamic, mechanical loading, such as exercise, stimulates a potent anabolic response in bone⁷³⁻⁷⁹. However, while there is a potent anabolic response to loading in young bone, this response diminishes with age⁸⁰⁻⁸². Our lab has shown that following loading, old mice upregulate fewer pathways at the transcript level, especially pathways related to proliferation and differentiation, processes thought to be necessary for bone formation⁸³.

Harold Frost expanded upon Wolff's Law to suggest bone has a mechanism similar to a thermostat he deemed the "mechanostat". Some mechanism, now thought to be the osteocytes^{26,39,84-86}, must monitor the mechanical demands and usage of the bone. If there are

large mismatches or errors between the current bone mass and the needed bone mass to meet mechanical demands, the mechanostat would turn on and initiate needed changes^{87,88}. If the mechanical demands were above a threshold or “minimum effective strain”, the mechanostat would initiate bone formation⁸⁷⁻⁸⁹.

1.5 Mouse Models of Mechanical Loading

To research bone mechanobiology, many labs, including ours, utilize murine long bone loading models^{22,90-94}. The current methods for loading bones have evolved considerably from the first models relying on surgical intervention to place pins through the bone that can be gripped and manipulated to overload the bone^{95,96}. To eliminate the injury response associated with surgical intervention, Turner proposed a non-invasive, *in vivo*, four-point bending model to produce controlled strain on long bones of rodents⁹⁷. This method of loading produces new bone formation, but confident analysis is restricted to the endocortical surface due to a woven bone (or injury) reaction response on the periosteum where the supports contacted the limb. To overcome this, Gross et al. developed a cantilever model where the knee and proximal tibia is held fixed while the distal tibia is displaced. This model elucidates bending in the medial-lateral direction about the anterior-posterior axis, which is non-physiological⁹⁸. In addition to the non-physiological loading direction, the knee is difficult to hold fixed. To more closely mimic physiologic loading, Torrance⁹⁹ and Lee¹⁰⁰ developed an axial loading model of the rodent forelimb. In this model, the proximal and distal ends of the ulna are held in cup-like fixtures while compressive loads are placed along the long-axis of the bone. This model was later replicated in the rodent tibia by Fritton¹⁰¹ and De Souza¹⁰². One advantage of the axial, tibial compression loading model is that no loads are directly applied to the tibia, but instead are transferred through the knee and ankle joints, which are held in fixtures (Fig 1.4). Due to the

natural curvature of the bone, the compressive forces also induce bending of the long bone placing the anterior-medial surface in tension and the posterior-lateral surface in compression^{80,103} (Fig 1.4). All the murine loading work done in this thesis utilizes the axial, tibial compression model following the guidelines established by Main et al¹⁰³.

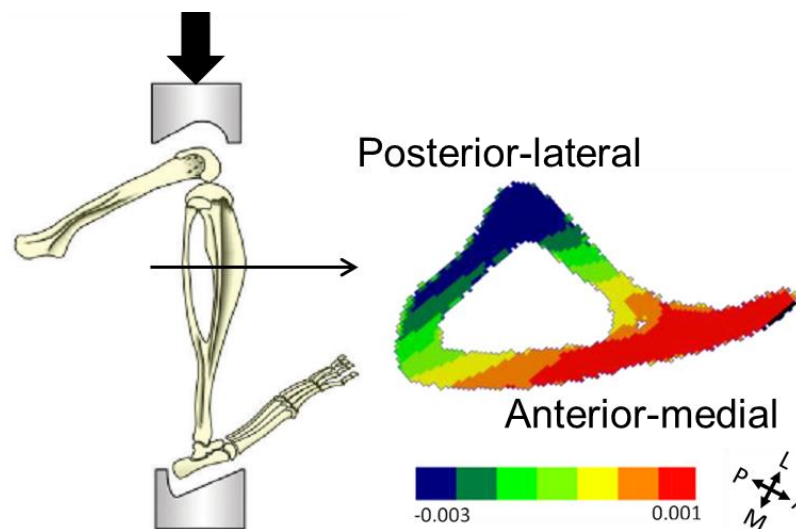


Figure 1.4: Schematic of axial, tibial loading. Adapted from Robling et. al.¹⁰⁴ and Patel et al.⁸⁰

Most loading studies are performed on a very limited range of mouse strains. In loading studies published between 2014 and 2020 (PubMed search terms: *mouse, bone, loading* – returned 94 studies), 96% use C57BL/6 (B6) mice or mutants that are a majority B6. The studies that didn't use B6, used only one of four other strains of mice (BALB/c¹⁰⁵⁻¹⁰⁷, CD1¹⁰⁰, DBA/2¹⁰⁸, and C3H/He^{108,109}). Additionally, the majority (64%) of loading studies were done in females, and while 15 included both sexes, most did not compare sexes. Work is needed to enhance rigor and translatability by using genetically diverse cohorts of both female and male mice.

1.6 Mouse Genetic Diversity

The laboratory mice typically used for research descend from the “fancy” mice kept as pets by the European and Asian elite. As mice were bred for special traits, like coat style and color, they became more and more inbred¹¹⁰. Eventually, these mice were used in research and the inbred

used in this thesis: *Mus musculus musculus* and *Mus musculus castaneus*. These two sub-species are from wild-derived mice (Fig 1.5 Group 7) and house over 11.6 million unique variants (SNPs, indels, and structural variants) compared to B6. These two sub-species are more closely related to each other than they are to most research mice (*Mus musculus domesticus*)¹¹⁴.

1.6.1 Diversity Outbred Mouse Population

To facilitate the investigations of the genetic basis of various diseases and phenotypes, Jackson Laboratory generated the Diversity Outbred (DO) mouse population by cross-breeding eight inbred founder strains to produce a population with random assortments of genes modeling the heterozygosity of the human population and the wide range of human diseases^{115,116}. These eight inbred strains consist of three wild-derived strains (CAST/EiJ, PWK/PhJ, and WSB/EiJ) and five classical laboratory strains (A/J, C57BL/6J, 129S1/SvImJ, NOD/ShiLtJ, and NZO/HILtJ) that together cover almost 90% of the genetic diversity found in the mouse genome¹¹⁷ (Fig 1.5). CAST are of sub-species *Mus musculus castaneus*, PWK are of sub-species *Mus musculus musculus*, and the remaining 6 strains are of the sub-species *Mus musculus domesticus*¹¹⁸. The DO mice each have a unique combination of over 44.7 million variants distributed across its genome, all inherited from one of the eight founders¹¹⁴. In comparison to the human population, scientists have discovered over 600 million single nucleotide polymorphisms (SNPs) around the world and any pair of humans differs by approximately 3 million base pairs¹¹⁹. In 17 inbred mouse strains genotyped by Keane et al, they discovered 56.7 million SNPs, considerably lower than the number seen in humans. However, the two closest inbred lines (B6 and 129S1) had over 4.5 million SNPs¹¹⁴, more than what is seen between a pair of humans.

Over the last decade, use of these genetically diverse populations has increased in the bone field, and these mice have been used to evaluate the heritability and candidate genes regulating cancellous bone microarchitecture in the growing skeleton¹²⁰, the response to hindlimb unloading

via casting in the femur¹²¹, and the heritability of femur properties and genes influencing cortical bone accrual in the growing skeleton¹²². These studies provide motivation and rationale to use these populations of genetically diverse mice to study the heritability of cortical bone traits.

1.7 Heritability of Bone Traits

From studies of twins and generations of sisters, it has been shown that about 70% of variability in bone density and about 60% of variability in osteoporotic fractures is genetically based³⁻⁵.

Classically, heritability is estimated using twin, adoption, or family clinical study designs^{123,124}.

Heritability is sensitive to age, GDP, and economic growth rates showing the importance of considering environmental factors in addition to genetic factors¹²⁵. The Framingham Offspring Study has been tracking multiple generations of nuclear families of European ancestry since 1971, making it a powerful resource for genetic studies. Karasik et al reported heritability of bone microarchitecture as high as 98.3% (tibia cortical area fraction) estimated from bone microarchitecture data collected from an offshoot of the Framingham study participants¹²⁶. With the increase in availability and decrease in cost of whole-genome arrays, heritability estimate from genome-wide association studies (GWAS) have become more standard¹²³. However, almost 80% of all genome-wide association study (GWAS) participants are of European descent despite those of European ancestry only accounting for approximately 16% of the world population¹²⁷. The conclusions of bone heritability from these studies therefore have limited applicability to broader populations.

Using mouse models, more complex bone traits can be investigated compared to studies done on humans. Additionally, due to the high homology between mammalian genomes, results from mouse studies are useful to assist in understanding the complicated role of genetics in humans¹²⁴.

In a GWAS performed on 31 diverse mouse strains, 11 genes were correlated to cancellous bone

properties¹²⁰. A recent study in mice by Al-Barghouthi et. al. showed that all 55 complex skeletal phenotypes measured in 12 wk old genetically diverse mice had non-zero heritability¹²². Additionally, they identified nineteen novel genes “not previously implicated in the regulation of bone traits”. Specifically, from their GWAS analysis and subsequent knockout experiments, they discovered *Qsox1* highly regulates bone accrual in the medial-lateral direction. In addition to static bone traits, different inbred mouse strains have been shown to respond differently to mechanical loading and multiple groups have highlighted the complex relationship between genetics, bone morphology, and response to loading, indicating interactions between multiple genomic regions^{128–132}. In a study by Akhter et al., two mouse strains were loaded to the same force, yet only one mouse strain produced a robust anabolic response¹⁰⁹. Robling and Turner compared the loading response of adult, female mice from three different strains, also showing significantly different responses¹⁰⁸. These studies revealed B6 mice were more responsive than C3H, motivating Kesavan et al. to perform a genome-wide search of loci regulating bone adaptive response in a B6XC3H intercross after tibial 4-pt bending¹²⁸. They calculated the broad-sense heritability of morphology changes between 70% and 86% and discovered multiple loci across multiple chromosomes. Additionally, Friedman et al¹²¹ showed the response of mouse bone to mechanical *unloading* in the Inbred Founders is heritable. These studies motivate further investigation of bone response to loading, incorporating more genetic variation and allele combinations to enhance rigor and translatability.

1.8 Goals of the Dissertation

There is a complex interplay between genetics and bone tissue, for both bone morphology and the ability to remodel. Understanding the genetic basis of bone traits in the adult skeleton can facilitate the discovery of novel genes or pathways as therapeutic targets for low bone mass.

Therefore, the goals of this dissertation are to investigate 1) the effect of genetic diversity on bone phenotype across length scales, 2) the effect of genetic diversity on bone response to loading, and 3) the correlation of phenotype to loading response in genetically diverse populations. First (Chapter 2), I took an existing data set from an advance-intercross population where each mouse has a unique combination of alleles from two founder strains and span a large range of body size. Using these mice, I investigated cortical bone phenotypes and how they correlate within a single bone and between bones. Second (Chapter 3), I utilized the Diversity Outbred (DO) mice and their eight Inbred Founders to phenotype cortical bone at the whole-body, whole-bone, lacunar, and material length scales. Third (Chapter 4), using the DO and Inbred Founders again, I mechanically loaded these genetically diverse mice and measured the variation in response to loading. Finally (Chapter 4), using the results from phenotyping and loading of the DO and Inbred Founders, I investigated which phenotype traits most correlate to loading outcomes. This led to the development of a working model that intrinsic osteocyte mechanosensitivity drives the morphology of bone to maintain a homeostatic mechanical strain state.

Chapter 2: Cortical Bone Relationships are Maintained Regardless of Sex and Diet in a Large Population of LGXSM Advanced Intercross Mice*

*Paper published in Bone Reports 2022: Migotsky N, Brodt MD, Cheverud JM, Silva MJ. Cortical bone relationships are maintained regardless of sex and diet in a large population of LGXSM advanced intercross mice. Bone Rep. 2022 Aug 26;17:101615. doi: 10.1016/j.bonr.2022.101615. PMID: 36091331; PMCID: PMC9449555.

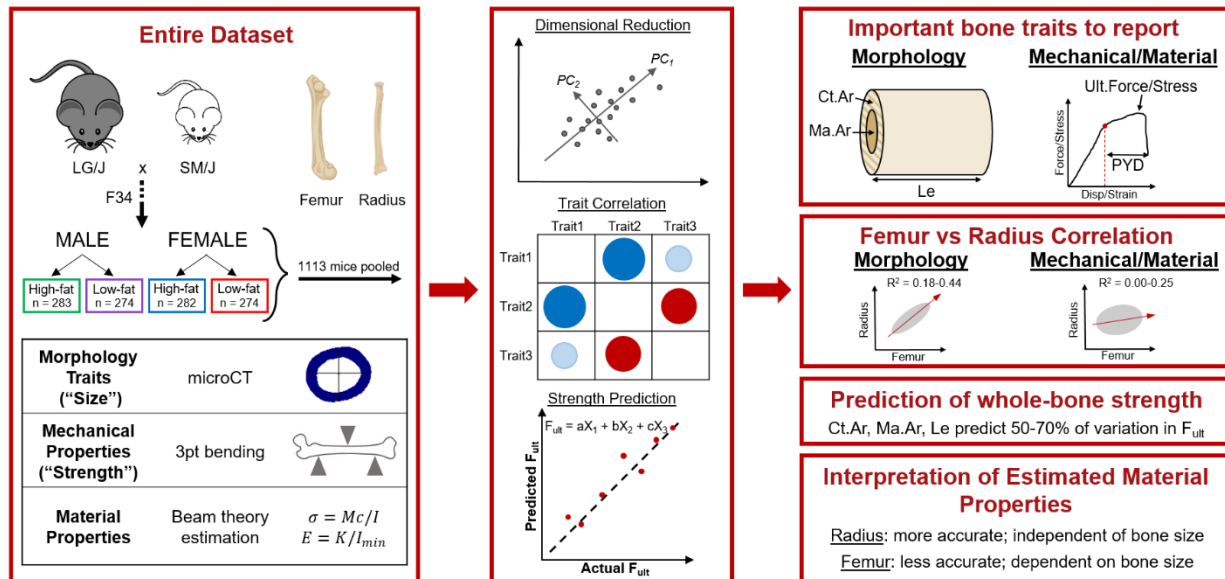


Figure 2.1: Graphical abstract

2.1 Abstract

Knowledge of bone structure-function relationships in mice has been based on relatively small sample sets that limit generalizability. We sought to investigate structure-function relationships of long bones from a large population of genetically diverse mice. Therefore, we analyzed previously published data from the femur and radius of male and female mice from the F34 generation of the Large-by-Small advanced intercross line (LGXSM AI), which have over a two-fold continuous spread of bone and body sizes (Silva et al. 2019 JBMR).

Morphological traits, mechanical properties, and estimated material properties were collected from the femur and radius from 1113 LGXSM AI adult mice (avg. age 25 wks). Males and females fed a low-fat or high-fat diet were evaluated to increase population variation. The data were analyzed using principal component analysis (PCA), Pearson's correlation, and multivariate linear regression.

Using PCA groupings and hierarchical clustering, we identified a reduced set of traits that span the population variation and are relatively independent of each other. These include three morphometry parameters (cortical area, medullary area, and length), two mechanical properties (ultimate force and post-yield displacement), and one material property (ultimate stress). When comparing traits of the femur to the radius, morphological traits are moderately well correlated (r^2 : 0.18-0.44) and independent of sex and diet. However, mechanical and material properties are weakly correlated or uncorrelated between the long bones. Ultimate force can be predicted from morphology with moderate accuracy for both long bones independent of variations due to genetics, sex, or diet; however, predictions miss up to 50% of the variation in the population. Estimated material properties in the femur are moderately to strongly correlated with bone size parameters, while these correlations are very weak in the radius.

Our results indicate that variation in cortical bone phenotype in the F34 LGXSM AI mouse population can be adequately described by a reduced set of bone traits. These traits include cortical area, medullary area, bone length, ultimate force, post-yield displacement, and ultimate stress. The weak correlation of mechanical and material properties between the femur and radius indicates that the results from routine three-point bending tests of one long bone (e.g., femur) may not be generalizable to another long bone (e.g., radius). Additionally, these properties could not be fully predicted from bone morphology alone, confirming the importance of mechanical testing. Finally, material properties of the femur estimated based on beam theory equations showed a strong dependence on geometry that was not seen in the radius, suggesting that differences in femur size within a study may confound interpretation of estimated material properties.

2.2 Introduction

Investigating the mechanical strength of long bones is a well-established concept in biology and engineering^{133,134}. Turner and Burr laid a foundation for biomechanical testing of rodent bones by describing techniques and defining terminology⁶⁰. These methods have become a staple in phenotyping musculoskeletal mouse models, allowing researchers to identify quantitative trait loci (QTL)¹³⁵, analyze gene functions^{136–138}, assess responses to pharmacological interventions¹³⁹ and alterations in mechanical loading^{105,140}, and quantify changes with growth and aging^{141,142}.

Knowing the strength of bones alongside morphology allows the investigation of structure-function relationships. It has been shown that bone material can redistribute, especially if quality is altered, to preserve adequate whole-bone (structural) strength^{136–138,143,144}. Jepsen et al identified three adaptations to meet the needs of the skeletal loading environment: changing the amount of bone, the distribution of bone, or the quality of bone¹⁴⁵. For example, in a mouse

model of osteogenesis imperfecta (OI), mutant mice compensate for deficient collagen production by developing larger bones which leads to an increase in whole-bone strength¹³⁶. Conversely, mice with BMP-5 deficiency, which have smaller body and muscle mass, develop smaller, weaker bones, while maintaining bone composition and material properties consistent with lower mechanical demands^{137,138}. These examples highlight the importance of examining mechanical and morphological properties of bones together¹⁴².

While mechanical testing of mouse bones has provided insights into bone structure-function, there remain some limitations. First, many studies use only one strain of mouse^{141,146}, and those that use more than one typically use discrete inbred strains^{147,148}. This can lead to groupings or clusters of data at two extremes instead of a continuous distribution of values, making correlations between traits difficult to assess¹⁴⁹. Second, despite knowing there are differences in regulation of bone strength and morphology between females and males^{150,151}, many studies only evaluate one sex^{140,141}. Third, sample sizes are typically tens of mice^{145,147}. Fourth, most studies only evaluate a single bone per mouse. Collectively, these drawbacks limit the opportunity for generalizable conclusions. Lang et al. addressed these limitations by testing mice from the F2 generation of C57 x DBA mice, using males and females, a sample size of 200 per sex, and evaluating both the tibia and femur¹³⁵. However, the focus of that study was to identify gene loci that influence bone properties and not to examine structure-function relationships.

We sought to investigate structure-function relationships of multiple bones from a large population of genetically diverse mice of both sexes. Accordingly, we analyzed data from the femur and radius of male and female mice from the F34 generation of the Large-by-Small advanced intercross line (LG,SM AI), which have over a two-fold continuous spread of bone sizes¹⁵². We utilized this F34 LG,SM AI population of mice in a previous study and reported the

effects of diet, sex, and body mass on cortical bone traits evaluated by microCT and mechanical testing of more than 2200 bones. In brief, we showed female and male mice raised on a high-fat diet had increased body weight and developed larger, stronger bones compared to mice fed a low-fat diet¹⁵².

One challenge with any in-depth phenotyping study is the volume of data, which can make analysis and interpretation overwhelming. For example, for the LG,SM AI mice, we reported 25 bone traits (14 for the radius, 11 for the femur) for 1113 animals from four experimental groups. Coulombe et al. recently highlighted limitations in comparing groups based on individual bone traits¹⁵³. As an alternative, they proposed principal component analysis (PCA), k-means clustering, and Support Vector Machine classification (SVM) as complimentary methods to concurrently evaluate all traits within a data set. Specifically, PCA was used to explain the variation of bone trait values within the population using a smaller number of independent variables resulting in three principal components that explain over 90% of the population variation in ten individual traits^{153,154}. Herein, we apply some of these approaches to the LG,SM AI data set to identify a reduced set of traits that still captures the variation in morphology or mechanical properties between animals.

Mechanical properties at the whole-bone (structural) scale are dependent on bone size and material properties. Material properties of rodent bone have traditionally been estimated from mechanical tests using engineering beam theory equations⁶⁰. These equations assume a uniform cross-section, homogenous and isotropic material properties, and a slender test specimen. Our group and others have shown mouse bones, especially femurs, do not meet these assumptions and calculations underestimate the true values of material properties^{60,155–157}. Schriefer et al. compared the measurement error of various long bones and recommended the radius as the

preferred bone for three-point bend testing due to its consistently round shape and slender aspect ratio¹⁵⁵. Despite this recommendation, over 80% of studies reporting mechanical testing in the last 10 years tested the femur and over 60% of those testing the femur reported material properties calculated using engineering beam theory (PubMed terms: mouse, bone, mechanical testing; published since 2011). Thus, there is a need to re-examine methods used to estimate mouse bone material properties that remain in widespread use.

Our objective in this study was to mine the dataset from the LG,SM AI population¹⁵² to investigate relationships between and within bone traits in a mouse population with a large variation of body size and bone size. Specifically, we asked four questions: 1) What are a reduced set of traits that can describe the morphology and mechanical properties of mouse long bones? 2) Do traits correlate between long bones? 3) Can the reduced set of morphology traits accurately predict whole-bone strength? and 4) What are the implications of using beam theory to estimate material properties in the femur compared to the radius?

2.3 Methods and Materials

2.3.1 Mice

All mouse work was completed with approval of the Washington University Institutional Care and Use Committee (IACUC). Data analyzed herein were previously published¹⁵². Briefly, long bones from 1139 mice from the F34 generation of the LG/J by SM/J AI line (Wustl:LG,SM-G34) were analyzed. Males and females were divided into two diet groups and fed either a relatively high-fat (42% calories from fat) or low-fat (15% calories from fat) diet beginning at weaning (3 wk of age). This resulted in four experimental groups: FL (female low-fat), FH (female high-fat), ML (male low-fat), and MH (male high-fat). Mice were euthanized at skeletal maturity (avg 24.7 wks, range = 21.0-28.7 wks). Female and male mice raised on a high-fat diet

had 32% greater body mass, on average, than sex-matched mice fed a low-fat diet. Body mass was 17% greater in males than females¹⁵².

2.3.2 Phenotyping

Femur and radius cortical bone phenotyping was completed as described¹⁵². Briefly, bone cross-sectional morphology was assessed with microCT spanning a 3 mm region of the mid-diaphysis (16 μm voxel size). Bone length was measured using calipers. Whole-bone mechanical properties were assessed using three-point bending with a support span of 7 mm. Material properties were estimated using simple beam theory equations. Fourteen properties were reported per bone: six morphology traits (five that describe the cross-section, and one the length), five whole-bone mechanical properties, and three bone material properties (Table 2.1). Traits were transformed as necessary to normalize the data. Any trait that was normalized is indicated with a prefix of l (natural log transform; femur yield force), i (inverse transform; femur post-yield displacement), or s (square root transform; femur work to fracture). Any mouse exhibiting extreme values (judged to be either biologically or physically implausible) in one or more traits were excluded from analysis, leaving 1113 mice (FL: n = 274; FH: n = 282; ML: n = 274; MH: n = 283).

Table 2.1: List of phenotype variables measured for both the femur and radius

Morphology Traits (n = 6)	Length (Le), Cortical Area (Ct.Ar), Total Area (Tt.Ar), Marrow Area (Ma.Ar), polar moment of inertia (J), average Cortical Thickness (Ct.Th)
Mechanical Properties (n = 5)	Ultimate Force (F_u), Yield Force (F_y), Stiffness (K), Post-yield Displacement (PYD), Work to Fracture (Wfx)
Estimated Material Properties (n = 3)	Ultimate Stress (S_u), Yield Stress (S_y), Elastic Modulus (E)

2.3.3 Analysis Software

Analysis and statistical comparison was done using R or GraphPad Prism. R version 4.0.2 (2020-06-22 – “Taking Off Again”) was used with RStudio (Version 1.2.5042) and the Global CRAN repository to calculate the principal component analysis and correlation matrix. GraphPad Prism (version 9) was used to perform bivariate and multivariate linear analyses.

2.3.4 Principal Component Analysis

Principal component analysis (PCA) was performed on four datasets: 1) femur morphology, 2) radius morphology, 3) femur mechanical properties and 4) radius mechanical properties.

Initially, the four experimental groups (2 sexes x 2 diets) were analyzed separately, but no differences were found between groups (Suppl. Fig 2.10) so all 1113 animals were pooled and analyzed together. Each variable was centered and scaled to have a distribution mean of 0 and standard deviation of 1 within the *prcomp* function. Because signs are arbitrarily assigned to variable weights, the weightings in dataset 2 (radius morphology) were multiplied by negative one (-1) to match the signs from dataset 1 (femur morphology). Coordinates (weightings) of each variable in each principal component dimension and the variance of each principal component were extracted from the PCA. Using the PCA analysis we identified reduced sets of morphological and mechanical traits that span the principal components and are relatively independent of each other (based on 2.5 - *Correlation Matrix* below).

2.3.5 Correlation Matrix

A matrix of Pearson’s correlation coefficients was computed on two datasets: 1) all femoral traits and 2) all radial traits. Correlations between all traits within a single bone were computed using the *cor* function in R and visualized using the *corrplot* function. Variables were automatically hierarchically clustered into five groups using the *ward.D2* algorithm.

2.3.6 Bivariate Linear Analysis

Bivariate linear regression was performed to 1) compare bone traits between long bones (radius vs femur) and 2) compare elastic modulus (material property) to bone size parameters (Ma.Ar, Tt.Ar, J) per bone. For all bivariate regressions, each sex/diet group was first plotted and analyzed individually, then pooled and analyzed again. The slopes were compared between groups by calculating a two-sided p-value. If slopes were determined to be not significantly different ($p > 0.05$) the intercepts were also compared. This method of slope and intercept comparison is equivalent to Analysis of Covariance (ANCOVA). Additionally, the slopes for each group were compared to zero using an F-test with $p < 0.05$ for significance. To compare traits between long bones, the value of a single trait measured in the radius was plotted against the same trait measured in the femur. This resulted in 14 bivariate analyses. To compare elastic modulus to bone size, the elastic modulus of the femur was plotted against either the marrow area, total area, or polar moment of inertia of the femur. The same was repeated for the radius. This resulted in 6 bivariate analyses (3 for femur and 3 for radius).

2.3.7 Multivariate Linear Regression

Multivariate linear regressions were performed to estimate ultimate force of the femur and radius individually. To create the multivariable model for ultimate force, the predicted value was set to ultimate force while the independent variables were initially set to all morphology traits ($n = 6$). First, backward elimination was used to reduce the variable set to only those significantly and independently contributing to the model. Briefly, the variable with the highest p-value was removed from the model and the analysis was re-run until all remaining variables had a significant contribution ($p < 0.05$). A second model was created using the three morphology parameters proposed in the reduced set of parameters (Ct.Ar., Ma.Ar., Le). The best fit of each model was assessed using the adjusted R^2 value.

2.4 Results

2.4.1 Correlation of traits within each bone

We used principal component analysis (PCA) to examine how bone traits cluster during dimensional reduction. Dimensional reduction can allow for fewer variables to characterize the data set while maintaining the majority of the variability in the population. In both the femur and radius, bone morphometry parameters can be reduced to three components that explain almost 99% of the variation between animals (Fig 2.2). Clustering of traits is almost identical in the femur and radius. While all variables contribute, the first principal component (PC1) is dominated by the bone size parameters total area, cortical area, and moment of inertia; these three variables are highly correlated ($r > 0.79$ for each pair) and fall into the same hierarchical cluster (Fig 2.4). PC2 is dominated by two additional cross-sectional parameters, marrow area and cortical thickness, which contribute to PC2 in opposite directions; these variables are not significantly correlated. Bone length is the only parameter that significantly contributes to PC3. Thus, the five measured bone traits that describe cortical cross-sectional morphology can be reduced to two principal components, while bone length adds a third component. Thus, cortical area, marrow area and length represent a reduced set of parameters that characterize long bone morphology in this mouse population.

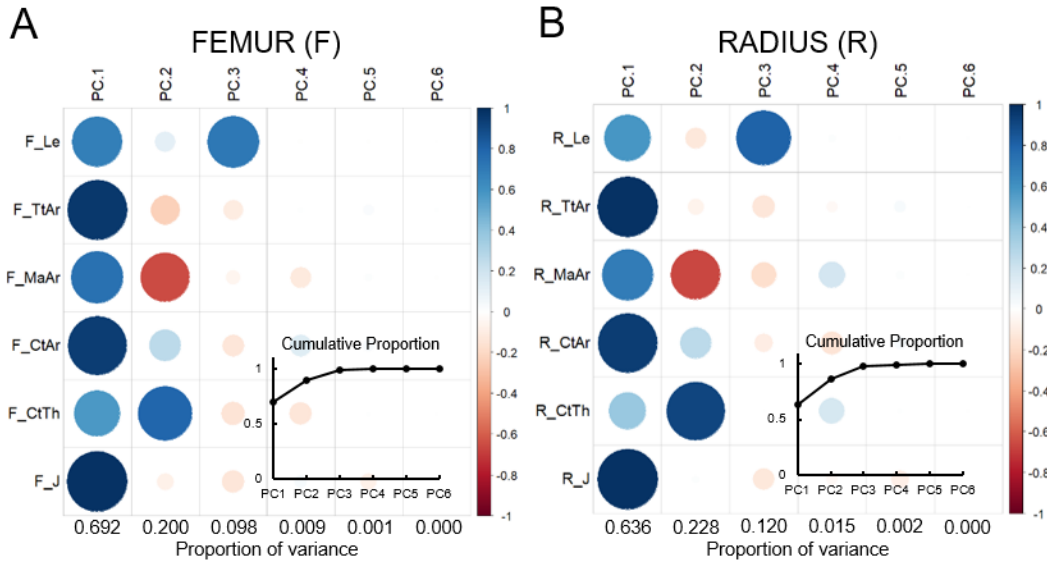


Figure 2.2: PCA of morphology parameters in the femur and radius
 Contribution of each morphology parameter collected from uCT of the femur (A) and radius (B) to the individual dimensions of a principal component analysis (PCA). For both bones, the first three components (PC) explain over 90% of variation between animals. TtAr, CtAr, and J contribute the most to PC1. MaAr and CtTh contribute the most to PC2. Le is the only variable highly contributing to PC3. Inset graphs show cumulative proportion of variance from each principal component.
 F: Femur, R: Radius, Le: Length, TtAr: Total Area, MaAr: Marrow Area, CtAr: Cortical Area, CtTh: Cortical Thickness, J: Moment of Inertia, PC: Principal Component

Similarly, the five measured mechanical properties reduce to two dimensions that explain 80% and 90% of the variation between animals in the femur and radius, respectively (Fig 2.3). PC1 is mainly defined by bone stiffness and strength. PC2 is defined by properties that reflect bone ductility (PYD and Wfx); these two properties are highly and almost exclusively correlated to each other and cluster together (Fig 2.4). Thus, ultimate force and post-yield displacement represent a reduced set of parameters that characterize long bone mechanical properties.

The three estimated material properties moderately or highly correlate with each other in both the femur and radius, but this correlation is stronger in the radius (Fig 2.4). Within the femur, material properties (especially elastic modulus) have negative correlations with multiple bone morphology parameters, whereas these correlations are absent in the radius.

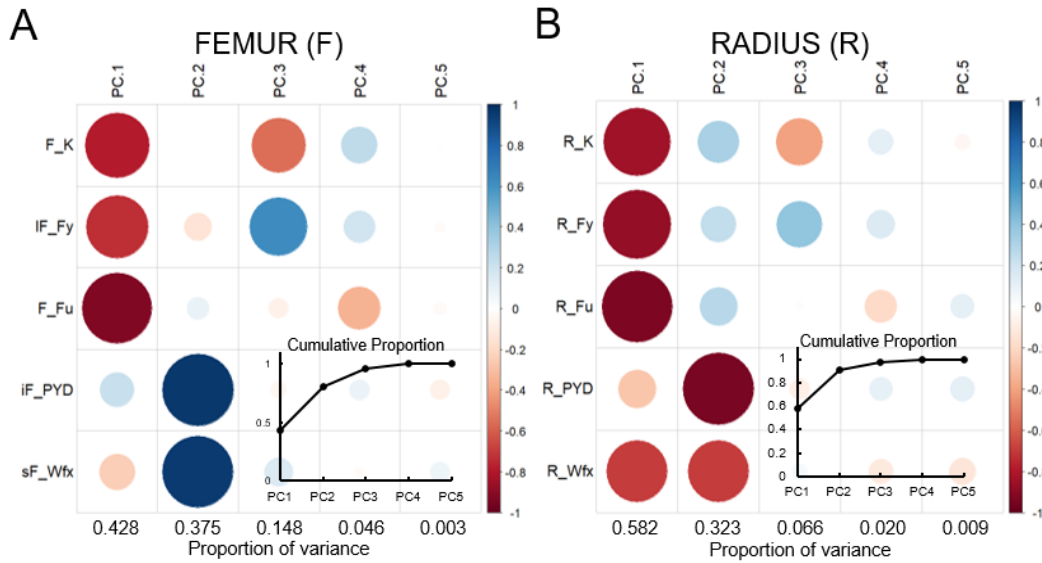


Figure 2.3: PCA of mechanical properties in the femur and radius
 Contributions of each mechanical property collected from 3pt bending of the femur (A) and radius (B) to the individual dimensions of a principal component analysis (PCA). For the femur, the first two components (PC) explain over 80% of variation between animals. For the radius, the first two components explain over 90% of variation between animals. K, Fy, and Fu (stiffness and strength properties) contribute the most to PC1. PYD and Wfx (ductility properties) contribute the most to PC2. Inset graphs show cumulative proportion of variance from each principal component.
 F: Femur, R: Radius, Fu: Ultimate Force, Fy: Yield Force, K: Stiffness, PYD: Post-Yield Displacement, Wfx: Work to Fracture, PC: Principal Component

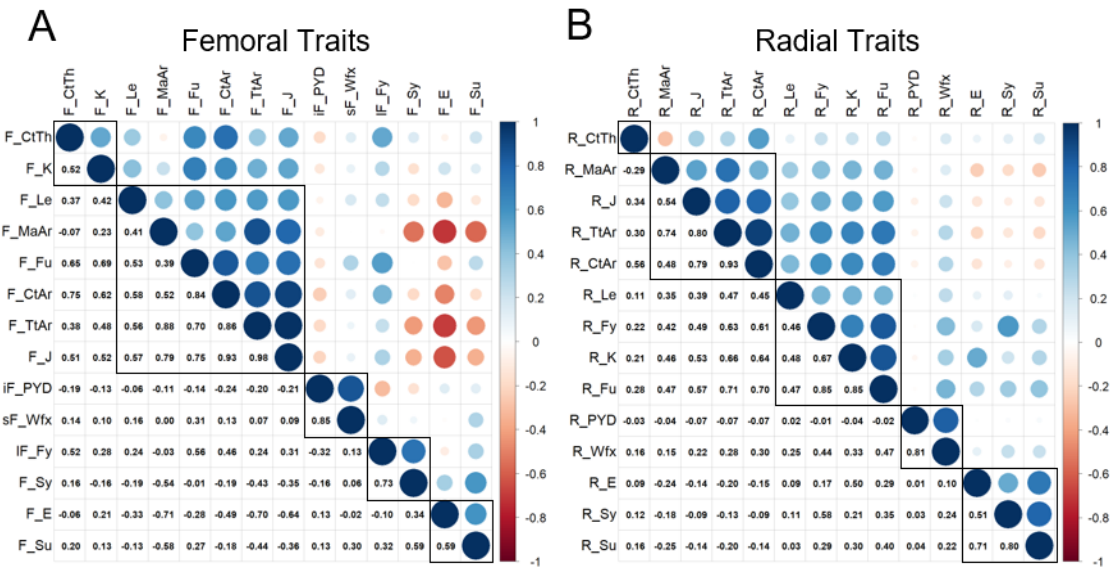


Figure 2.4: Pearson's correlation matrix for all measured bone traits in the femur and radius
 Correlation matrix of all 14 bone properties measured for the femur (A) and radius (B). Black boxes surround variables that cluster together using hierarchical clustering. Material properties (Sy, Su, E) highly correlate with each other for both bones. E in the femur has negative correlation with many morphometry parameters, a relationship absent in the radius. Lower triangle shows Pearson's r values.
 F: Femur, R: Radius, Le: Length, TtAr: Total Area, MaAr: Marrow Area, CtAr: Cortical Area, CtTh: Cortical Thickness, J: Moment of Inertia, Fu: Ultimate Force, Fy: Yield Force, K: Stiffness, PYD: Post-Yield Displacement, Wfx: Work to Fracture, Su: Ultimate Stress, Sy: Yield Stress, E: Elastic Modulus

2.4.2 Correlation of traits between bones

We used bivariate linear regression to investigate how each trait correlates between two long bones, the femur and radius. All morphology traits are positively and significantly correlated between bones. Notably, the relationships between bones do not depend on sex or diet (i.e., slopes of regression lines are not different between groups; Fig 2.5). We note that there are significant differences in intercepts between groups, but intercepts from the pooled data are within the 95% confidence interval of the intercept for each group. The R^2 values for each sex-diet group are generally similar, which is further indication that there is a similar relationship between bones across the four groups (Supp. Table 2.2). When sex/diet groups are pooled, cortical area and moment of inertia have the strongest correlations between bones ($R^2 = 0.44$ and 0.43 , respectively; Fig 2.5), while medullary area and cortical thickness have the weakest correlations ($R^2 = 0.25$ and 0.18 , respectively; Fig 2.5). Thus, morphological traits related to size of the radius and femur are moderately well correlated in this mouse population and these relationships are similar across sex and diet.

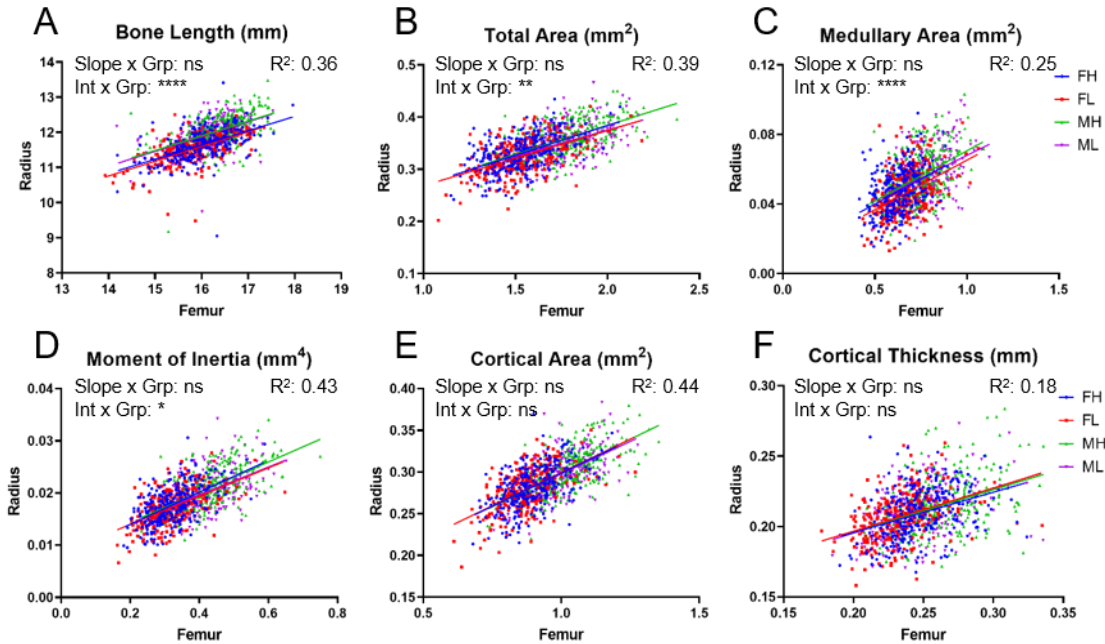


Figure 2.5: Morphology correlations between femur and radius
 Correlation of morphology traits between the femur (x-axis) and radius (y-axis) with linear regression lines displayed per sex/diet group. Slopes are not significantly different between sex/diet groups, for any variable. Intercept values are significantly different for bone length (A), total area (B), medullary area (C), and moment of inertia (D). For all traits and all groups, the slopes of the linear regression line are significantly different from zero. Goodness of fit (R^2) for all groups pooled is shown on each graph.
 Slope: significance of different slopes between groups, Int: significance of different intercepts between groups, ns: not significant, * $p < 0.05$, ** $p < 0.01$, *** $p < 0.001$, **** $p < 0.0001$, FH: female high fat, FL: female low fat, MH: male high fat, ML: male low fat

Mechanical properties are weakly correlated between long bones (Fig 2.6). Ultimate force is the only mechanical property where the slopes are different between sex/diet groups ($p = 0.03$); individual group slopes range from 32% lower to 12% higher than the pooled slope (Supp. Table S2). For post-yield displacement, all four sex/diet groups have slopes not different from zero indicating no correlation between the femur and radius. Additionally, despite having no significant differences in slopes between groups, only female low-fat (FL) and male high-fat (MH) have slopes not different from zero for work-to-fracture. Material properties are not correlated between long bones, where all four sex/diet groups for the three material properties have slopes not significantly different from zero (Fig 2.7). The estimated values for each material property are approximately two times higher in the radius than the femur. Thus, whole-bone

mechanical properties of the radius and femur are only weakly correlated, while estimated material properties are not correlated.

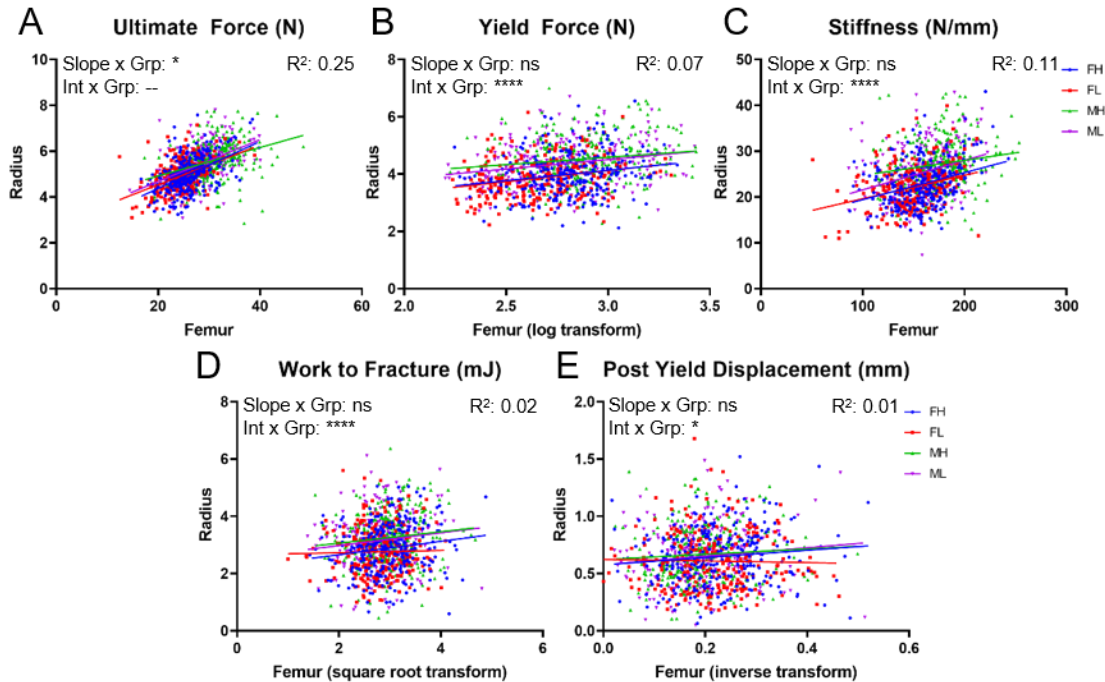


Figure 2.6: Mechanical property correlations between femur and radius

Correlation of mechanical properties between the femur (x-axis) and radius (y-axis) with linear regression lines displayed per sex/diet group. Slopes are not significantly different between sex/diet groups, except for ultimate force (A). Intercept values are significantly different for all other traits (B-E). For ultimate force (A), yield force (B), and stiffness (C), the slopes of the linear regression line are significantly different from zero. For work to fracture, best fit lines from the FL and MH groups are not significantly different from zero. The post-yield displacement regression lines are not significantly different from zero for all sex/diet groups.

Slope: significance of different slopes between groups, Int: significance of different intercepts between groups, ns: not significant, --: not evaluated, * $p < 0.05$, ** $p < 0.01$, *** $p < 0.001$, **** $p < 0.0001$, FH: female high fat, FL: female low fat, MH: male high fat, ML: male low fat

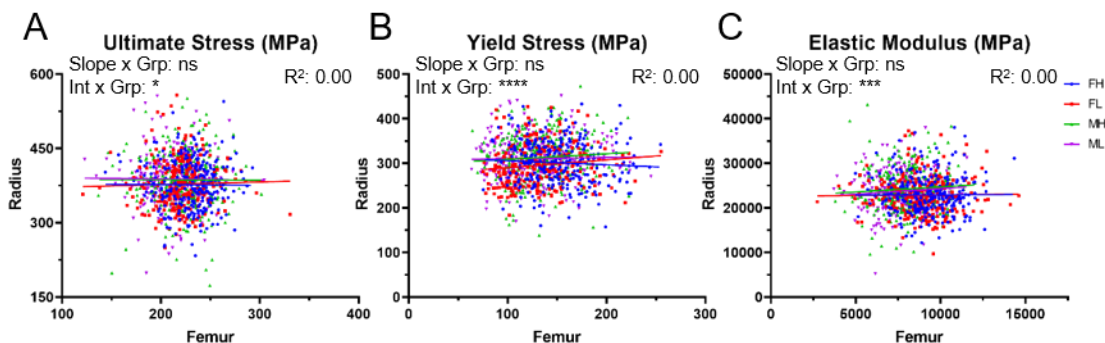


Figure 2.7: Material property correlations between femur and radius

Correlation of material properties between the femur (x-axis) and radius (y-axis) with linear regression lines displayed per sex/diet group. The slopes of the linear regression line are not significantly different from zero for any material property trait, and are not significantly different between sex/diet groups. Intercept values are significantly different for all traits (A-C).

*Slope: significance of different slopes between groups, Int: significance of different intercepts between groups, ns: not significant, * $p < 0.05$, ** $p < 0.01$, *** $p < 0.001$, **** $p < 0.0001$, FH: female high fat, FL: female low fat, MH: male high fat, ML: male low fat*

2.4.3 Prediction of whole-bone strength

We created a multivariate linear regression to predict ultimate force, a measure of whole-bone strength, from morphology parameters (Fig 2.8). Ultimate force can be predicted with moderate accuracy for both bones, with the femur prediction being more accurate (adj $R^2 = 0.72$ (fem) vs. 0.54 (rad)) (Fig 2.8 A,B). After using backwards elimination to exclude non-significant contributing variables, the femur ultimate force can be well predicted from cortical area, moment of inertia, cortical thickness, and length (Fig 2.5 A). Note that these four parameters span the three main PCs explaining a majority of the intra-bone variation (Fig 2.2 A). For the radius, only total area, marrow area, and length are needed to predict ultimate force (Fig 2.8 B), which corresponds to one variable per PC cluster (Fig 2.2 B). For both bones, the largest contributing variable is a measure of cross-sectional bone size. We compared this non-biased model to a model using a pre-selected reduced set of morphology traits (Ct.Ar, Ma.Ar, Le; determined in *3.1 - Correlation of traits within each bone*). The goodness of fit is almost identical to that of the un-biased model (adj $R^2 = 0.71$ (fem) and 0.54 (rad); Fig 2.8 C,D) supporting the finding that these three parameters are a functionally meaningful set.

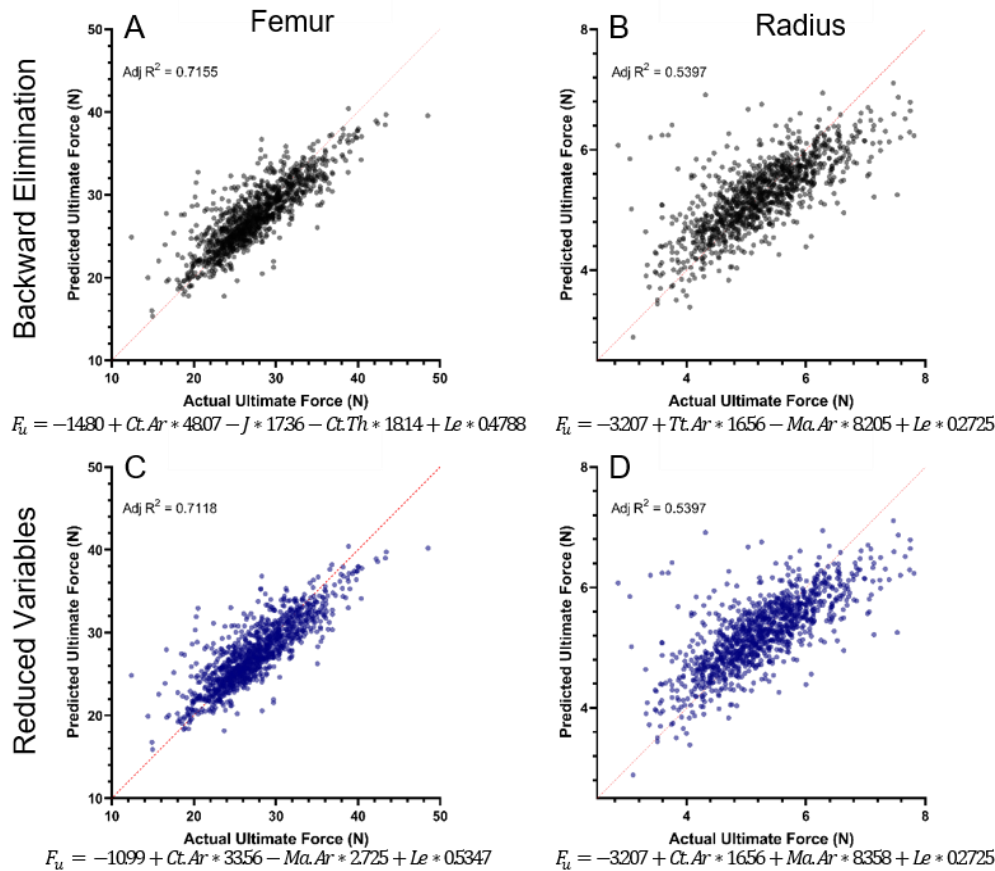


Figure 2.8: Prediction of ultimate force

Multivariate linear regression of ultimate force for the femur (A&C) and radius (B&D). (A&B) All morphology parameters were initially included in the model. Backwards elimination was used to narrow down only significantly contributing variables. (C&D) Only the reduced set of morphology parameters (Ct.Ar, Ma.Ar, Le) were included in the model. The R^2 value is extremely similar between models within each bone. Ultimate force is more accurately predicted in the femur compared to the radius, as shown by the larger adjusted R^2 value.

2.4.4 Implications of using beam theory to predict material properties

Finally, we further examined the negative correlations between material properties and

morphology parameters identified in the correlation matrix (Fig 2.4). In the femur, elastic

modulus correlated strongly with marrow area, total area, and moment of inertia ($r = -0.64$ to -

0.71 ; $p < 0.0001$). These same correlations in the radius were much weaker, albeit significant (r

$= -0.16$ to -0.25 ; $p < 0.0001$). We used bivariate linear regression to investigate these

relationships individually (Fig 2.9). Marrow area correlates the most strongly to elastic modulus

and this correlation is much stronger in the femur than radius ($R^2 = 0.51$, fem [Fig 2.9 A] vs

0.061 , rad [Fig 2.9 D]). Total area correlates moderately to elastic modulus in the femur (Fig 2.9

B) yet very weakly in the radius (Fig 2.9 E). Moment of inertia had the weakest correlation to elastic modulus, but was still moderately correlated in the femur ($R^2 = 0.40$; Fig 2.9 C). The radius shows a very weak correlation between elastic modulus and moment of inertia ($R^2 = 0.025$; Fig 2.9 F). Taken together, these analyses indicate that beam theory-estimated material properties for the femur have a strong dependence on morphology, while the estimated material properties of the radius have only a weak dependence on morphology.

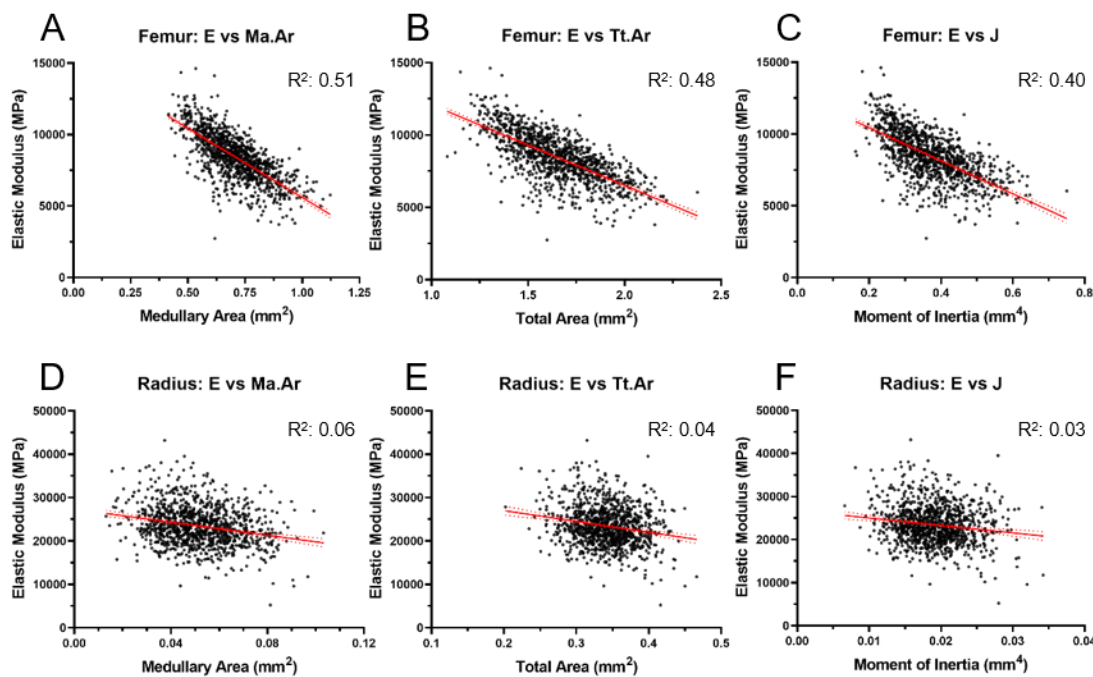


Figure 2.9: Correlation of elastic modulus with morphology parameters
Correlation of elastic modulus with morphology parameters in the femur (A-C) and radius (D-F). Medullary area correlates most strongly with elastic modulus for both bones (A&D), but the correlation is stronger in the femur. For each trait, the correlation is stronger in the femur (top row) compared to the radius (bottom row). All slopes from the linear regression are significantly different from zero. All 4 sex/diet groups were combined for analysis.

2.5 Discussion

We reported previously that long bone traits are different between sexes and are altered by diet in LG,SM AI mice¹⁵². Using these same data from more than 1100 mice, here we focused on the intra- and inter- bone relationships to address four questions: 1) What are a reduced set of traits that can describe the morphology and mechanical properties of mouse long bones? 2) Do traits correlate between bones? 3) Can the reduced set of morphology traits accurately predict bone

strength? and 4) What are the implications of using beam theory to estimate material properties in the femur compared to the radius? We find that PCA and correlation analysis reveals similar relationships between morphological and mechanical properties across the sex/diet groups for both the femur and radius, which implies that relationships between bone parameters were conserved across sex, diet, and bone. This suggests that the reduced set of parameters we report here may be useful to describe mouse long bones from other populations. Correlations of individual traits between long bones reveal that morphology parameters are positively and strongly correlated, whereas mechanical and material properties have weak to no correlations between bones. These correlations are again independent of sex or diet. Multivariate regression reveals that 54-72% of variation in ultimate force can be predicted from bone morphology measured using microCT. Finally, elastic modulus and bone morphology are moderately correlated for the femur but not the radius. The dependency of material property estimates in the femur on morphology raises the possibility of a size-dependent error when using beam theory to estimate material properties of mouse femurs.

We investigated *intra*-bone relationships of cortical bone traits using principal component analysis (PCA) to evaluate which combination of variables contribute the most to bone variability in the F34 LGXSM AI population. Reducing dimensionality using PCA can simplify interpretation while minimizing data loss. Additionally, we built a correlation matrix to investigate the relationship of each pair of traits. Using these analyses, we identified a minimal set of cortical bone properties (traits) to describe mouse long bones that may be useful when assessing differences between experimental groups or variations within other mouse populations. For morphometry we identified *cortical area*, *medullary area*, and *bone length*; these parameters span the first three principal components and together can describe bone expansion periosteally,

endosteally, and axially. For mechanical properties we identified *ultimate force* and *post-yield displacement*; these two parameters are independent, contribute almost exclusively to different principal components, and represent a force measurement and deformation measurement.

Compared to other measurements that describe whole-bone function (e.g., stiffness), ultimate force is more accurately computed since it is independent of deformation measurements, and ultimate force had the strongest correlations to morphology parameters in our data set (Fig 2.4).

For material properties, we identify *ultimate stress*. Calculations of ultimate stress do not depend on strain estimation and are therefore less variable and more accurate than modulus estimations¹⁴².

We investigated *inter*-bone relationships between the femur and radius using bivariate linear regressions for each of the fourteen traits reported. Morphometry traits are all significantly and positively correlated between long bones. The lack of significant difference in slopes between the sex/diet groups in all these correlations indicates that morphometry traits scale between long bones independently of sex or diet. In contrast to the moderately strong correlations between bones for morphometric properties, mechanical properties are only weakly correlated. Ultimate force is the most strongly correlated ($R^2 = 0.25$) between the radius and femur, followed by bone stiffness ($R^2 = 0.11$). The correlation between radius and femur for ultimate force reported here for mice is comparable to the correlation reported in Patton et al for humans¹⁵⁸. However, work-to-fracture and post yield displacement do not correlate between long bones indicating yielding behavior and ductility assessed by three-point bending are bone-dependent properties. Estimated material properties have no correlation between long bones. While this result could mean that murine bone material properties differ between bones, it may be an artifact of inaccurate estimations of femur material properties using beam theory. To answer this question, more direct

methods to estimate material properties are required. Regardless, the lack of strong correlation of mechanical and material properties between the radius and femur indicates that the results from routine three-point bending tests of one long bone (e.g., femur) may not be generalizable to another long bone (e.g., radius).

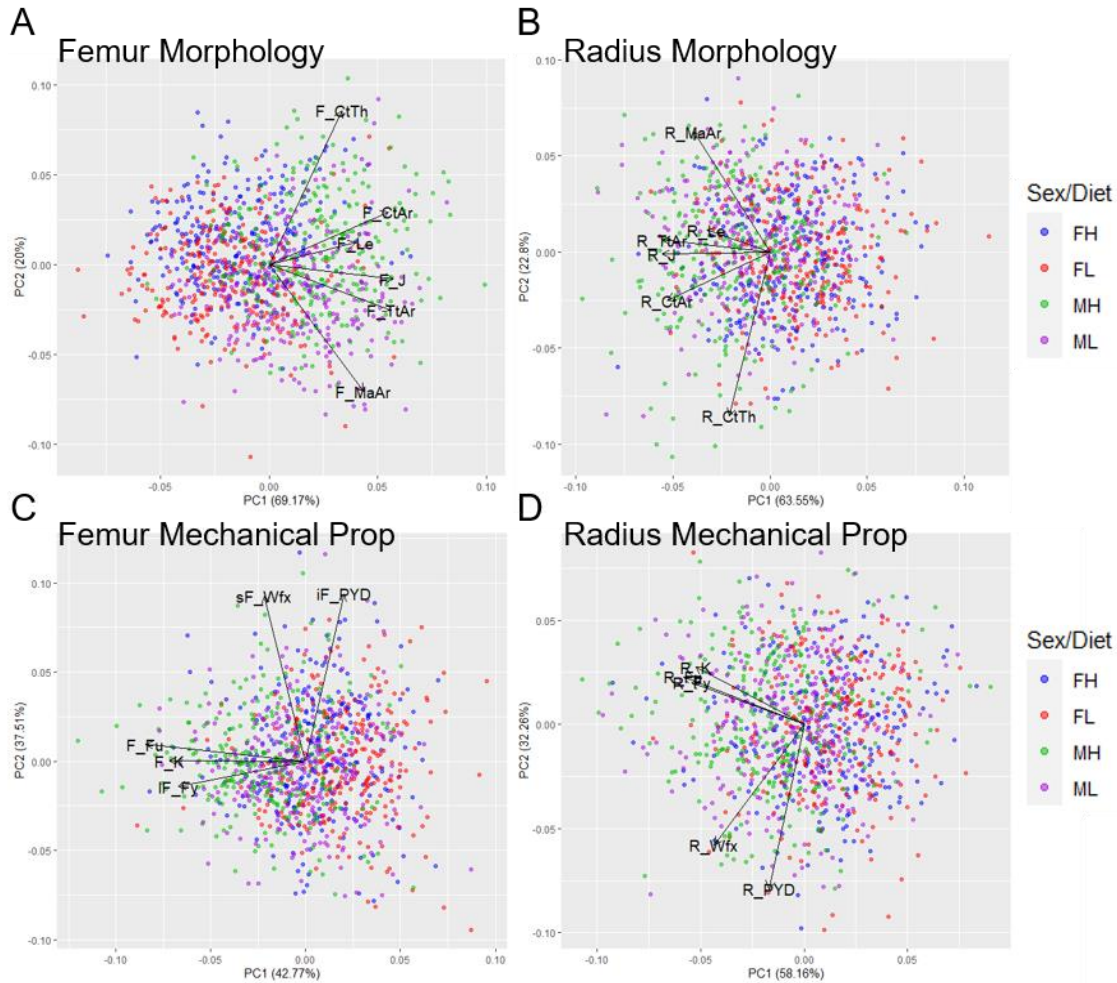
Next, we investigated the feasibility of predicting bone strength using bone morphology determined by microCT. If variation in bone strength can be estimated using non-destructively measured parameters, physically breaking bones may be unnecessary and bone samples could be used for other outcomes (e.g., histology). The unbiased multi-variable model we report here can predict nearly 72% of the variation in ultimate force in the femur and nearly 54% in the radius. A reduced set of morphology parameters predict the same amount of variation as the unbiased model for both bones. Additionally, using just one of the morphometry parameters in the reduced set (cortical area) explains nearly the same amount of variation in ultimate force (71% for femur, 49% for radius). Bone mineral density alone can explain 50-75% of the variation in ultimate strength in various mammalian models, and around 57% for rat humerus⁵⁶, which is similar to the range of variation explained by our model. Additionally, other groups have used similar multivariable models and have been able to predict almost 80% of femur strength using bone volume, cortical thickness, and total area¹⁴⁹. The higher goodness of fit of the model in that study might be due to the differences in mouse number, range of bone sizes, and measurement technique. While morphometry-based estimation of bone strength is an appealing concept, 28-46% of variation in ultimate force was not explained by our model leading us to conclude that mechanical testing is still essential to assess differences in bone strength between experimental groups.

Finally, we investigated the implications of using beam theory to estimate bone material properties. Three- (or four-) point bending is the preferred method to mechanically test bones of small animals¹⁴². Typically, material properties are estimated using engineering beam theory where the test specimen is assumed to have a constant cross-section, homogenous and isotropic properties, and a large length-to-width ratio. The femur, which is the most common bone used for mechanical testing, does not meet these assumptions and therefore estimated values of material properties are generally underestimated^{142,155,156}. The radius is a longer, more slender bone that more accurately meets beam theory assumptions, but can be more difficult to handle and requires more sensitive testing equipment due to its small size. A previous study comparing the accuracy between the radius and femur did so in mouse bones of two genetic backgrounds having distinctly different bone size (B6, C3H)¹⁵⁵. The mice in the current study have a more continuous range of bone sizes and strengths and include larger variations of genetic backgrounds, allowing us to test if the limitations of applying beam theory to mouse bones are more broadly applicable. We found strong correlations of elastic modulus with bone morphometry parameters in the femur only, with 40-50% of variation in elastic modulus being explained by bone geometry. These correlations are almost entirely absent in the radius, with only 2.5-6% of the variation in elastic modulus being explained by bone geometry. This suggests that size differences in bones may bias femur-estimated values of material properties much more so than radius-estimated properties. These findings provide additional support to previous recommendations for mechanical testing of the radius when a goal is to estimate material properties^{142,155}.

In summary, we used a large, data set (Chapter 2) from mice spanning a large range of body size and weight to investigate the structure-function relationship of two long bones and the

dependency on sex and diet. In both the femur and radius, bone traits similarly cluster together using PCA and correlation analysis. Additionally, how bone traits cluster did not change based on sex/diet groups. The independence on bone type, sex, and diet provide support that these correlations are more broadly applicable to cortical traits of long bones from various mouse populations. We identified a reduced set of parameters for morphometry, mechanical properties, and material properties that are fairly independent yet span the various principal components to explain the most variation in the population. For morphometry, we identified cortical area, medullary area, and bone length; for mechanical properties, we identified ultimate force and post-yield displacement; for material properties, we identified ultimate stress. We observed that up to 50% of the variation in femur-estimated elastic modulus could be explained by size parameters, which suggests that caution should be taken when interpreting estimated material properties of the femur. Finally, while many morphometry parameters are highly correlated with mechanical properties, predicting ultimate force from morphometry alone did not account for up to 50% of the variation between animals in our study, highlighting the value of destructive mechanical testing. Our results support that testing be done on the bone of interest because mechanical, and especially material, properties correlated poorly between the femur and radius.

2.6 Supplemental Material



Supplemental Figure 2.10: PCA analysis on each sex/diet group
 PCA was done on each sex/diet group individually for both morphology (A&B) and mechanical properties (C&D). There is no clear division of sex/diet groups indicating no large difference between groups.

Supplemental Table 2.2: R^2 and p -values of each sex/diet group separately for correlations between the femur and radius. R^2 represents the goodness of fit while the p -value indicates if the slope is significantly non-zero.

Outcome	FH		FL		MH		ML		Pooled	
	R^2	p -val	R^2	p -val						
Length (Le)	0.311	<0.0001	0.372	<0.0001	0.250	<0.0001	0.271	<0.0001	0.363	<0.0001
Total Area (Tt.Ar)	0.280	<0.0001	0.278	<0.0001	0.327	<0.0001	0.263	<0.0001	0.386	<0.0001
Medullary Area (Ma.Ar)	0.165	<0.0001	0.185	<0.0001	0.187	<0.0001	0.171	<0.0001	0.250	<0.0001
Moment of Inertia (J)	0.315	<0.0001	0.290	<0.0001	0.370	<0.0001	0.295	<0.0001	0.427	<0.0001
Cortical Area (Ct.Ar)	0.329	<0.0001	0.341	<0.0001	0.413	<0.0001	0.358	<0.0001	0.439	<0.0001
Cortical Thickness (Ct.Th)	0.136	<0.0001	0.152	<0.0001	0.155	<0.0001	0.190	<0.0001	0.178	<0.0001
Ultimate Force (Fu)	0.251	<0.0001	0.196	<0.0001	0.120	<0.0001	0.234	<0.0001	0.273	<0.0001
Yield Force (Fy)	0.037	0.001	0.063	<0.0001	0.021	0.016	0.056	<0.0001	0.072	<0.0001
Stiffness (K)	0.105	<0.0001	0.089	<0.0001	0.026	0.007	0.106	<0.0001	0.120	<0.0001
Work to Fracture (Wfx)	0.022	0.014	0.001	0.709	0.012	0.065	0.017	0.036	0.014	<0.0001
Post Yield Displacement (PYD)	0.013	0.058	0.001	0.705	0.005	0.264	0.014	0.058	0.004	0.049
Ultimate Stress (Su)	0.000	0.921	0.001	0.678	0.000	0.981	0.000	0.858	0.000	0.631
Yield Stress (Sy)	0.004	0.320	0.015	0.051	0.005	0.230	0.001	0.692	0.000	0.491
Elastic Modulus (E)	0.000	0.955	0.000	0.857	0.005	0.253	0.006	0.209	0.000	0.833

FH: female high-fat FL: female low-fat MH: male high-fat ML: male low-fat

Supplemental Table 2.3: Slope and intercept values of each sex/diet group separately for correlations between the femur and radius. The values for each sex/diet group are similar to the results when all four groups are pooled.

† slopes significantly different between groups, * intercepts significantly different between groups, ^ slope not significantly different from zero

Outcome	FH		FL		MH		ML		Pooled	
	Slope	Int	Slope	Int	Slope	Int	Slope	Int	Slope	Int
Length (Le)	0.406	5.152	0.420	4.885	0.418	5.224	0.421	5.150	0.483	4.025*
Total Area (Tt.Ar)	0.114	0.157	0.106	0.163	0.111	0.162	0.100	0.175	0.111	0.159*
Medullary Area (Ma.Ar)	0.057	0.011	0.057	0.008	0.058	0.013	0.053	0.015	0.060	0.009*
Moment of Inertia (J)	0.031	0.008	0.027	0.009	0.029	0.009	0.027	0.009	0.029	0.008*
Cortical Area (Ct.Ar)	0.159	0.140	0.160	0.140	0.162	0.137	0.155	0.143	0.158	0.141
Cortical Thickness (Ct.Th)	0.288	0.138	0.307	0.135	0.300	0.136	0.317	0.132	0.299	0.136
Ultimate Force (Fu)	0.103	2.323	0.087	2.805	0.062	3.673	0.091	2.851	0.092 [†]	2.723
Yield Force (Fy)	0.721	1.972	0.771	1.809	0.511	3.053	0.657	2.537	0.875	1.752*
Stiffness (K)	0.059	13.510	0.051	14.51	0.033	21.50	0.064	15.120	0.067	13.67*
Work to Fracture (Wfx)	0.234	2.191	0.040 [^]	2.649	0.199 [^]	2.666	0.223	2.533	0.206	2.426*
Post Yield Displacement (PYD)	0.319 [^]	0.576	-0.072 [^]	0.625	0.229 [^]	0.623	0.370 [^]	0.578	0.183	0.606*
Ultimate Stress (Su)	-0.013 [^]	379.4	0.053 [^]	366.4	-0.003 [^]	387.2	-0.023 [^]	392.9	-0.030 [^]	388.9*
Yield Stress (Sy)	-0.091 [^]	315	0.174 [^]	272.9	0.125 [^]	296.4	0.033 [^]	306.6	0.031 [^]	301.2*
Elastic Modulus (E)	0.010 [^]	22840	0.028 [^]	22635	0.226 [^]	22452	0.250 [^]	21823	-0.017 [^]	23606*

FH: female high-fat

FL: female low-fat

MH: male high-fat

ML: male low-fat

† slopes significantly different between groups

* intercepts significantly different between groups

[^] slope not significantly different from zero

Chapter 3: Multi-Scale Cortical Bone Traits Vary in Two Mouse Models of Genetic Diversity

Multi-scale cortical bone traits have high heritability (H^2)

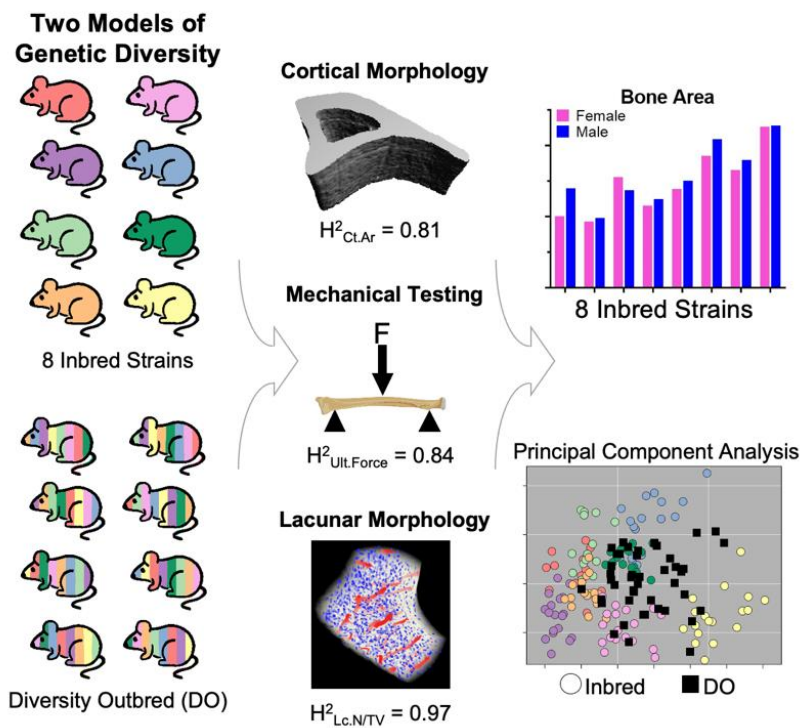


Figure 3.1: Graphical abstract

3.1 Abstract

Understanding the genetic basis of cortical bone traits can facilitate the discovery of novel genes or biological pathways regulating bone health. Mice are the most widely used mammalian model for skeletal biology and allow for the quantification of traits that can't easily be evaluated in humans, such as osteocyte lacunar morphology. The goal of our study was to investigate the effect of genetic diversity on multi-scale cortical bone traits of three long bones in skeletally-mature mice. We measured bone morphology, mechanical properties, material properties, lacunar morphology, and mineral composition of mouse bones from two populations of genetic diversity. Additionally, we compared how intra-bone relationships varied in the two populations. Our first population of genetic diversity included 72 females and 72 males from the eight Inbred Founder strains used to create the Diversity Outbred (DO) population. These eight strains together span almost 90% of the genetic diversity found in mice (*Mus musculus*). Our second population of genetic diversity included 25 genetically unique, outbred females and 25 males from the DO population. We show that multi-scale cortical bone traits vary significantly with genetic background; heritability values range from 21% to 99%, indicating genetic control of bone traits across length scales. We show for the first time that lacunar shape and number are highly heritable. Comparing the two populations of genetic diversity, we show each DO mouse does not resemble a single Inbred Founder but instead the outbred mice display hybrid phenotypes with the elimination of extreme values. Additionally, intra-bone relationships (e.g., ultimate force vs. cortical area) were mainly conserved in our two populations. Overall, this work supports future use of these genetically diverse populations to discover novel genes contributing to cortical bone traits, especially at the lacunar length scale.

3.2 Introduction

Osteoporosis is a large and growing public health burden affecting over 54 million people in the United States over the age of 50 and substantially contributes to increased fracture risk^{1,159,160}.

Many individuals are pre-disposed to osteoporosis or low BMD due to their genetic background.

Studies of twins and generations of sisters have shown that about 70% of variability in bone density and about 60% of variability in osteoporotic fractures is genetically based^{3,161,162}.

Clinically, osteoporosis is defined using bone mineral density (BMD) from DEXA scans, however many traits in addition to BMD contribute to bone strength and fracture risk such as morphology, mineralization, and stiffness¹⁶³; it is important to understand if these bone traits are also heritable.

Classically, heritability is estimated using twin, adoption, or family clinical study designs^{123,124}.

A review of heritability studies of body mass index using twins from 12 different countries showed high variability between studies and that heritability is sensitive to age, GDP, and economic growth rates showing the importance of considering environmental factors in addition to genetic factors¹²⁵. The Framingham Offspring Study has been tracking multiple generations of nuclear families of European ancestry since 1971, making it a powerful resource for genetic studies. Karasik et al reported heritability of bone microarchitecture as high as 98.3% (tibia cortical area fraction) estimated from bone microarchitecture data collected from an offshoot of the Framingham study participants¹²⁶. With the increase in availability and decrease in cost of whole-genome arrays, heritability estimates from genome-wide association studies (GWAS) have become more standard¹²³. Due to the high homology between mammalian genomes, results from mouse studies can assist in understanding the complicated role of genetics in humans¹²⁴.

Additionally, environmental factors can be controlled in mice and more complex phenotypes can be measured (e.g., bone strength or lacunar morphology). A recent study in mice by Al-

Barghouthi et al. showed that all 55 skeletal phenotypes measured in 12-week-old genetically diverse mice had non-zero heritability¹²². Understanding the genetic basis of cortical bone traits in adult skeletons can allow for the discovery of novel genes or pathways as therapeutic targets for low bone mass⁶.

There remain gaps in the current literature regarding the heritability of bone traits. First, almost 80% of all GWAS participants are of European descent despite only accounting for approximately 16% of the world population¹²⁷. Likewise, the bone data collected in the Framingham Study is only from people European descent¹²⁶, limiting the applicability of results to broader populations. Second, previous mouse studies only investigated a single long bone, primarily the femur¹²⁰⁻¹²². Many bone traits are skeletal site dependent, so heritability of traits may also vary between long bones. Third, measured traits also focused on the whole-bone or tissue length scale, but none have investigated the tissue or cellular length scale. Finally, phenotyping of and heritability measurements for cancellous or cortical bone was previously done using skeletally-developing mice (11-13 week old) or elderly humans (avg 72 years old), leaving a gap to investigate the heritability of traits in the young-adult, skeletally-mature skeleton, i.e. when bone mass is maximized. Bone mass and fracture risk later in life depends on the peak bone mass attained as a young-adult; a 10% increase in peak bone mass reduces fracture risk in older adults by 50%⁵⁸ making it important to study what factors affect the young-adult skeleton.

To facilitate the investigations of the genetic basis of various diseases and phenotypes, The Jackson Laboratory (JAX) generated the Diversity Outbred (DO) mouse population by cross-breeding eight inbred founder strains to produce a population with random assortments of genes modeling the heterozygosity of the human population and the wide range of human diseases^{164,165}. These eight inbred strains consist of three wild-derived strains (CAST/EiJ, PWK/PhJ, and WSB/EiJ) and five classical laboratory strains (A/J, C57BL/6J, 129S1/SvImJ,

NOD/ShiLtJ, and NZO/HILtJ) that together cover almost 90% of the genetic diversity found in the mouse genome and represent the three sub-species of the common house mouse (*Mus musculus domesticus*, *Mus musculus musculus*, and *Mus musculus castaneus*)¹⁶⁶. Over the last decade, use of these genetically diverse populations has increased in the bone field, and these mice have been used to evaluate the heritability and candidate genes regulating cancellous bone microarchitecture in the growing skeleton¹²⁰, the response to hindlimb disuse via casting of one femur¹²¹, and the heritability of femur properties and genes influencing cortical bone accrual in the growing skeleton¹²². These studies provide motivation and rationale to use these populations of genetically diverse mice, both the Inbred Founders and DO, to study the heritability of cortical bone traits.

In this study, we aimed to calculate the heritability of multi-scale cortical bone traits of the three long bones – the radius, tibia, and femur – in skeletally-mature mice. We used two models of genetic diversity with each population containing the same pool of possible alleles. First, a cohort of males and females from the eight Inbred Founder strains used to create the Diversity Outbred (DO) population, and second, a cohort of males and females from the DO population. Comparing the individual inbred strains, we hypothesized that cortical bone traits vary with genetic background and sex. Comparing the Inbred Founder cohort to the DO cohort, we hypothesized the DO cohort has a similar spread and mean per trait as the Inbred Founder cohort. Comparing the correlations between traits within a single animal, we hypothesized that relationships between cortical bone traits are conserved in these two models.

3.3 Methods

3.3.1 Mouse Populations

All mouse work was completed with approval of the Washington University Institutional Care and Use Committee (IACUC). Two mouse populations were used to model genetic diversity: (1) Eight Inbred Founder strains and (2) Diversity Outbred (DO) mice. The eight Inbred Founder strains (CAST/EiJ – JAX stock #000928, PWK/PhJ - #003715, WSB/EiJ - #001145, A/J - #000646, C57BL/6J - #000664, 129S1/SvImJ - #002448, NOD/ShiLtJ - #001976, and NZO/HILtJ - #002105) have been continuously outbred by Jackson Laboratory to create and maintain the Diversity Outbred population (#009376) (Fig 3.2 A). Inbred Founder strains (n = 9/strain/sex) were delivered at 8 wks of age and aged to 22 wks in our animal facilities. Of the N = 144 that arrived, eight were lost (3 NOD and 5 CAST) leaving N = 136 for analysis. DO mice (n = 25/sex, G46 and G47) were delivered between 3 and 5 wks of age and aged to 22 wks in our animal facilities. One female DO mouse died prematurely leaving n = 24 for analysis. Inbred mice were group housed up to 5 in a cage. Male DO mice were housed individually, and female DO mice were housed up to 3 in a cage according to recommendations by JAX to reduce in-fighting. All mice were kept on a 12 hr light-dark schedule with *ad libitum* access to food and water.

3.3.2 Longitudinal Measurements

After one week of acclimation, Inbred Founder strains were monitored for whole body growth. Mouse weights, dual-energy x-ray absorptiometry (DEXA) scans, and fasting blood glucose (FBG) were collected at 9, 12, 15, 18, and 22 wks of age. Briefly, mice were fasted for 6 hrs, weighed, and FBG was measured using a drop of blood from the tail (Glucocard Vital, Arkray Inc) to track glycemic status; hyperglycemia was defined as a level over 250 mg/dL. Mice were then anesthetized with isoflurane (1.5-4%) for 10-15 minutes to ensure full sedation during the

DEXA scan. Whole-body (excluding the head) bone mineral content (BMC) and areal bone mineral density (aBMD) were measured from DEXA (UltraFocus, Faxitron, 4 x 40 kV and 6 x 80 kV scans). At 22 wks old, Inbred Founder mice were euthanized, bones collected for analysis (Table 3.1), and bodies stored frozen at -20°C.

DO mice were evaluated *in vivo* at 22 wks. Briefly, mice were fasted for 6 hrs, weighed, and FBG was measured. The next day mice were anesthetized with isoflurane for DEXA and subsequent tibial microCT (*see Cortical Bone Morphology*). DO mice were subjected to right limb tibial loading (findings in Chapter 4), euthanized at 25 wks age, femora and radii collected for analysis (Table 3.1), and bodies stored frozen at -20°C. Only tibial μ CT from before loading in the DO mice were analyzed in this study. No Inbred Founder mice were loaded.

Table 3.1: Bones evaluated for various outcomes in both the Inbred Founders and Diversity Outbred (DO) mice.

Inbred Founder Bone Outcomes

Bone	Outcome
Left Tibia	XRM
Right Tibia	μ CT (Suppl)
Left Femur	μ CT (Suppl)
Right Femur	Raman
Right Radius	μ CT - 3pt bend

Diversity Outbred Bone Outcomes

Bone	Outcome
Right Tibia	μ CT (Suppl)
Left Femur	μ CT (Suppl)
Right Radius	μ CT - 3pt bend

3.3.3 Cortical Bone Morphology

The right tibia was microCT scanned (vivaCT 40, Scanco Medical, Switzerland - 70kVP, 8W, 300ms integration time) at 10.5 μ m/pixel resolution either *ex vivo* (Inbred Founders) or *in vivo*

(DO mice). A 1.05 mm long region (100 slices) centered 5 mm proximal to the distal tibiofibular junction (TFJ) was analyzed.

The entire right radius was microCT scanned (μ CT50, Scanco Medical, Switzerland-70kVP, 4W, 700ms integration time) at 7.4 μ m/pixel resolution *ex vivo*. A 1.48 mm long region (200 slices) centered at the radius midpoint was analyzed.

The left femur was microCT scanned (μ CT50, 70kVP, 4W, 700ms integration time) at 7.4 μ m/pixel resolution *ex vivo*. A 1.11 mm long region (150 slices) centered at the femur midpoint was analyzed.

All bones were analyzed following published guidelines¹⁶⁷ for total area (Tt.Ar), bone area (Ct.Ar), medullary area (Ma.Ar), cortical thickness (Ct.Th), polar moment of inertia (pMOI), and tissue mineral density (TMD).

3.3.4 Mechanical Testing

The right radius was cleaned of all tissue and stored at -20°C in PBS-soaked gauze until testing.

The radius was selected for mechanical testing because its relatively long, slender shape allows for more accurate estimation of material properties than the femur¹⁵⁵. On the day of testing, samples were brought to room temperature and kept hydrated in PBS. Bones were tested in three-point bending with a bottom span of 7 mm and the top point aligned with the bone center and held in place with a -0.1 N pre-load. Bones were pre-conditioned for 5 cycles at an amplitude of -0.4 N at 1Hz then loaded monotonically to failure at 0.1 mm/s. Force-displacement curves were analyzed for stiffness (K), ultimate force (F_u), yield force (F_y), post-yield displacement (PYD), and work-to-fracture (Wfx). Material properties (ultimate stress (S_u), yield stress (S_y), Young's elastic modulus (E)) were estimated using engineering beam theory¹⁶⁸.

3.3.5 Osteocyte Lacunar Morphology

Osteocyte lacunar morphology was quantified in the Inbred Founder population only. The left tibiae of Inbred Founders were dissected and fixed in 4% PFA overnight, then rinsed and stored in PBS until use. Bones were cut transversely 5 mm proximal to the TFJ using an Isomet saw, and the distal portion was scanned on an X-ray microscope (XRM, Xradia Versa 520, Zeiss) 4 mm proximal to the TFJ. A pre-scan, using the 4x objective, was acquired to locate the high-resolution scan region of interest, centered halfway between endocortical and periosteal surfaces at the postero-lateral apex (Suppl. Fig 3.15 A). Scanning parameters for the high-resolution scan were: 40 kV, 3 W, 1601 projections, 20x objective, bin = 2, 4800-5000 projection intensity (7-8 sec exposure), yielding a nominal resolution of 0.54 $\mu\text{m}/\text{voxel}$. Bones were segmented, filtered, and analyzed using custom scripts in Dragonfly (version 4.1, Object Research Systems, Montreal, Canada) for total lacunar volume, total vessel volume, and individual lacunar properties (volume, aspect ratio, phi, and sphericity), as described¹⁶⁹.

3.3.6 Raman Spectroscopy

Bone matrix composition was quantified in cortical bone from the Inbred Founder population only. The right femurs of Inbred Founders were dehydrated in ethanol and embedded in poly methyl methacrylate (PMMA) (Thermo Scientific AAA130300F, Thermo Fisher Scientific). Plastic blocks were cut at the midpoint perpendicular to the bone long-axis and trimmed to 5 mm in length. Blocks were polished using an Allied TechPrep polisher to 0.05 μm (600 grit silicon carbide sandpaper, 1200 grit silicon carbide sandpaper, 1 μm aluminum oxide, 0.05 μm aluminum oxide) on Rayon felt pads (Allied). Measurements were taken on the anterior side of the femur in lamellar bone excluding the periosteal and endocortical surfaces (Supp. Fig 3.8). Measurements were taken in a grid of 3 spots wide spanning the cortical width (5-9 spots long) spaced 20 μm apart. Data was collected using a red laser (785 nm wavelength) on a Renishaw

in Via confocal microscopy system (Renishaw, Wotton-under-Edge, Gloucestershire, UK). Each point was collected with 10 accumulations with a 6 second exposure time and post-processed using WiRE 4.1 software (baseline subtraction with 11th order polynomial fit, cosmic ray removal, spectra normalization). A single measurement of the PMMA for each sample was used for baseline subtraction. All data was analyzed in a custom MATLAB code to quantify area ratios of mineral:matrix (v2 phosphate: amide III, v1 phosphate:proline), carbonate:phosphate (v1 carbonate: v1 phosphate), and crystallinity (inverse of full-width at half-maximum of v1 phosphate)¹⁷⁰⁻¹⁷².

3.3.7 Correlation Matrix

A matrix of Pearson's correlation coefficients was computed using R (v4.0.2) on three separate datasets: 1) all lacunar traits in the Inbred Founders, 2) radial and whole-body traits in the Inbred Founders, and 3) radial and whole-body traits in the DO mice. Correlations were calculated using the *cor* function and visualized using the *corrplot* function. For the lacunar traits, variables were unbiasedly hierarchically clustered into three groups using the *ward.D2* algorithm. For the radial traits, variables were ordered by measurement technique consistently for each mouse population (Inbred Founders and DO).

3.3.8 Principal Component Analysis (PCA)

Principal component analysis (PCA) was performed using R on two datasets from the Inbred Founder population: 1) radial and whole-body traits (15 traits), and 2) lacunar traits (10 traits). Each trait was centered and scaled within the *prcomp* function to have a mean of 0 and standard deviation of 1. The contribution of each trait to each principal component (PC) was extracted from the PCA. To compare the Inbred Founders and DO population for dataset 1 (radial and whole-body traits), each DO animal was plotted onto the PCA space defined by the Inbred Founders. Briefly, the value for each DO trait was centered and scaled and linearly combined

according to PC weightings per variable from the Inbred Founder PCA. For visualization of the Inbred Founders, data points were grouped by mouse strain and encompassed by a normal data ellipse spanning one standard deviation (68%).

3.3.9 Heritability Calculations

Broad-sense heritability (H^2) was calculated for all traits measured in the Inbred Founder mice as the proportion of variance due to genetic differences according to Moran et al.¹⁷³. Heritability was calculated as $H^2 = \sigma^2_{\text{strain}} / (\sigma^2_{\text{strain}} + \sigma^2_{\text{sex}} + \sigma^2_{\text{res}})$ where σ^2_{strain} is the between-strain variance, σ^2_{sex} is the between-sex variance, and σ^2_{res} is the residual variance (equation on Table 3.2). Variances were calculated from the sum of squares from a 2-factor analysis of variance (ANOVA) with strain and sex and the two factors. Specifically, $\sigma^2_{\text{strain}} = SS_{\text{strain}} / n_{\text{avg}}$ (n_{avg} = average group size), $\sigma^2_{\text{sex}} = SS_{\text{sex}} / df_{\text{sex}}$, and $\sigma^2_{\text{res}} = SS_{\text{res}} / df_{\text{res}}$.

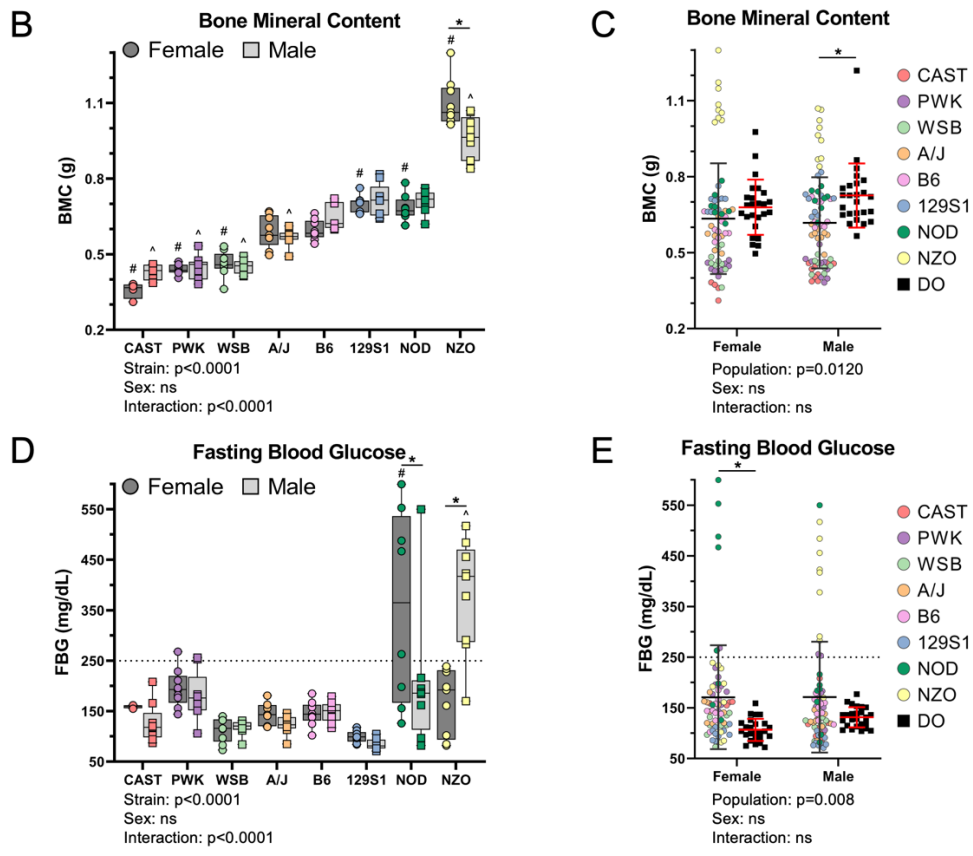
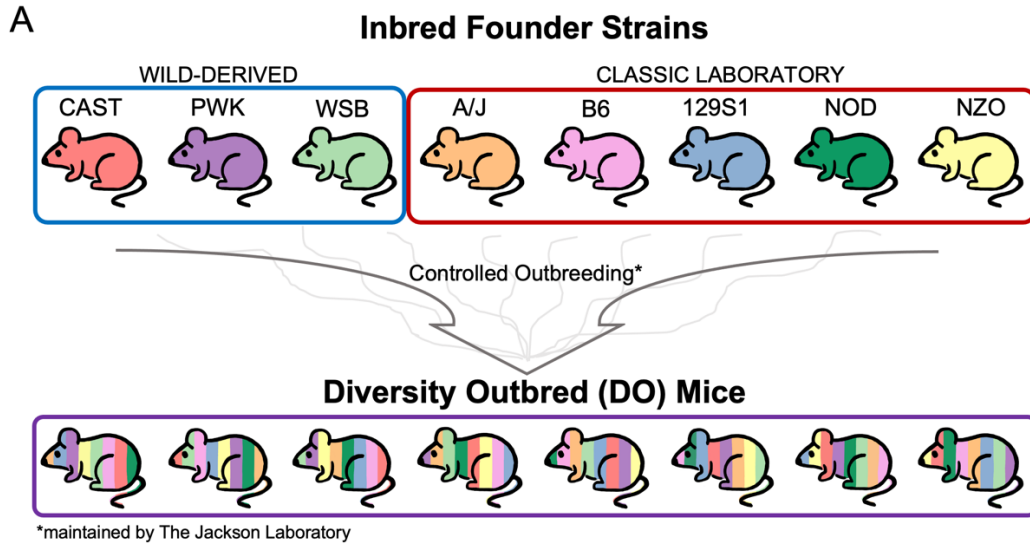
3.3.10 Statistical Analysis

Statistical analysis was done in GraphPad Prism (v9). First, outcomes from the eight Inbred Founders were analyzed using a 2-factor ANOVA with mouse strain and sex as the two factors. Second, outcome from the Inbred Founder population (all eight strains pooled) and the DO population were compared using a 2-factor ANOVA with population and sex as the two factors. Post-hoc tests were run with Sidak correction. Significance was set at $p < 0.05$. Body mass was evaluated as a co-variate using a full factorial general linear model in SPSS (IBM, Armonk, NY). Body mass adjusted values per animals were calculated according to guidelines in Jepsen et al¹⁶⁸ using the following equation $Trait_{\text{adjusted}} = Trait_{\text{unadjusted}} - slope * (body\ mass - mean\ body\ mass)$. Slopes were determined from a linear regression of each trait with body mass within each strain group (8 groups). To ensure statistically meaningful relationships, for any regression with a $p > 0.20$ the slope was set to 0 for that strain. The mean body mass was calculated as the mean of the means of each strain group (mean of 8 means).

3.4 Results

3.4.1 Young-adult mice from the Inbred Founder and Diversity Outbred populations span a large range of body size and bone mass

At the whole-body length scale, DEXA was used to assess skeletal mass. The eight Inbred Founder strains were skeletally mature by 22 wks; the average increase in BMC between 18 and 22 wks is less than 4% of final BMC (0.2% - 7.7%) (Supp Fig 3.9 A). At 22 wks, BMC of the Inbred Founders varied significantly between strains, with a 3-fold difference between CAST females and NZO females (Fig 3.2 B). (Note that Inbred Founder strains are ordered from smallest to largest BMC along the x-axis; this order is maintained for all graphs in this thesis.) The main effect of sex on BMC was not significant, although there was a significant strain-sex interaction, driven by a greater BMC in NZO females than males (Fig 3.2 B). The DO population had significantly higher BMC than the Inbred Founder population with a narrower range of values and higher minimum values (Fig 3.2 C). This result was more pronounced in the males. Similar trends across strains and between the two populations were seen with body weight (Supp Fig 3.9 D,E). About 12% of the Inbred Founders were hyperglycemic by 22 wks (Fig 3.2 D). NZO males became hyperglycemic between 12 and 15 wks of age (Supp Fig 3.9 B), which coincided with a halt in an increase in their BMC and weight (Supp Fig 3.9 A,C). NOD females became hyperglycemic between 18 and 22 wks of age (Supp Fig 3.9 B), which coincided with a loss in their weight (Supp Fig 3.9 C). In contrast, none of the DO mice were hyperglycemic at 22 wks (Fig 3.2 E).



* : $p < 0.05$ for comparison line
: F strain vs F B6 $p < 0.05$
^ : M strain vs M B6 $p < 0.05$

Figure 3.2: Overview of the two genetic mouse models and whole-body traits. A) Two mouse models of genetic diversity were used, eight inbred mouse strains and an outbred stock. The inbred strains were the founders used by The Jackson Laboratory to create the diversity outbred (DO) population. After controlled outbreeding of the founder lines, each DO mouse is genetically unique. Phenotyping was performed on 5 mo-old females and males of the eight Inbred Founder strains and DO mice from generations 46 and 47. B) Whole-body bone mineral content of the Inbred Founders shows a 3-fold difference in BMC between the largest (NZO F) and smallest (CAST F) mice. Strains on the x-axis are ordered from smallest to largest BMC. This order is maintained for all graphs in the study. C) The DO mice have a larger average BMC

*with less variation than the pooled Inbred Founder population. D) Fasting blood glucose shows that about 12% of the Inbred Founder mice become hyperglycemic (FBG > 250mg/dL), mostly NOD F and NZO M. E) All DO mice have FBG levels in the healthy range. * $p < 0.05$ for comparison line; # $p < 0.05$, F strain vs F B6; ^ $p < 0.05$, M strain vs M B6*

3.4.2 Cortical morphology of three different long bones varies with mouse strain and sex

Whole-bone morphology, assessed using μ CT, varied significantly between Inbred Founder strains in a sex-dependent manner (Fig 3.3 and Supp Fig 3.10). Radial bone area (Fig 3.3 A) spanned a 1.7-fold difference between smallest (PWK females) and largest (NZO males), while medullary area (Fig 3.3 B) spanned a 3.9-fold difference between smallest (WSB females) and largest (NZO males). Bone area was positively correlated with skeletal mass and body weight ($r=0.85$ and 0.75 respectively, Fig 3.5 A). While all strains contributed to these overall trends, WSB mice had larger bones and NOD mice had smaller bones than strains of similar BMC (Fig 3.3 A). Compared to the Inbred Founders, the DO population on average had significantly larger bones with a similar medullary area (Fig 3.3 D,E). Analysis of morphology from tibias (Supp Fig 3.12) and femurs (Supp Fig 3.13) showed similar population spreads and differences between mouse strains as observed for the radius, indicating consistency between long bones. Radius tissue mineral density also varied significantly between Inbred Founder strains, although there was no main sex effect or sex-strain interaction (Fig 3.3 C). The DO males, on average, had a lower TMD than Inbred Founder males, but no difference was observed between females (Fig 3.3 F). Similar results were seen in the femoral TMD (Supp Fig 3.13 K). However, in the tibia, the DO population had higher TMD as compared to the Inbred Founders, especially in females (Supp Fig 3.12 K). In summary, cortical morphology varied widely between Inbred Founder strains with outbred animals (DO) having larger bones on average.

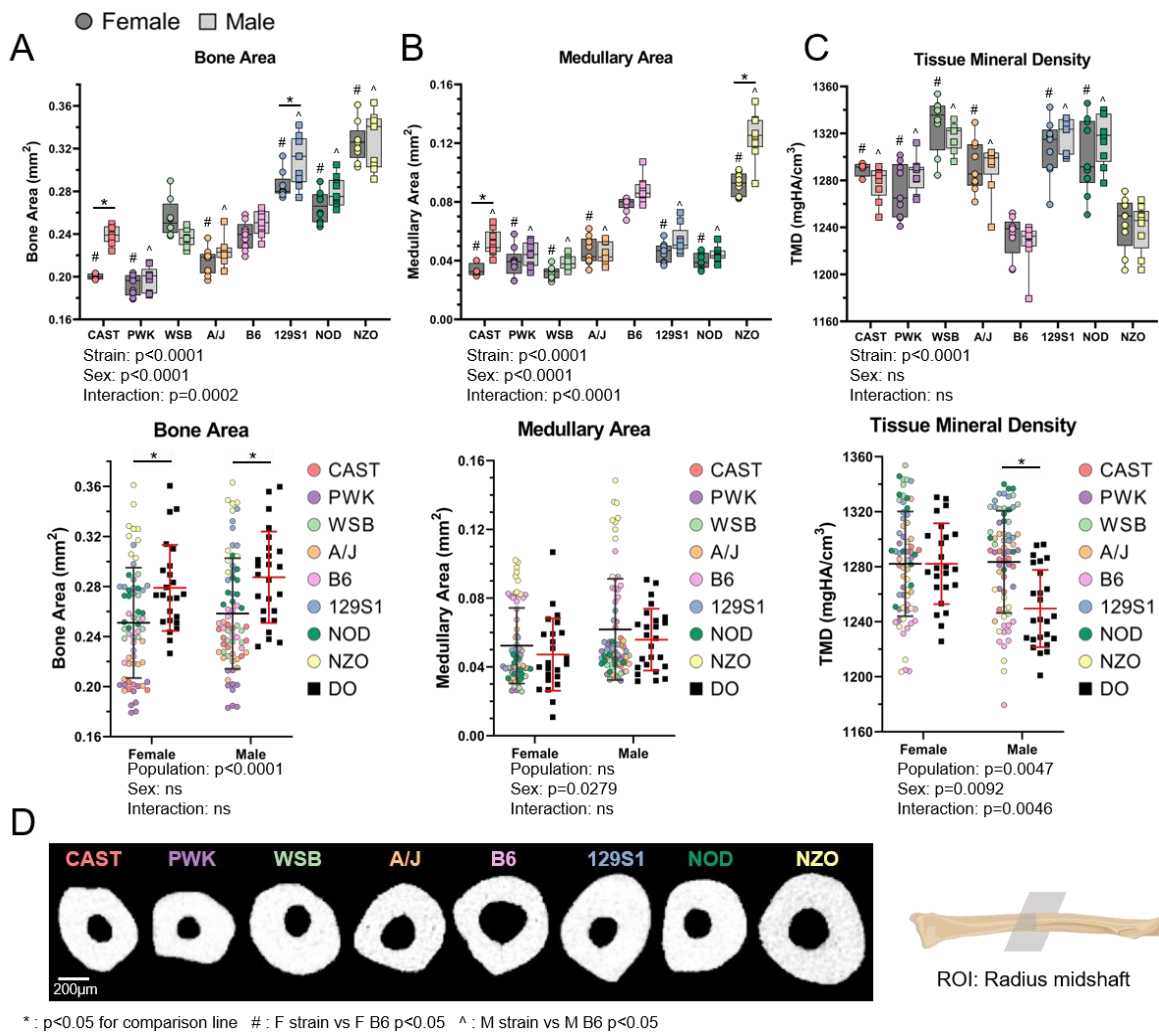
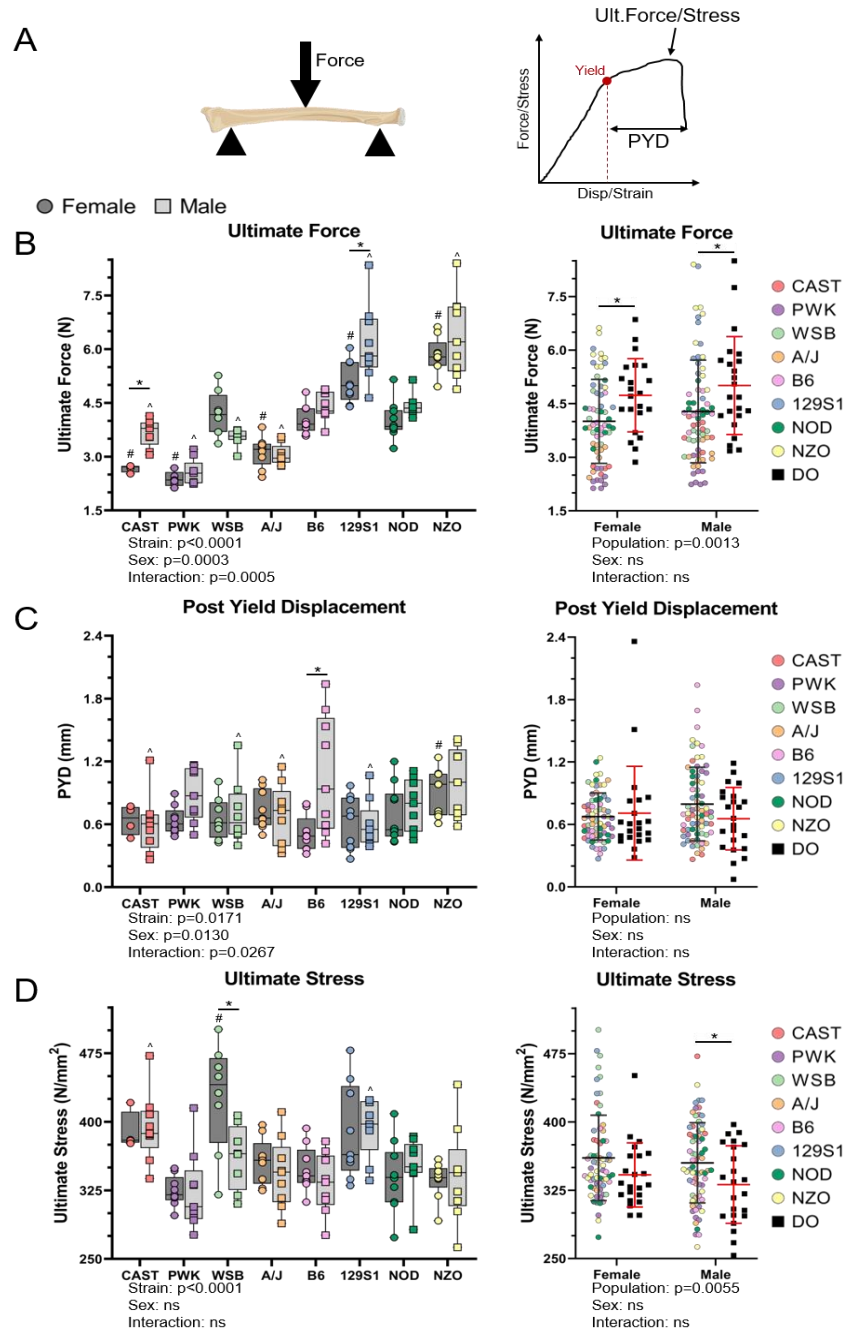


Figure 3.3: Radial morphology changes with strain in a sex dependent manner. A) Bone area and B) medullary area of Inbred Founder mice have significant strain, sex, and strain-sex interaction terms (ANOVA). C) Tissue mineral density shows significant strain differences in the Inbred Founder mice. D) The DO population has higher bone area than the pooled Inbred Founder population, but no difference in E) medullary area. F) The male DO population has lower TMD than the male Inbred Founders. This difference is not seen in females. G) Representative cross-sections at the radius mid-diaphysis show the variation in bone shape and size between the eight Inbred Founder strains (females). * $p < 0.05$ for comparison line; # $p < 0.05$, F strain vs F B6; ^ $p < 0.05$, M strain vs M B6

3.4.3 Cortical bone mechanical properties vary with mouse strain and sex, but material properties only vary with mouse strain

The radius was tested in three-point bending to determine whole-bone mechanical and estimated material properties (Fig 3.4 A). Only the radius was selected for testing since it closely fits the assumptions of beam theory, allowing for accurate estimation of material properties¹⁵⁵. In the Inbred Founder population, all mechanical properties varied between strains with significant strain, sex, and strain-sex interaction effects (Fig 3.4 B,D and Supp Fig 3.11 A-C). Ultimate

force, a measurement of whole-bone strength, spanned a 2.7-fold difference between the weakest strain (PWK females) and the strongest (NZO males) (Fig 3.4 B). Mouse strain accounted for about 80% of the total variation in ultimate force (ANOVA). Compared to the Inbred Founders, the DO population had stronger bones on average, and no DO mice had bones as weak as any of the weakest Inbred Founders (PWK) (Fig 3.4 C). Post-yield displacement (PYD), a measurement of ductility, varied only modestly with strain (Fig 3.4 D) and did not correlate strongly with BMC ($r=0.24$, Fig 3.5 A). The radius from B6 females were the least ductile and those from B6 males the most. PYD was highly variable within each strain/sex group and mouse strain only accounted for about 11% of the total variation. The PYD in the DO population did not differ from the PYD in the Inbred Founder population (Fig 3.4 E). All estimated material properties varied between Inbred Founder strains but did not differ between sexes. Ultimate stress had a 1.3-fold difference between PWK males (lowest) and WSB females (highest) (Fig 3.4 F). The DO population had slightly lower ultimate stress than the Inbred Founder population (Fig 3.4 G), which is also true of other material properties (Supp Fig 3.11 I,J). In summary, radial bone mechanical and material properties vary between the Inbred Founder strains, with the outbred mice (DO) having average higher mechanical but lower material properties than the average Inbred Founder.



*: $p < 0.05$ for comparison line # : F strain vs F B6 $p < 0.05$ ^ : M strain vs M B6 $p < 0.05$

Figure 3.4: Radius mechanical and material properties vary between inbred mouse strains.

A) The radius was tested using three-point bending to determine mechanical properties. Beam theory equations were used to estimate material properties. B) Ultimate force varies between Inbred Founder strains with significant strain, sex, and strain-sex interaction. C) The DO population has stronger bones (higher ultimate force) than the pooled Inbred Founder population. D) Post-yield displacement (a measure of ductility) also had significant strain, sex, and strain-sex interactions. E) The ductility of DO population is not significantly different from the Inbred Founders. F) Ultimate stress and other material properties varied with mouse strain with no significant sex differences. G) The DO population has lower material properties, such as ultimate stress, than the Inbred Founder population. * $p < 0.05$ for comparison line; # $p < 0.05$, F strain vs F B6; ^ $p < 0.05$, M strain vs M B6

3.4.4 Within-bone correlations are similar in both mouse populations, but stronger in the Inbred Founder population

Results from Chapter 2 showed that cortical bone traits are highly correlated within a single bone (femur or radius) in an Advanced Intercross mouse population (LGXSM). Here, we investigated the relationship between traits by calculating the Pearson's correlation coefficient for 15 whole-body and radial trait pairs in the Inbred Founder and DO populations (Fig 3.5). In the Inbred Founders, bone size traits (bone area, total area, medullary area, and pMOI) were all highly correlated with each other (Fig 3.5 A). Cortical thickness was only moderately correlated with other morphology parameters. Bone size traits were highly correlated with whole-bone mechanical properties (with exception of PYD) as well whole-body measurements (bone length, weight, BMC). Mechanical properties (except PYD) were also correlated with whole-body measurements. Bone material properties correlated with each other, but did not correlate with bone size parameters, which is expected because material properties are already normalized for bone size. Tissue mineral density had few strong correlations but was moderately correlated with cortical thickness ($r = 0.61$) and medullary area ($r = -0.68$). Bones with high tissue mineral density tend to have a thick cortex and a small medullary cavity.

Compared to the Inbred Founders, the DO population showed similar correlations between traits, but the magnitudes were generally weaker. In particular, correlations with body weight and length were much lower in DO mice (Fig 3.5 B). The correlation coefficient between total area and BMC was lower by 0.23 (0.88 in Founders vs 0.65 in the DO), while the correlation between total area and weight was lower by 0.54 (0.84 in the Founder vs 0.30 in the DO). Additionally, the direction (negative or positive) of many correlations with bone length were opposite in the two populations. The relationship between ultimate force and bone area was highly, positively

correlated ($r=0.95$ in Inbred Founders and 0.88 in DO) and extremely conserved in the two populations, sharing the same slope and intercept (Supp Fig 3.16).

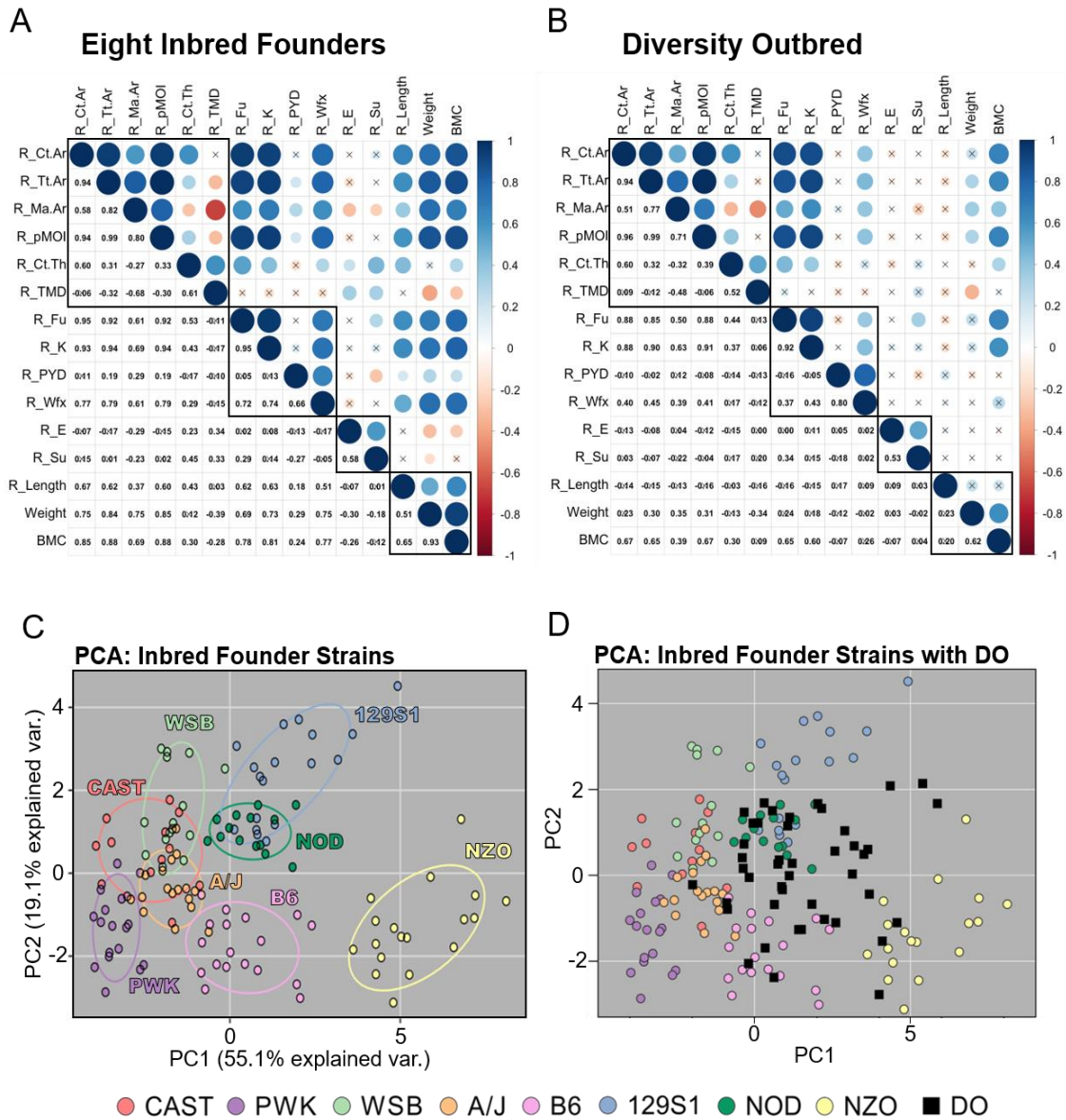


Figure 3.5: Within-bone correlations are maintained in outbred mice. Inbred mice cluster via mouse strain. A) Matrix of Pearson's correlations between traits measured in the radius in the eight Inbred Founder strains (A) and the Diversity Outbred mice (B). Black boxes separate different types of outcomes (morphology, mechanical properties, material properties, whole skeleton size). Similar correlations are seen between the two populations, but are generally weaker in the DO population. For A) and B) an X indicates a non-significant correlation ($p > 0.05$) C) PCA analysis showing how the Inbred Founders cluster by strain. D) The DO mice mapped onto the PCA space defined by the Inbred Founders; the DO population lays in a subset, hybrid space eliminating extreme values at the periphery of the PCA space. Ct.Ar: Cortical Area, Tr.Ar: Total Area, Ma.Ar: Medullary Area, Ct.Th: Cortical Thickness, TMD: Tissue Mineral Density, Fu: Ultimate Force, K: Stiffness, PYD: Post-yield displacement, Wfx: Work to fracture, E: Young's Elastic Modulus, Su: Ultimate Stress, BMC: Bone Mineral Content

3.4.5 Inbred Founder strains separate using PCA while Diversity Outbred mice overlap many individual strains and occupy gaps between strains

PCA was done to evaluate within and between strain differences based on multiple (15) traits from the radius of the Inbred Founders (Fig 3.5 C). The first two principal components (PC) explained almost 75% of the population variance, and mice strongly clustered by strain. Mouse and bone size and strength parameters (BMC, weight, Ct.Ar, Tt.Ar, pMOI, F_u , K) were the main contributors to PC1. Bone thickness and material properties (Ct.Th, TMC, S_u , E) were the main contributors to PC2 (Supp Fig 3.14 C). NZO was separate from all other strains, while B6 was mostly separate (small overlap with A/J only). 129S1 and NOD showed moderate overlap. The wild-derived strains showed moderate overlap with each other (CAST overlaps WSB and PWK), and with A/J. When the DO mice were mapped onto the PCA space defined by the Inbred Founders, they occupy a smaller, central region of the PCA space, eliminating extreme values at the periphery (Fig 3.5 D). Additionally, many DO mice filled the empty space between the NZO and 129S1 clusters indicating that individual DO mice have a unique combination of bone traits and do not necessarily phenotypically mimic a single Inbred Founder mouse.

3.4.6 Lacunar morphology varies between Inbred Founder strains

Osteocyte lacunar morphology was analyzed in the tibia of Inbred Founder mice using high-resolution XRM (Fig 3.6 and Supp Fig 3.15). Over 4,000 lacunae were individually analyzed per sample. Total lacunar number density (Lc.Num/TV) varied significantly between strains in a sex-dependent manner ranging from 53,189/mm³ in B6 females to 80,200/mm³ in 129S1 females (Fig 3.6 B). The total volume of lacunae only occupied 1-2% of the total bone volume (cortical bone tissue including pores), but varied significantly between Inbred Founders (Fig 3.6 C). Quantifying approximately 4,000 lacuna per mouse, the median lacunar volume also varied with mouse strain in a sex-dependent manner (Fig 3.6 D). Lacunar porosity (Lc.Vol/TV) highly,

positively correlated to median lacunar volume ($r = 0.65$), and moderately correlated with lacunar number density ($r = 0.49$), indicating that the total lacunar volume is increased mainly by increasing the volume of each lacuna rather than the number of lacunae (Fig 3.6 G).

Lacunae are ellipsoidal in shape, with the long-axis being parallel to the direction of loading¹⁷⁴, therefore we quantified the lacunar elongation and orientation in the Inbred Founders. Median lacunar aspect ratio, a measure of elongation, also varied significantly with mouse strain (Fig 3.6 E). In addition, we evaluated uniformity of the primary axis of the lacunae within each bone. For each lacuna, the angle of the lacunar long axis off the z-axis (ϕ) was calculated. We compared the SD of ϕ between mice, due to variation in bone placement in the XRM. Smaller SD of ϕ values represents greater uniformity of the primary axis of the population of osteocyte lacunae. The uniformity of alignment varied significantly with mouse strain (Fig 3.6 F). The lacunar elongation (aspect ratio) and uniformity of alignment (SD of ϕ) are positively correlated with each other and lacunar number density (Fig 3.6 G), indicating that in bones where lacunae are more densely packed, the lacuna tend to be more elongated and more aligned with each other. The lacunar traits that cluster together also contributed similarly to explain the population variance (Fig 3.6 H). In summary, all osteocyte lacunar morphology traits are dependent upon mouse strain.

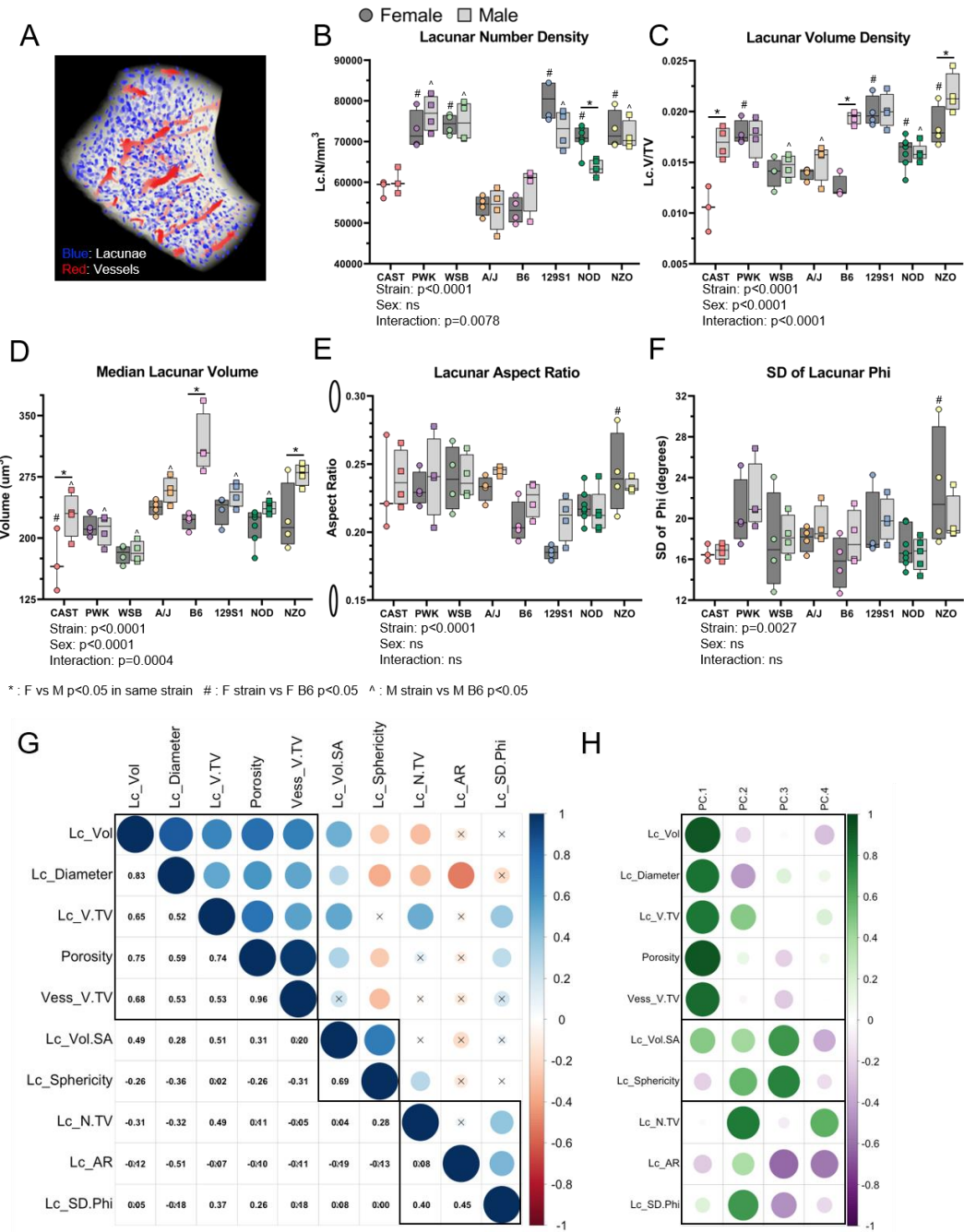
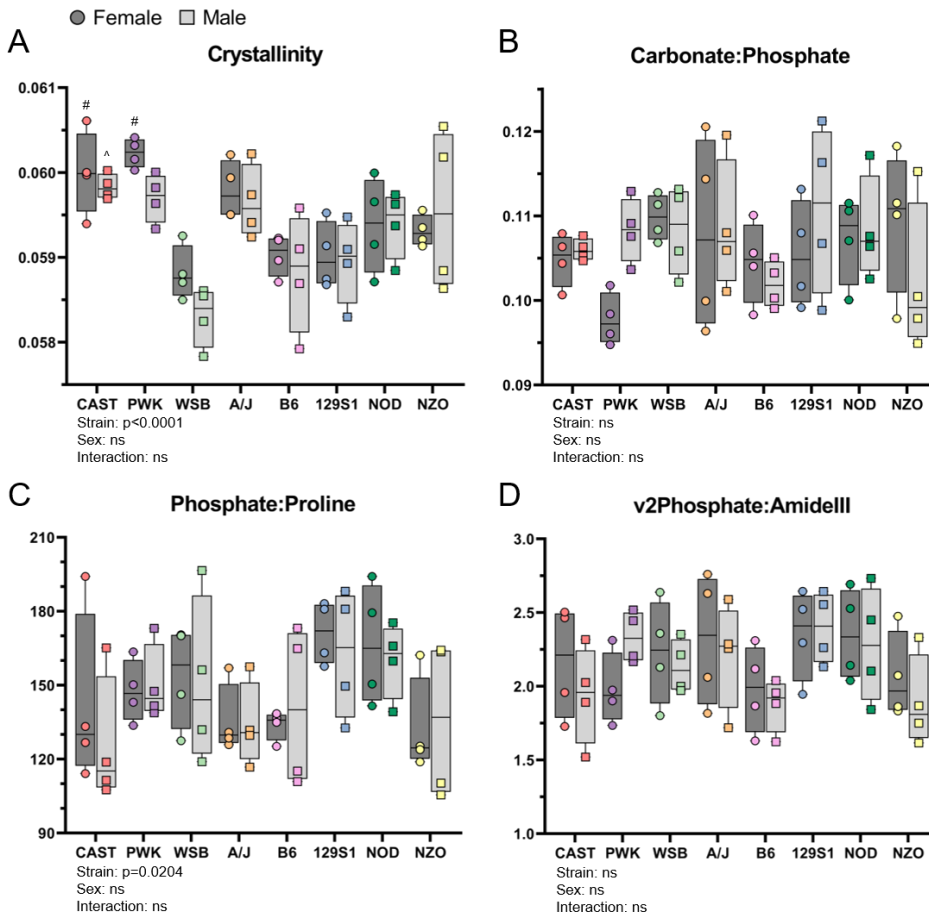


Figure 3.6: Lacunar morphology was visualized using x-ray microscopy (XRM). A) Lacunae were imaged using x-ray microscopy (XRM). Representative cross-section of the field of view (FOV) imaged. Intracortical pores were defined as lacunae (blue) or vasculature (red) based on size and shape. B) Lacunar number density had significant strain and strain-sex interaction effects. NOD have a significant sexual dimorphism. C) Lacunar volume density has significant strain, sex, and strain-sex interaction effects with significant sex differences in CAST, B6, and NZO mice. D) The median lacunar volume for each sample was determined based on all lacunae in the FOV. Lacunar volume varied significantly with strain and sex, with a strain-sex interaction. B6 M have 1.8 times larger lacunae than CAST F. E) The aspect ratio of each lacuna in the FOV was analyzed as a measure of elongation. An aspect ratio of 0 corresponds to a straight line while 1 is a perfect circle. Ellipses along the y-axis represent aspect ratios of 0.15 and 0.30. Lacunar aspect ratio varies with mouse strain. 129S1 F have a 1.3 times lower aspect ratio (i.e., more elongated) than AJ M. F) Phi (angle from z-axis) was calculated for each lacuna. The standard deviation (SD) of phi represents how uniformly aligned the lacunae are, with a smaller value being more aligned. The uniformity in alignment varies with mouse strain. NZO F have a 1.5 times larger SD of phi than B6 F. G) Pearson's correlation matrix of all the lacunar traits measured in the Inbred Founder population. Black boxes group traits that cluster using hierarchical clustering. H) Contributions of each lacunar trait to the first four principal components of a PCA analysis.

*Traits that correlate highly contribute similarly to explain the variance in the population. * $p < 0.05$, F vs M in same strain; # $p < 0.05$, F strain vs F B6; ^ $p < 0.05$, M strain vs M B6 $p < 0.05$*

3.4.7 Mineral composition minimally varies between Inbred Founder mice

Bone composition was analyzed using Raman spectroscopy on the transverse cross-section of the femur midsection (Supp Fig 3.8). Crystallinity, a measure affected by mineral length and organization, varied significantly between mouse strains (Fig 3.7 A). The carbonate:phosphate ratio, which varies with architecture, age, and crystallinity^{171,175}, did not significantly vary between mouse strains (Fig 3.7 B). One measurement of mineral:matrix (phosphate:proline) also varied significantly between mouse strains (Fig 3.7 C). However, when mineral:matrix was measured using phosphate:amideIII, there was no significant variation (Fig 3.7 D). In summary, the crystalline structure of the mineral varies modestly between Inbred Founders strains, but bone composition is mainly conserved.



: F strain vs F B6 p<0.05 ^ : M strain vs M B6 p<0.05

Figure 3.7: Raman spectroscopy was used to evaluate bone mineral composition. A) Crystallinity and C) Phosphate:Proline ratio vary significantly between strains. B) Carbonate:Phosphate ratio and D) vsPhosphate:amidellIII ratio are not significantly different between strains.

3.4.8 Multi-scale cortical bone traits are moderately to highly heritable in the Inbred Founder population

Broad-sense heritability was calculated for traits measured in the Inbred Founder strains using variance calculated from the two-factor ANOVA (Table 3.2). BMC had the highest heritability of 99.3% ($H^2 = 0.993$) indicating almost all the variance in the population is attributed to genetic differences. In general, lacunar traits had lower heritability, but a few lacunar traits had very high levels of heritability, such as lacunar number density ($H^2 = 0.966$). Heritability values were also similar between long bones. For the radius, femur, and tibia, cortical thickness and cortical area were the most heritable morphology traits. The rank order of μ CT morphology traits in the femur and tibia are identical, with the femur always having a slightly higher value. Overall, of the 43

whole-body, whole-bone (radius, tibia, and femur), tissue, and lacunar traits, 35 (~80%) had a heritability above 60% which is similar or greater than the reported heritability of BMD in humans^{3,161,162}.

Table 3.2: Broad sense heritability was calculated using data for the Inbred Founders for each trait as the fraction of total variation due to strain using the equation shown.

Trait	Heritability (H ²)	Trait	Heritability (H ²)
BMC	0.993	Lc.AspectRatio	0.755
Cortical Thickness	0.985	Ult. Stress	0.746
TMD	0.967	Work-to-Fx	0.741
Lc.No Density	0.966	Phos:Amidelll	0.741
FBG	0.910	Medullary Area	0.722
Lc.Sphericity	0.887	Yield Force	0.718
Cortical Area	0.884	Yield Stress	0.717
Crystallinity	0.844	Porosity	0.689
Weight	0.840	Modulus (E)	0.684
Ult. Force	0.836	Lc.Diameter	0.634
Lc.SD.Phi	0.835	Carb:Phos	0.574
V.Vol Density	0.827	Lc.Vol/SA	0.535
Phos:Proline	0.806	Lc.Vol Density	0.516
pMOI	0.799	Lc.Vol	0.383
Total Area	0.799	PYD	0.209
Stiffness (K)	0.776		

Whole Body

Whole Bone

Tissue Level

Cellular Level

$$\sigma_{strain}^2 = \frac{SS_{strain}}{n}$$

$$\sigma_{sex}^2 = \frac{SS_{sex}}{df_{sex}}$$

$$\sigma_{res}^2 = \frac{SS_{res}}{df_{res}}$$

$$H_{broad}^2 = \frac{\sigma_{strain}^2}{\sigma_{strain}^2 + \sigma_{sex}^2 + \sigma_{res}^2}$$

3.4.9 Whole-body mass significantly contributes to trait differences, but variation due to mouse strain remains significant

Many of the bone traits we analyzed correlated with body weight (Fig 3.5 A). There data were re-analyzed using an ANCOVA with body mass as a covariate to test if the effects of mouse strain remained after accounting for body mass. While body mass was a significant covariate for 22 out of 42 traits measured, the significant effect due to strain was maintained for 39/40 (98%) traits that were significant before body mass adjustment (Supp Table 3.3). PYD was the only trait that lost significance for strain after adjusting for body mass, but the significance of the strain-sex interaction was maintained. Notably, all lacunar level traits did not have weight as a significant covariate. To evaluate the effect of body weight on the separation of strains in the PCA, the PCA was re-run with body-weight adjusted traits. After adjustment, Inbred Founders

still separated by strain with even more distinct clustering for PWK and CAST strains when compared to the PCA using unadjusted values (Supp Fig 3.14 B). After body mass adjustment, CAST radii more closely resemble radii of much larger mice (129S1) than from mice of similar size (PWK). NZO and B6 still fully separate from the other inbred strains. Additionally, how traits contribute to each principal component mainly remains the same after body-weight adjustment (Supp Fig 3.14 C,D). Heritability was also recalculated after body weight adjustment. The heritability of all traits except BMC, lacunar sphericity, and tibial cortical thickness increased or stayed the same after adjustment (Supp Table 3.4 and Supp Table 3.5). The lowest heritability value after body mass adjustment was 77.4% (phosphate:amideIII ratio). Therefore, while weight is an important factor when considering differences in skeletal traits between animals, the differences between mouse strains does not exclusively depend on mouse size (body mass).

3.5 Discussion

Using two mouse models of genetic diversity we show that all measured cortical bone traits, from the whole-body to the osteocyte-lacunar length scale, vary with genetic background and are heritable. In the radius, whole-bone traits (morphology and mechanical properties) vary with both mouse strain (genetic background) and sex. Tissue level traits (tissue mineral density, material properties, and bone composition) vary with genetic background but not sex.

Differences between inbred mouse strains for single traits are bone dependent (i.e., may be different between femur, radius, and tibia). Comparing the two populations, the Diversity Outbred (DO) mice are on average larger and protected from hyperglycemia. The DO population also has larger, stronger bones, but also has bone-dependent differences in tissue level properties. When all whole-body and radial traits are evaluated together, the DO population occupies a

subset of the principal component space defined by the Inbred Founders although many DO mice do not resemble a single inbred strain, implying that complex gene interactions determine skeletal traits. Overall, genetic background significantly contributes to cortical bone phenotype, which indicates genetic control of bone traits across length scales.

We posed three hypotheses, which were tested using the two populations of genetically diverse animals. Our data support the first hypothesis that cortical bone traits vary with genetic background, consistent with a previous report that compared inbred mice¹⁷⁶. Of the 43 traits we measured in the Inbred Founder strains, only two (carbonate:phosphate and phosphate:amideIII ratios) did not have strain as a significant factor. Additionally, broad-sense heritability, which represents the proportion of variability due to genetic difference, was greater than 20% for all traits, and after adjusting for body size heritability was greater than 77% for all traits. These values are higher than those reported by Al-Barghouthi et al¹²², who determined heritability values in DO mice as low as 12% after covariate adjustment. The mice used in that study were 12-weeks old, so there could be more non-genetic variation due to different rates of skeletal growth in mice that were not yet skeletally mature. Furthermore, in the current study heritability was calculated using data from the eight Inbred Founder strains, where each group has genetically identical replicates reducing the intra-strain variation. The greatest variation we found between strains was for morphology and mechanical properties (e.g. cortical area and ultimate force). These traits tend to have higher heritability values, larger fold-differences between high and low groups, and contribute to the first principal component (PC1) of the PCA, which explains 55% of population variation. This same trend was reported in Al-Barghouthi et al., where morphology traits had the highest heritability values¹²². In contrast, we observed that the tissue-level properties (e.g. ultimate stress, TMD, and mineral:matrix) tend to have less

variability between strains and more variability within a strain. These traits have lower fold-differences and mainly contribute to PC2, which explains only about 20% of the population variance. Overall, these results indicate that bone material properties are fairly conserved between strains, whereas how this bone is distributed varies markedly between strains.

To our knowledge, this is the first study to quantify osteocyte lacunar morphology across different mouse strains, as all previous work has been done on mice from a C57BL/6 background. At the cellular length scale, lacunar size traits (e.g., diameter, volume) tend to have moderate heritability ($H^2 = 0.38-0.63$). By contrast, the number of lacunae (e.g., lacunar number density) and their shape (e.g., sphericity, aspect ratio) have relatively high heritability (0.76-0.97). Therefore, the shape of the lacunae and how densely they are packed are strongly determined genetically in the Inbred Founder mice, whereas the volume of a single lacunae is less so.

Contrary to our second hypothesis, many traits of the DO population have different means and smaller ranges than the Inbred Founder population. For 24 out of the 29 traits measured in both Inbred Founders and DO mice, there was a significant difference in mean values between the populations. As a population, the DO had larger skeletal size (BMC), body weight, and healthier glucose levels than Inbred Founders. For the radius, tibia, and femur, the DO bones were larger (e.g., greater cortical area), although medullary area was not different. The DO had higher mechanical properties, but diminished material properties. The combination of higher total area but lower tissue mineral density seen in the DO population matches the preferred bone trait set established in Jepsen et al.¹⁷⁷, and resulted in greater ultimate force. The range of values for each trait in DO mice was generally lower than in Founders, and extreme values were eliminated. For example, for each μ CT parameter, the DO have a smaller coefficient of variation (CV) compared

to the Inbred Founders. For whole-body traits, both maximum and minimum extreme values were eliminated in the DO. For morphology traits, only minimum extremes were eliminated; there were no DO mice with bones as small as the smallest Inbred Founder bones, however there were DO mice with bones as large as the largest Inbred Founder bones. When the DO mice were plotted onto the PCA space defined by the Inbred Founders, the DO population resided in a subset, hybrid space emphasizing the elimination of extreme values and the mixing of phenotypes. The elimination of extreme values in the outbred population implies epistasis in the Inbred Founder strain with the extreme phenotypes since disruption of the exact allele combination removes the phenotype.

While other groups have reported bone phenotypes for either the Inbred Founders¹²¹ or the DO mice¹²² no one has directly compared the two populations. Turner et al.¹⁷⁸ compared two inbred strains (B6 and C3H) to multiple recombinant inbred lines (BXH RI) and showed that none of the measured traits grouped the RI strains into subsets resembling either of the two progenitors. Additionally, none of the RXH RI strains had ultimate force values approaching the high-strength C3H femurs, supporting epistasis of bone traits as our data suggest. In contrast, Jepsen et al.¹⁷⁷ compared A/J and B6 inbred strains to multiple recombinant inbred lines (AXB/BXA RI) and showed many RI lines with femurs smaller than A/J and larger than B6. Depending on the alleles available and the specific combination per animal, bone phenotypes vary considerably, indicating that complicated interactions between genomic regions control skeletal phenotypes.

In support of our third hypothesis, many relationships between traits seen in the Inbred Founder population are maintained in the DO population, especially those between morphology and mechanical properties. However, correlations between most traits and body weight or bone

length were greatly diminished. In the Inbred Founder strains, a relatively large mouse (by body weight) would typically have a large bone. However, in the DO mice, this relationship is disrupted. For example, the correlation between cortical area and weight is non-significant in the DO population ($r = 0.75$ for the Inbred Founders, $r = 0.23$ in the DO population). On the other hand, across both populations, one of the strongest correlations is between bone area and ultimate force, with larger bones being stronger. In fact, we observed an almost identical relationship (slope and intercept are not significantly different) between cortical area and ultimate force in the two populations of genetic diversity, suggesting that this relationship is conserved in all *Mus musculus*. Previously, we evaluated the relationships between traits in a large population of advanced intercross mice (F34 LGXSM AI), which have a large range of body weight and bone size (Chapter 2)¹⁷⁹. We see many similar relationships between traits in that study as we discovered herein. Specifically, in both studies morphology traits are highly correlated with each other except for cortical thickness, which only has low correlations with other traits. Morphology traits also highly correlate with stiffness and strength but not brittleness (PYD). All material properties are highly correlated with each other but relatively independent of morphology. The current study provides additional support that our proposed reduced set of parameters (Ct.Ar, Ma.Ar, Ult.Force, PYD, Ult. Stress)¹⁷⁹ are useful to describe variation in mouse long bones from any population. Jepsen et al. compared femurs from multiple RI lines, and showed a complex, biologically important relationship between bone morphology and tissue quality¹⁷⁷. Specifically, there was a positive correlation between tissue mineral density and cortical thickness in the femurs in that study, which holds true for the radii in both the Inbred Founder population and the DO population herein. Thus, our data add support to the idea that there is a coordinated, biological regulation of the relative rates of periosteal and endocortical expansion (which determine cortical thickness) and tissue mineral density¹⁷⁷.

Many measured traits correlated significantly with body weight, which had a 4.5-fold range from smallest to largest strain of the Inbred Founders. Therefore, we asked whether differences in traits between strains were due solely to differences in body size. After adding body weight as a covariate to the ANOVA analysis, all traits maintained a significant strain or strain/sex effect. The clustering of inbred strains on the PCA also became more distinct and separate after body weight adjustment. Additionally, the heritability increased for most traits after body weight adjustment. This analysis indicates that variations in body size alone do not explain variations in bone traits and indicates that there are genes that independently control bone traits and body size.

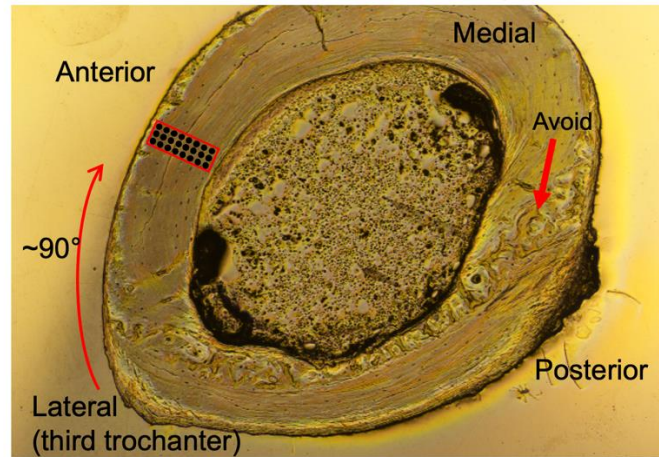
We acknowledge some limitations of our study. First, while we were able to collect data from 188 individual animals, some strain/sex groups had small sample size. Although 9 mice per strain per sex were ordered, we ended up with only 4 female CAST mice due to attrition of this difficult-to-handle strain. Additionally, only 4 samples per sex per strain were evaluated for lacunar (XRM) and bone composition (Raman spectroscopy) analysis. The interpretation from these outcomes, especially those with high variability within a strain/sex group should be supported by more data. When comparing the Inbred Founder mice to the Diversity Outbred population, only 25 DO animals per sex were sampled. We are confident this sample size provides a reasonable estimate of the population mean and distribution, but it is possible adding more DO animals would alter the differences we observed. Second, because two of the inbred strains (NOD, NZO) are commonly used as models for diabetes, we tracked the glycemic status of our mice. Only two groups consistently became hyperglycemic (NOD female and NZO males). No mice were treated with insulin or other means to manage their hyperglycemia, in order to avoid any influence of treatments on bone traits. For NOD and NZO mice, most traits did not exhibit a large sex difference even though hyperglycemia only occurred in one sex by 22

weeks old, which suggests that these traits were not significantly altered by high glucose levels in our study.

In summary, we find that multi-scale cortical bone traits vary with genetic background and are moderately to highly heritable. While we noted significant variations in bone composition, these were less pronounced than variations in bone morphology, indicating that the bone composition between mice is well conserved while bone distribution varies widely. There are several novel findings from this study. First, this is the first study to report osteocyte lacunar traits for genetically diverse mice and to show that these traits are genetically regulated. Second, this is the first study to directly compare bone phenotypes between the DO mice and their inbred progenitors (Inbred Founders). This provides insight into how traits change with outbreeding. Lastly, this is the first study to evaluate the conservation of intra-bone relationships in multiple genetically diverse populations, providing support for how robust these relationships are for *Mus musculus*. This work supports future use of these genetically diverse populations to discover novel genes contributing to cortical bone traits, especially at the lacunar length scale.

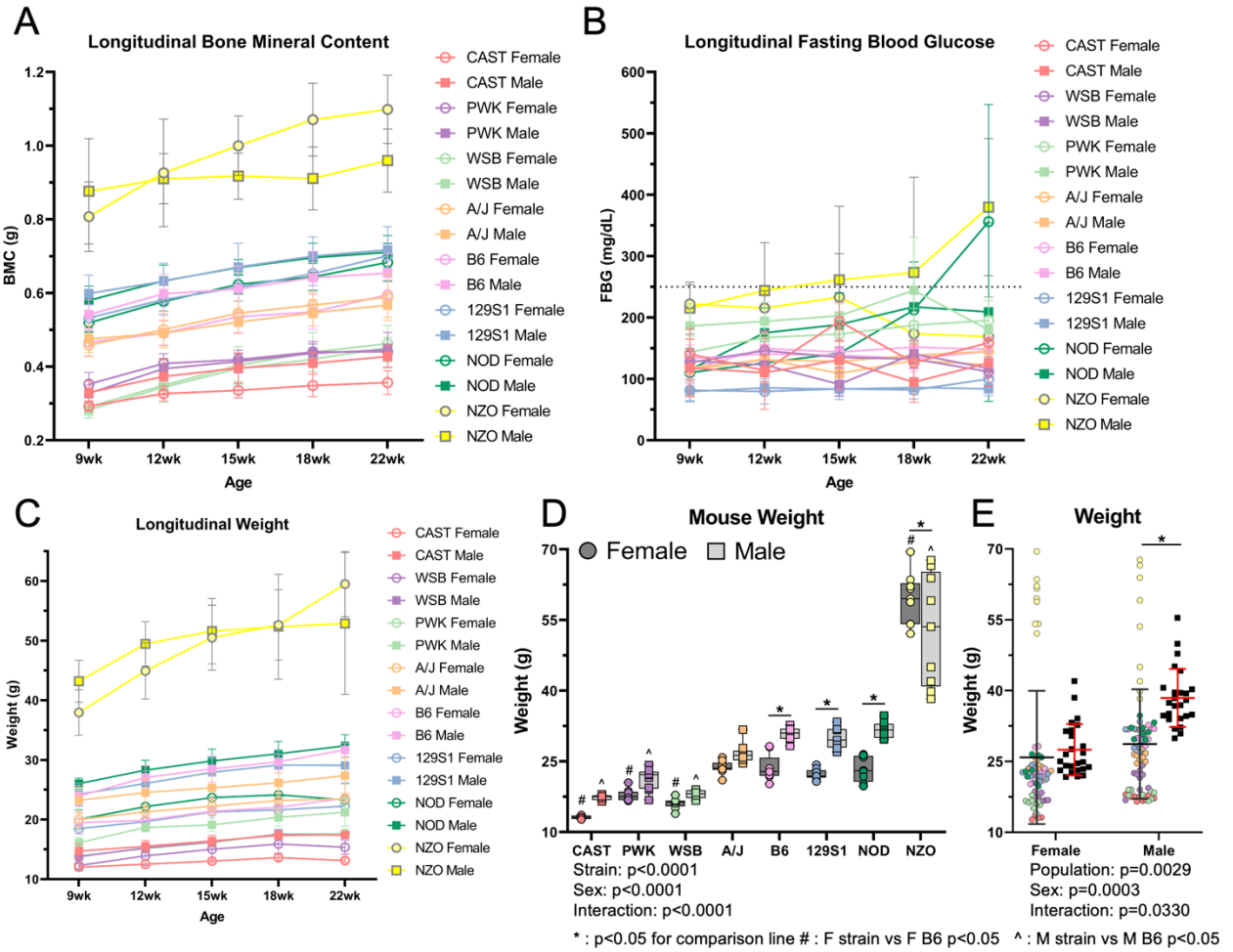
3.6 Supplemental Material

Raman Spectroscopy ROI



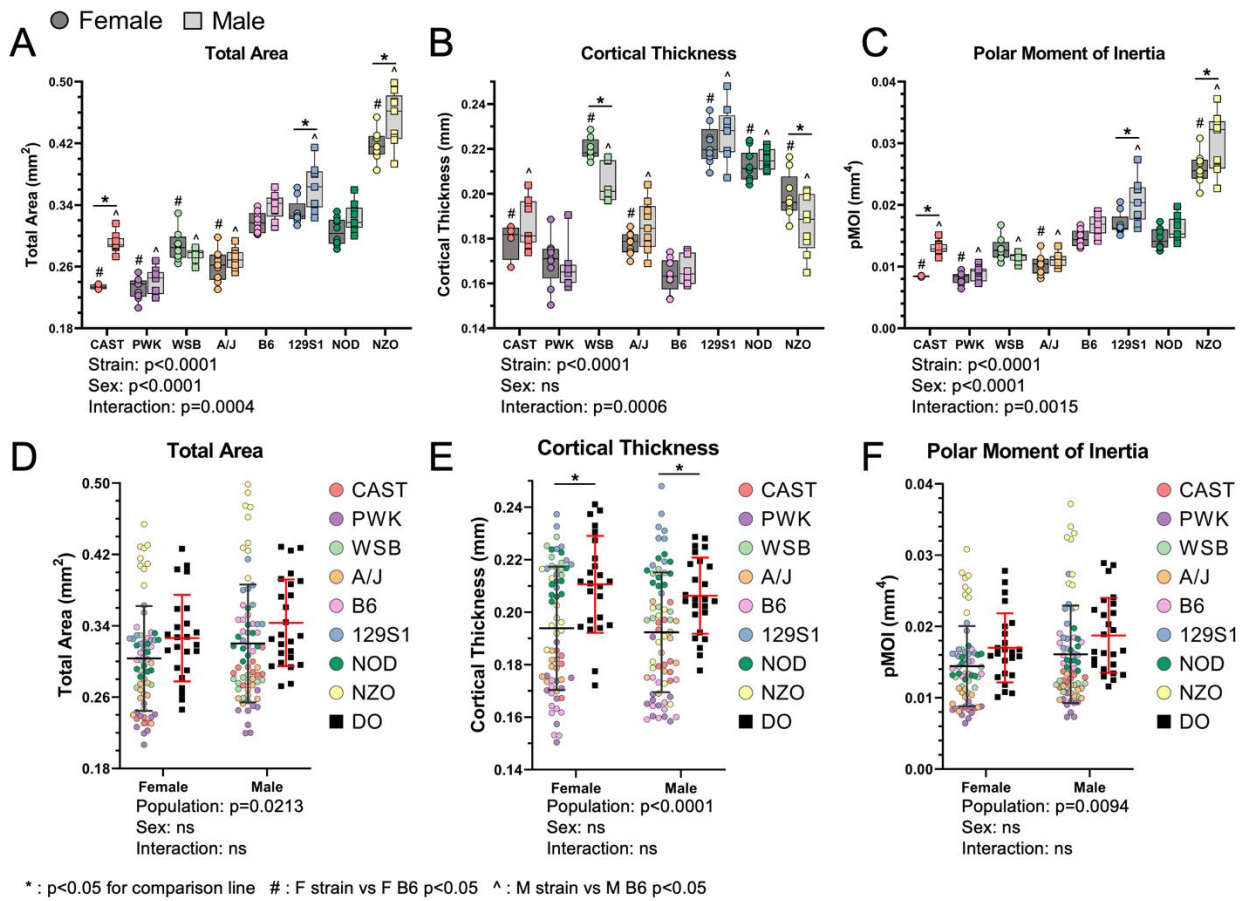
20 μm spacing between spots
Lamellar bone only

Supplemental Figure 3.8: Region of interest for Raman spectroscopy on the transverse cross-section of the femur. Bones were embedded in PMMA and polished to a smoothness of 0.05 μm . The red box shows the region where measurements were taken.

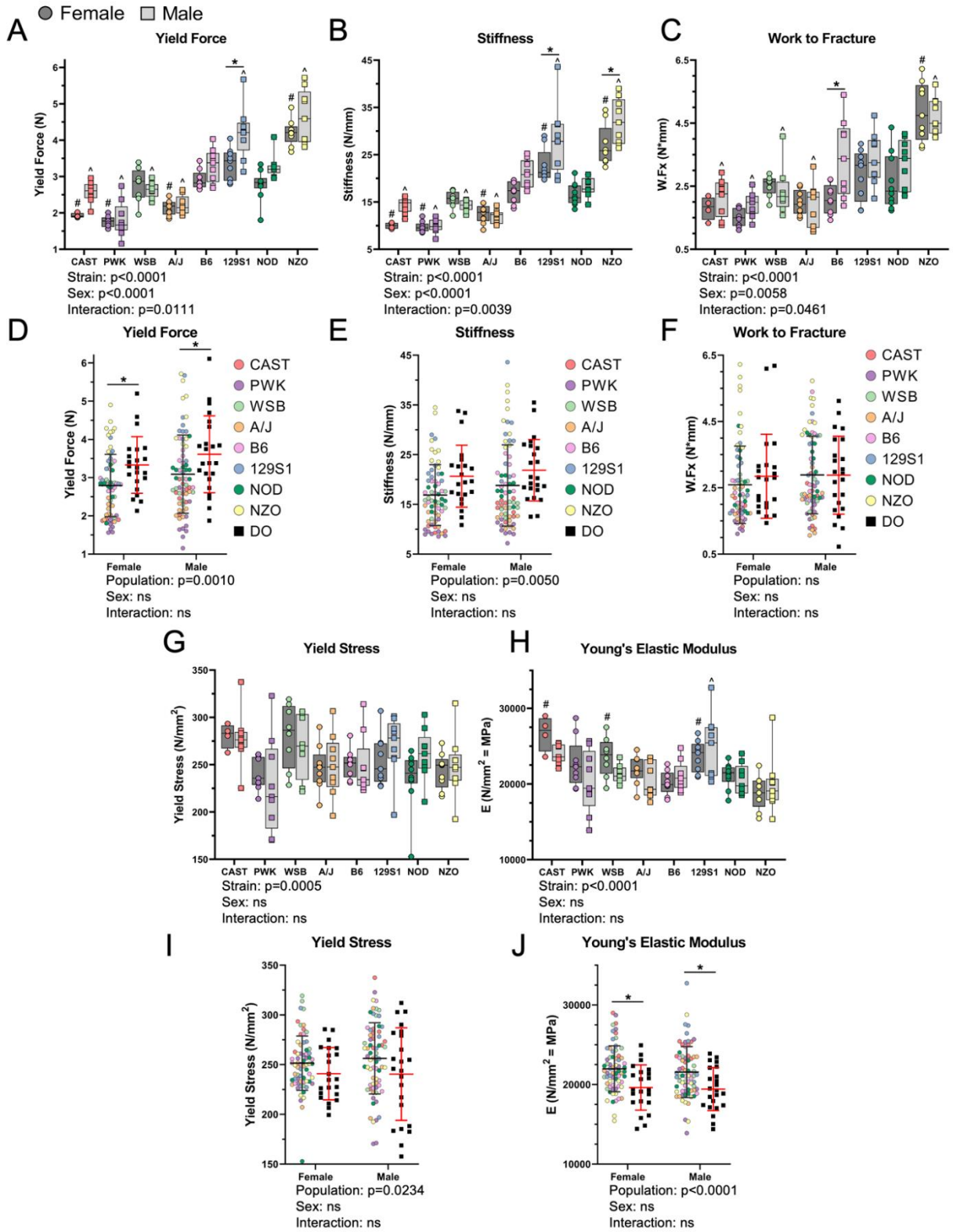


Supplemental Figure 3.9: Longitudinal whole-body measurements.

A) BMC of founder strain mice overtime showing healthy skeletal growth. BMC has plateaued around 22wks of age, with no significant differences between 18wk and 22wk values for any group. B) FBG of founder strains overtime showing the onset of hyperglycemia. NOD F become hyperglycemic between 18wk and 22wk of age. NZO M become hyperglycemic earlier, between 12wk and 15wk of age. C) Trends in body weight match those of BMC. NOD F begin to lose weight around the onset of hyperglycemia. D) At 22wks of age, the Inbred Founder have significant variations due to strain, sex, and a sex-strain interaction. E) At 22wks the DO mice have a higher weight with less variation than the Inbred Founder population. * : $p < 0.05$ for comparison line; # : F strain vs F B6 $p < 0.05$; ^ : M strain vs M B6 $p < 0.05$

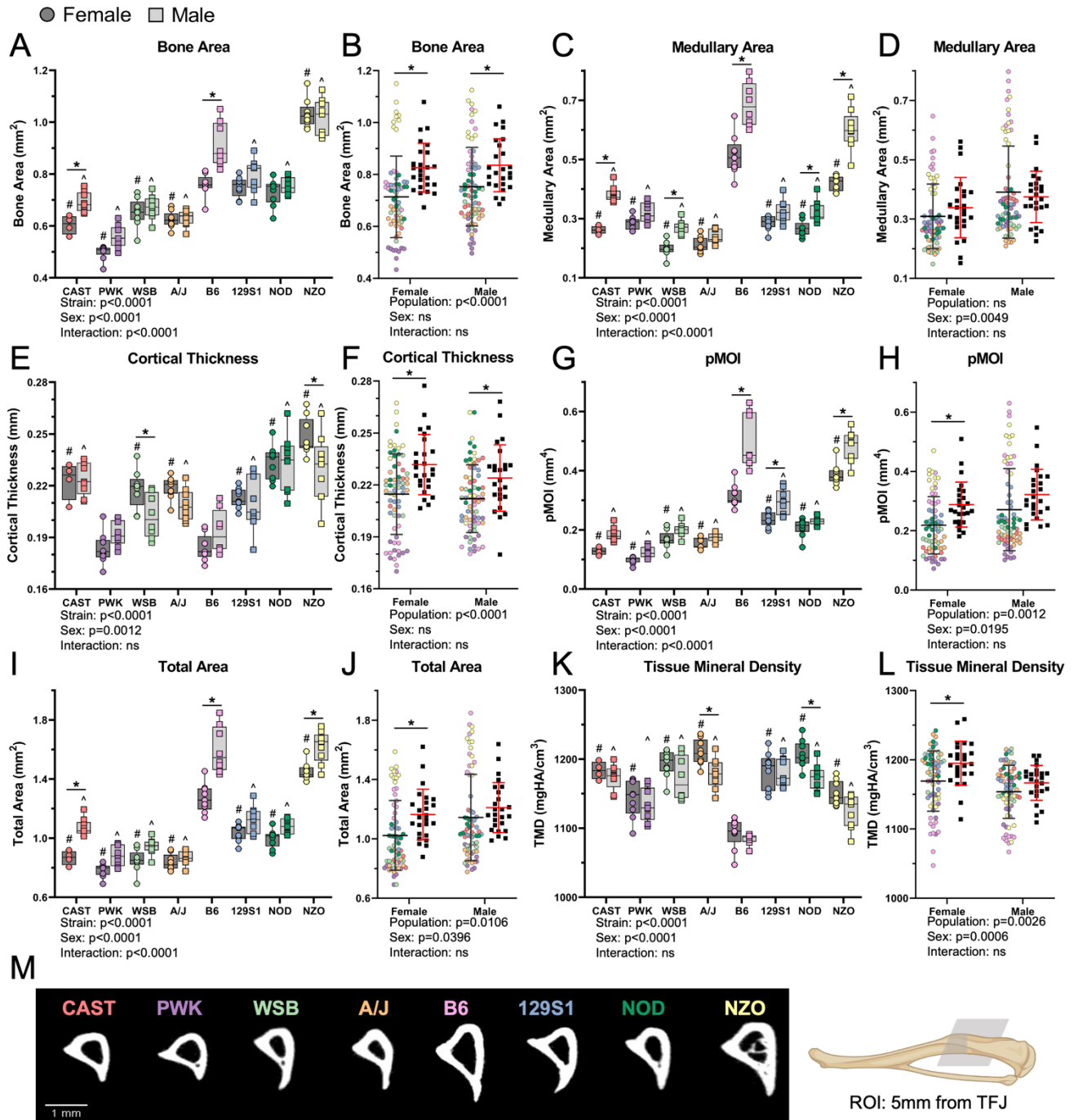


Supplemental Figure 3.10: Radial morphology changes with strain in a sex dependent manner. Additional radial traits not reported in Fig 3.3. * : $p < 0.05$ for comparison line; # : F strain vs F B6 $p < 0.05$; ^ : M strain vs M B6 $p < 0.05$



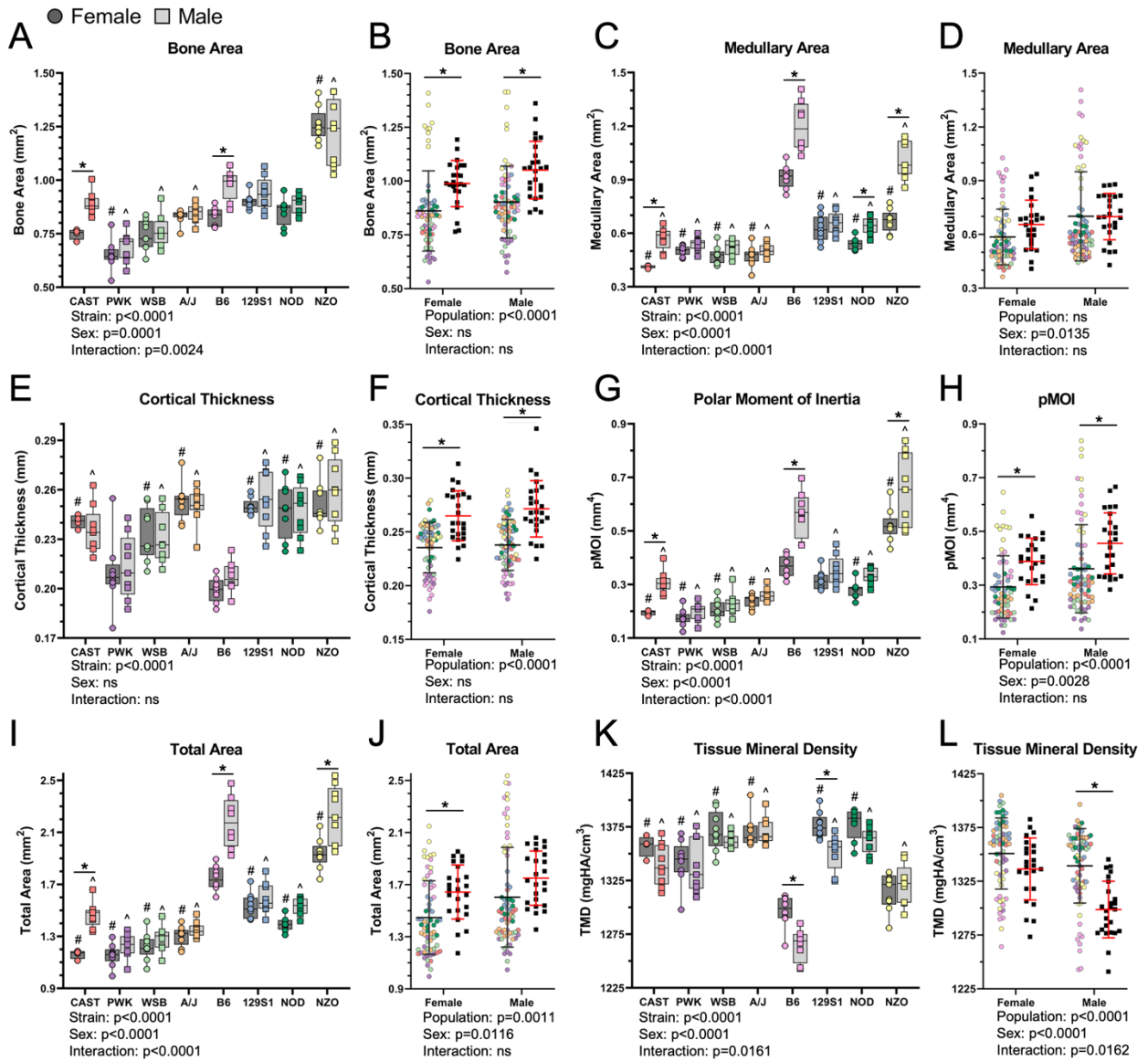
* : $p < 0.05$ for comparison line # : F strain vs F B6 $p < 0.05$ ^ : M strain vs M B6 $p < 0.05$

Supplemental Figure 3.11: Radial material and mechanical properties changes with strain in a sex dependent manner. Mechanical (A-F) and material properties (G-J) not reported in Fig 3.4. * : $p < 0.05$ for comparison line; # : F strain vs F B6 $p < 0.05$; ^ : M strain vs M B6 $p < 0.05$



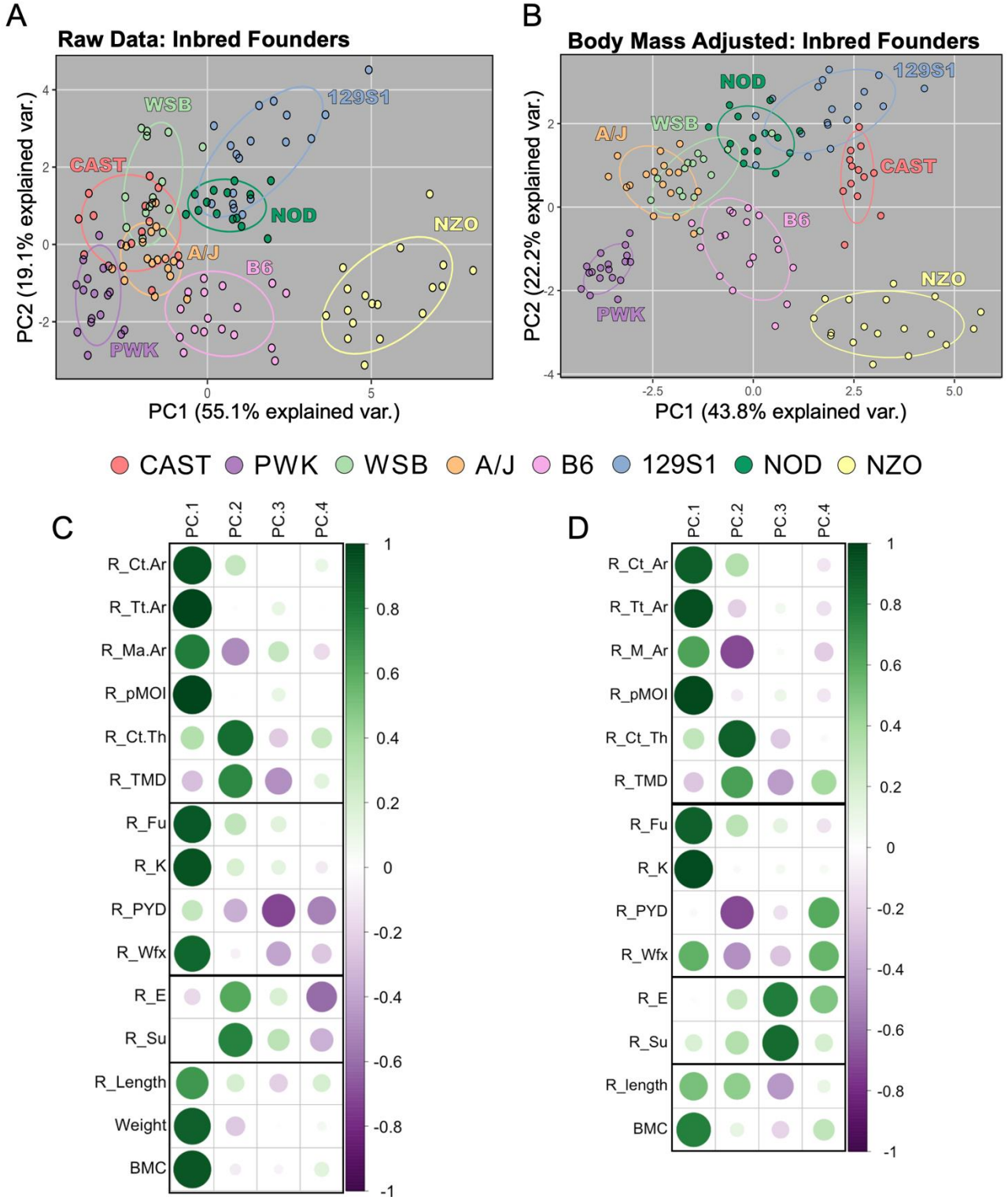
* : $p < 0.05$ for comparison line # : F strain vs F B6 $p < 0.05$ ^ : M strain vs M B6 $p < 0.05$

Supplemental Figure 3.12: Tibial morphology changes with strain in a sex dependent manner. Representative cross-sections 5mm proximal of the tibia-fibula junction (TFJ) show the variation in bone shape and size between the eight inbred founder strains. * : $p < 0.05$ for comparison line; # : F strain vs F B6 $p < 0.05$; ^ : M strain vs M B6 $p < 0.05$

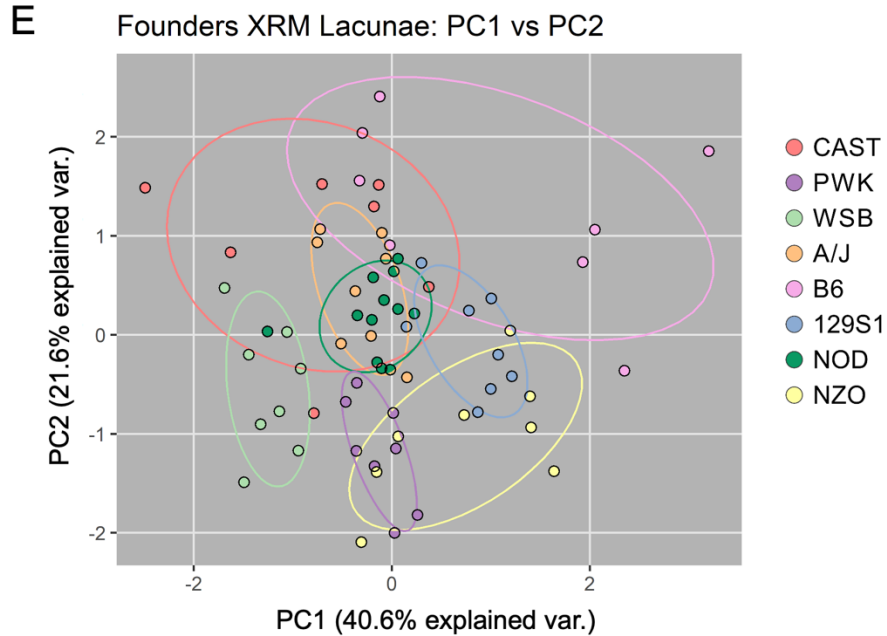
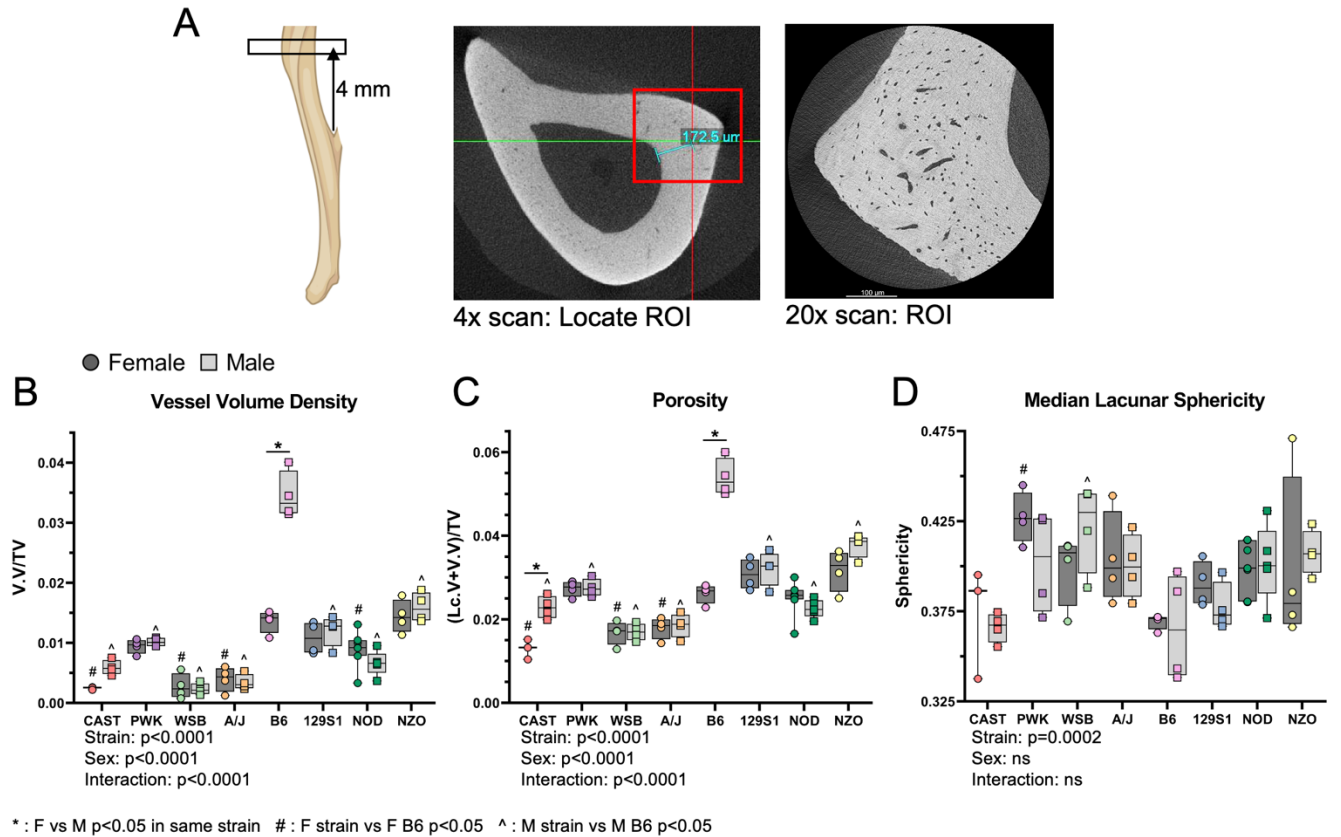


* : p<0.05 for comparison line # : F strain vs F B6 p<0.05 ^ : M strain vs M B6 p<0.05

Supplemental Figure 3.13: Femoral morphology changes with strain in a sex dependent manner. * : p<0.05 for comparison line; # : F strain vs F B6 p<0.05; ^ : M strain vs M B6 p<0.05

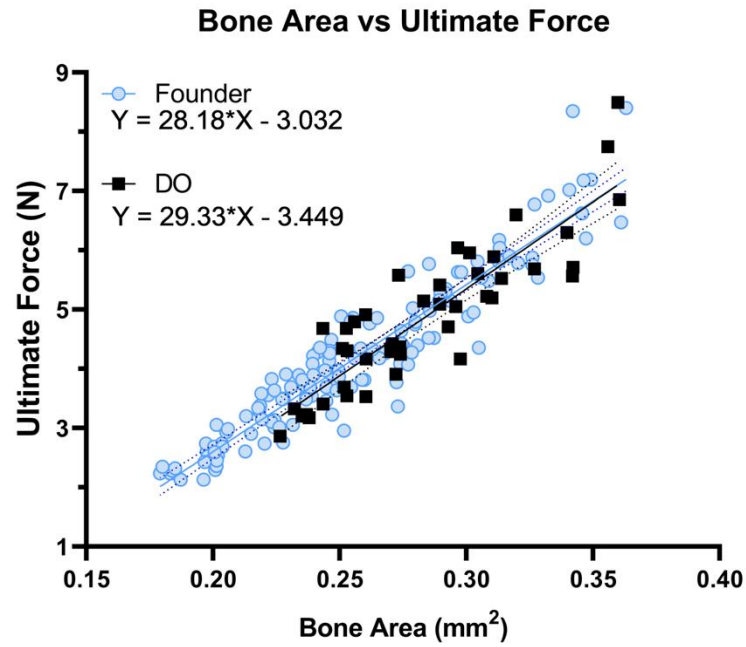


Supplemental Figure 3.14: PCA of raw and body mass adjusted data from Inbred Founder mice. A) PCA of raw data repeated from Fig 3.5 C for ease of contrast. B) The Inbred Founder strains cluster more tightly after body weight adjustment. Contributions of each trait to the first four principal components for the C) raw data and D) body mass adjusted data.



Supplemental Figure 3.15: Additional XRM parameters.

A) Schematic showing the region of interest scanned and analyzed. The scanning region of approximately $500 \mu\text{m} \times 500 \mu\text{m} \times 500 \mu\text{m}$ centered 4 mm proximal to the distal TFJ at the postero-lateral apex. B-D) XRM outcomes not reported in Fig 3.6. E) PCA using all the lacunar traits shows the Inbred Founder strains do not clearly separate. * : F vs M $p < 0.05$ in same strain; # : F strain vs F B6 $p < 0.05$; ^ : M strain vs M B6 $p < 0.05$



Supplemental Figure 3.16: Bivariate plot highlighting how the relationship between cortical area and ultimate force is highly conserved. The slopes and intercepts between the two linear-regression lines are not significantly different.

Supplemental Table 3.3: ANCOVA p-value results with body weight as a co-factor.

		Factor p-value			
Trait		Weight	Strain	Sex	Strain*Sex
Radius	Cort. Area	0.001	0.001	0.181	0.001
	Total Area	0.001	0.001	0.001	0.001
	Med. Area	0.609	0.001	0.001	0.001
	Cort. Thickness	0.001	0.001	0.029	0.022
	pMOI	0.001	0.001	0.005	0.001
	TMD	0.381	0.001	0.881	0.398
Radius	Stiffness (K)	0.001	0.001	0.044	0.001
	Ult. Force	0.001	0.001	0.227	0.001
	Yield Force	0.001	0.001	0.011	0.004
	PYD	0.414	0.266	0.010	0.022
	Wfx	0.128	0.001	0.070	0.219
	Ult. Stress	0.005	0.001	0.013	0.043
	Yield Stress	0.011	0.001	0.450	0.520
	Elastic Modulus	0.016	0.001	0.008	0.065
Tibia	Lc.Vol Density	0.233	0.001	0.001	0.001
	Vess.Vol Density	0.805	0.001	0.001	0.001
	Porosity	0.619	0.001	0.001	0.001
	Lc.No Density	0.837	0.001	0.942	0.032
	Lc.Vol	0.189	0.001	0.001	0.001
	Lc.AspectRatio	0.432	0.001	0.074	0.507
	Lc.SD.Phi	0.196	0.004	0.289	0.529
	Lc.Vol/SA	0.252	0.002	0.031	0.040
	Lc.Diameter	0.300	0.001	0.008	0.034
	Lc.Sphericity	0.659	0.001	0.590	0.579
Femur	Phos:Proline	0.915	0.028	0.634	0.985
	v2Phos:AmideIII	0.568	0.086	0.726	0.670
	Carb:Phos	0.361	0.325	0.823	0.564
	Crystallinity	0.378	0.001	0.093	0.642
Body	BMC	0.001	0.001	0.001	0.025
	FBG	0.001	0.001	0.070	0.001
Tibia	Cort. Area	0.001	0.001	0.003	0.001
	Total Area	0.001	0.001	0.001	0.001
	Med. Area	0.471	0.001	0.001	0.001
	Cort. Thickness	0.001	0.001	0.001	0.031
	pMOI	0.001	0.001	0.001	0.001
	TMD	0.179	0.001	0.001	0.367
Femur	Cort. Area	0.001	0.001	0.399	0.005
	Total Area	0.001	0.001	0.001	0.001
	Med. Area	0.017	0.001	0.001	0.001
	Cort.Thickness	0.036	0.001	0.738	0.596
	pMOI	0.001	0.001	0.001	0.001
	TMD	0.517	0.001	0.001	0.098

Supplemental Table 3.4: Heritability of all traits reported in main paper (left is repeated from Table 3.2) (right is body-weight adjusted)

Raw Data: Inbred Founders

Trait	Heritability (H ²)
BMC	0.993
Cortical Thickness	0.985
TMD	0.967
Lc.No Density	0.966
FBG	0.910
Lc.Sphericity	0.887
Cortical Area	0.884
Crystallinity	0.844
Weight	0.840
Ult. Force	0.836
Lc.SD.Phi	0.835
V.Vol Density	0.827
Phos:Proline	0.806
pMOI	0.799
Total Area	0.799
Stiffness (K)	0.776
Lc.AspectRatio	0.755
Ult. Stress	0.746
Work-to-Fx	0.741
Phos:AmideIII	0.741
Medullary Area	0.722
Yield Force	0.718
Yield Stress	0.717
Porosity	0.689
Modulus (E)	0.684
Lc.Diameter	0.634
Carb:Phos	0.574
Lc.Vol/SA	0.535
Lc.Vol Density	0.516
Lc.Vol	0.383
PYD	0.209

Body Mass Adjusted: Inbred Founders

Trait	Heritability (H ²)
BMC	0.800
Cortical Thickness	0.993
TMD	0.973
Lc.No Density	0.975
FBG	0.936
Lc.Sphericity	0.881
Cortical Area	0.992
Crystallinity	0.873
Weight	NA
Ult. Force	0.984
Lc.SD.Phi	0.835
V.Vol Density	0.969
Phos:Proline	0.806
pMOI	0.960
Total Area	0.989
Stiffness (K)	0.983
Lc.AspectRatio	0.871
Ult. Stress	0.983
Work-to-Fx	0.958
Phos:AmideIII	0.774
Medullary Area	0.959
Yield Force	0.968
Yield Stress	0.897
Porosity	0.975
Modulus (E)	0.962
Lc.Diameter	0.775
Carb:Phos	0.866
Lc.Vol/SA	0.780
Lc.Vol Density	0.969
Lc.Vol	0.893
PYD	0.804

Whole Body
Whole Bone
Tissue Level
Cellular Level

Supplemental Table 3.5: Heritability of uCT parameters from all three bones. Radial heritability values are repeated from Table 3.2. Right side shows heritability for body weight adjusted values.

Raw Data: Inbred Founders

Trait	Bone	Heritability (H ²)
Ct.Th	Radius	0.985
TMD	Radius	0.967
Ct.Th	Femur	0.937
Ct.Th	Tibia	0.886
Ct.Ar	Radius	0.884
Ct.Ar	Femur	0.861
Ct.Ar	Tibia	0.807
pMOI	Radius	0.799
Tt.Ar	Radius	0.799
TMD	Femur	0.741
Ma.Ar	Radius	0.722
TMD	Tibia	0.636
Tt.Ar	Femur	0.621
Tt.Ar	Tibia	0.614
pMOI	Femur	0.607
pMOI	Tibia	0.597
Ma.Ar	Femur	0.522
Ma.Ar	Tibia	0.503

Body Mass Adjusted: Inbred Founders

Trait	Bone	Heritability (H ²)
Ct.Th	Radius	0.993
TMD	Radius	0.973
Ct.Th	Femur	0.956
Ct.Th	Tibia	0.870
Ct.Ar	Radius	0.992
Ct.Ar	Femur	0.991
Ct.Ar	Tibia	0.991
pMOI	Radius	0.960
Tt.Ar	Radius	0.989
TMD	Femur	0.969
Ma.Ar	Radius	0.959
TMD	Tibia	0.917
Tt.Ar	Femur	0.957
Tt.Ar	Tibia	0.968
pMOI	Femur	0.909
pMOI	Tibia	0.947
Ma.Ar	Femur	0.837
Ma.Ar	Tibia	0.926

Radius
Femur
Tibia

Chapter 4: Bone Response to Mechanical Loading is Highly Heritable and Correlates with Osteocyte Lacunar Morphology in Mice

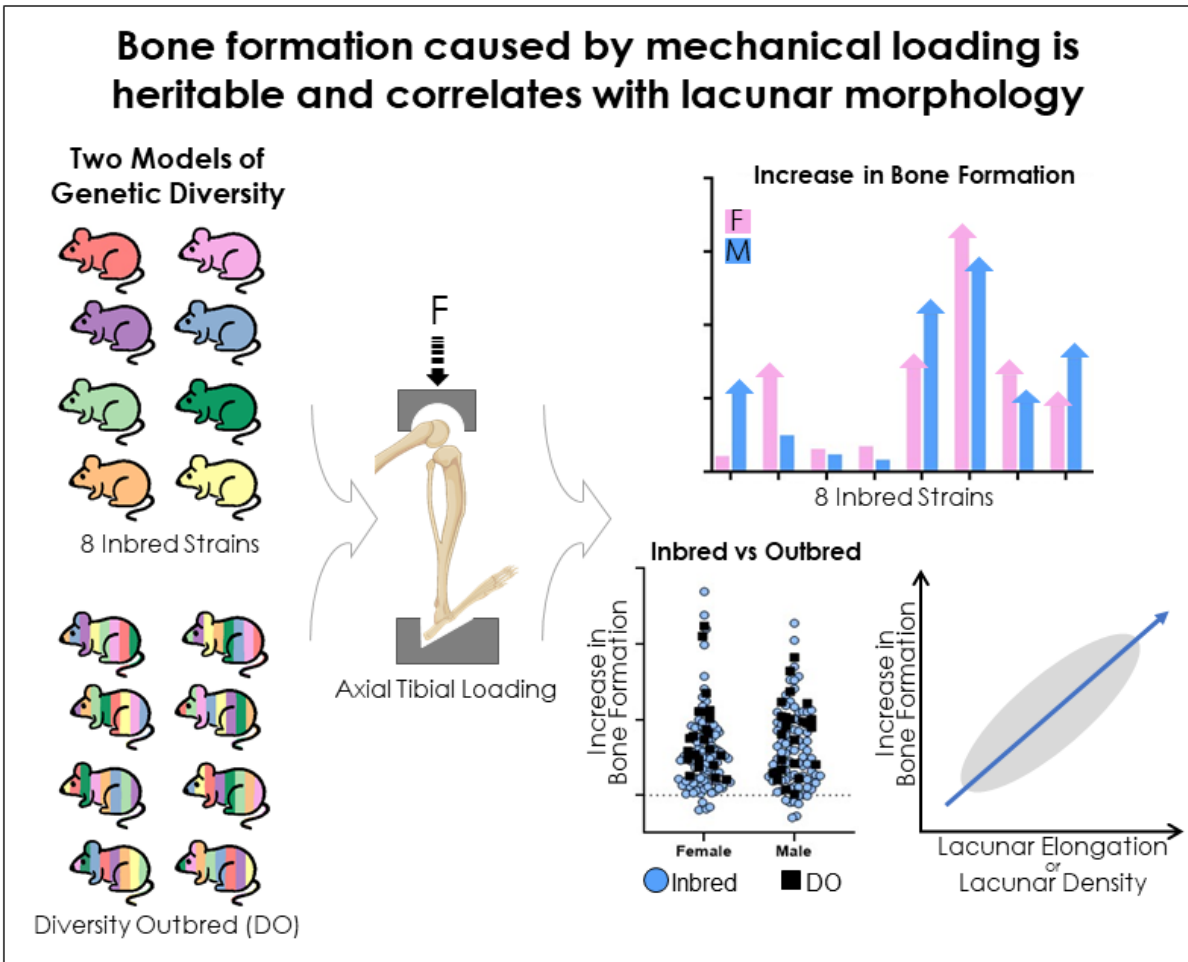


Figure 4.1: Graphical Abstract

4.1 Abstract

The ability of bone to adapt and remodel in response to external demands is a key trait maintaining skeletal health and preventing fracture risk. This phenomenon has only been studied in a limited range of mouse strains; therefore, a more comprehensive study is needed that incorporates more genetic variation and allele combinations to enhance rigor and translatability. The objective of this study was to investigate the effect of genetic diversity on bone response to mechanical loading. Specifically, we aimed to assess the variation in bone response to loading in two models of genetic diversity using the axial, tibial loading model to induce cortical bone formation. Additionally, we explored the correlation between bone phenotype and the response to mechanical loading. Similar to the approach in Chapter 3, our first population of genetic diversity included 96 female and 96 male young-adult (5-month) mice from the eight Inbred Founder strains used to create the Diversity Outbred (DO) population. The second population included 25 females and 25 males from the DO population. We show the response to loading varies with genetic background and is highly heritable; heritability values range from 32% to 97% with all measurements of periosteal formation being near or above 80%. On average, the DO population showed a more robust response to mechanical loading compared to the Inbred Founders with all DO mice showing positive net increases in all bone formation measurements. Additionally, bone axial stiffness and lacunar traits (determined in Chapter 3) correlate with the magnitude of loading-induced bone formation. Stiffer bones and bones with more elongated lacunae respond more robustly to mechanical loading. This work provides the groundwork and rationale to perform genome wide association studies (GWAS) or quantitative trait loci (QTL) analysis in these populations to identify candidate genes regulating the response to loading.

Uncovering novel genes can provide new targets for therapeutics to increase bone mass, especially in patients where weight-bearing exercise is unsafe or less feasible.

4.2 Introduction

Bone mechanobiology explores the intricate relationship between mechanical forces and bone tissue, shedding light on how bone adapts and remodels in response to external stimuli. Our lab and others have shown that mechanical loading promotes a potent anabolic response in bone^{22,90–94}. However, most loading studies are performed on a very limited range of mouse strains. In loading studies published between 2014 and 2020 (PubMed search terms: *mouse, bone, loading* – returned 94 studies), 96% use C57BL/6 (B6) mice or mutants that are a majority B6. The studies that didn't use B6, used only one of four other strains of mice (BALB/c^{105–107}, CD1¹⁰⁰, DBA/2¹⁰⁸, and C3H/He^{108,109}). This is problematic because classical laboratory strains share the majority of their genetic backgrounds and are derived from a small pool of ancestors, with 97% of the mouse genome being explained by fewer than 10 haplotypes¹¹². In recent years, there has been increasing recognition of the impact of genetic diversity on bone physiology and its response to mechanical loading.

Different inbred mouse strains have been shown to respond differently to mechanical loading. Several research groups have highlighted the complex relationships between genetics, bone morphology, and response to loading, indicating interactions between multiple genomic regions^{128–132}. In a study by Akhter et al., two mouse strains were loaded to the same force, yet only one mouse strain produced a robust anabolic response¹⁰⁹. Robling and Turner compared the loading response of adult, female mice from three different strains, also showing significantly different responses¹⁰⁸. These studies revealed B6 mice were more responsive than C3H,

motivating Kesavan et al. to perform a genome-wide search of loci regulating bone adaptive response in a B6XC3H intercross subjected to tibial 4-pt bending¹²⁸. They estimated broad-sense heritability of morphology changes ranging from 70% and 86%, and discovered multiple loci across different chromosomes that were correlated to changes in morphology and gene expression in response to loading^{128,129}. These studies, however, only compared or crossed a small number of inbred laboratory mouse strains. A more comprehensive study that incorporates more genetic variation and allele combinations will extend the prior work and enhance rigor and generalizability.

Thus, there is a need to for a genetically diverse set of mice so researchers can better understand the role of genetics on many phenomena, including bone response to loading. To help fulfill this need, the Jackson Laboratory has developed the Diversity Outbred (DO) mouse resource, which is an outbred population derived from eight founder lines (A/J, C57BL/6J, 129S1/SvImJ, NOD/ShiLtJ, NZO/HILtJ, CAST/EiJ, PWK/PhJ, and WSB/EiJ)^{115,180}. These eight Inbred Founder lines contain five classical laboratory mouse strains (A/J, B6, 129S1, NOD, and NZO) and three wild-derived strains (CAST, PWK, WSB). Altogether, they cover almost 90% of the genetic diversity found in mice (*Mus musculus*)¹¹⁸. Comparing the loading responses of the Inbred Founder lines and the DO mice will provide insight into how genetics contributes to bone responsiveness to mechanical loads.

The objective of this study is to investigate the effect of genetic diversity on bone response to mechanical loading. Specifically, we aim to assess the variation in bone response to loading among the eight Inbred Founder strains and DO mice. In addition to evaluating the loading response, we also aim to explore the correlation between bone phenotype and the response to mechanical loading. Using our two models of genetic diversity (Inbred Founders and DO mice)

we set out to test three hypotheses; 1) the response to loading varies between mice of different genetic backgrounds, 2) outbred mice (DO) have the same average response to loading as the Inbred Founder population, and 3) the magnitude of the loading response correlates significantly with homeostatic bone phenotypes, especially of the osteocyte lacunae. Investigating the effect of genetic diversity on bone response to mechanical loading is a crucial step toward unraveling the complex interplay between genetics and mechanobiology in bone tissue.

4.3 Methods

4.3.1 Mouse Populations

The mouse experiments were conducted in compliance with the guidelines and regulations set forth by the Washington University Institutional Care and Use Committee (IACUC). All mice were obtained from The Jackson Laboratory (JAX). To model genetic diversity, two mouse populations were utilized: (1) Eight Inbred Founder strains: CAST/EiJ (JAX Stock #000928), PWK/PhJ (#003715), WSB/EiJ (#001145), A/J (#000646), C57BL/6J (#000664), 129S1/SvImJ (#002448), NOD/ShiLtJ (#001976), and NZO/HILtJ (#002105); and (2) Diversity Outbred (DO) mice (#009376). The Diversity Outbred population are derived and maintained by continuous outbreeding, starting from the eight Inbred Founder strains (Fig 4.2 A).

Inbred Founder strains ($n = 12/\text{strain}/\text{sex}$) were received at 8 weeks of age and subsequently aged to 22 weeks in our animal facilities. Due to attrition, a total of $N = 169$ Inbred Founder mice were analyzed at the end of the study. The DO mice ($n = 25/\text{sex}$, generation G46 and G47) were obtained between 3 and 5 weeks of age and aged to 22 weeks in our animal facilities. One female DO mouse died during μCT ; a total of $N = 49$ DO mice were analyzed at the end of the study. Inbred mice were group-housed, with up to 5 individuals per cage. Male DO mice were housed individually, while female DO mice were housed in groups of up to 3 individuals per cage,

following recommendations from JAX to minimize intra-group aggression. All mice were maintained under a 12-hour light-dark cycle and provided *ad libitum* access to food and water.

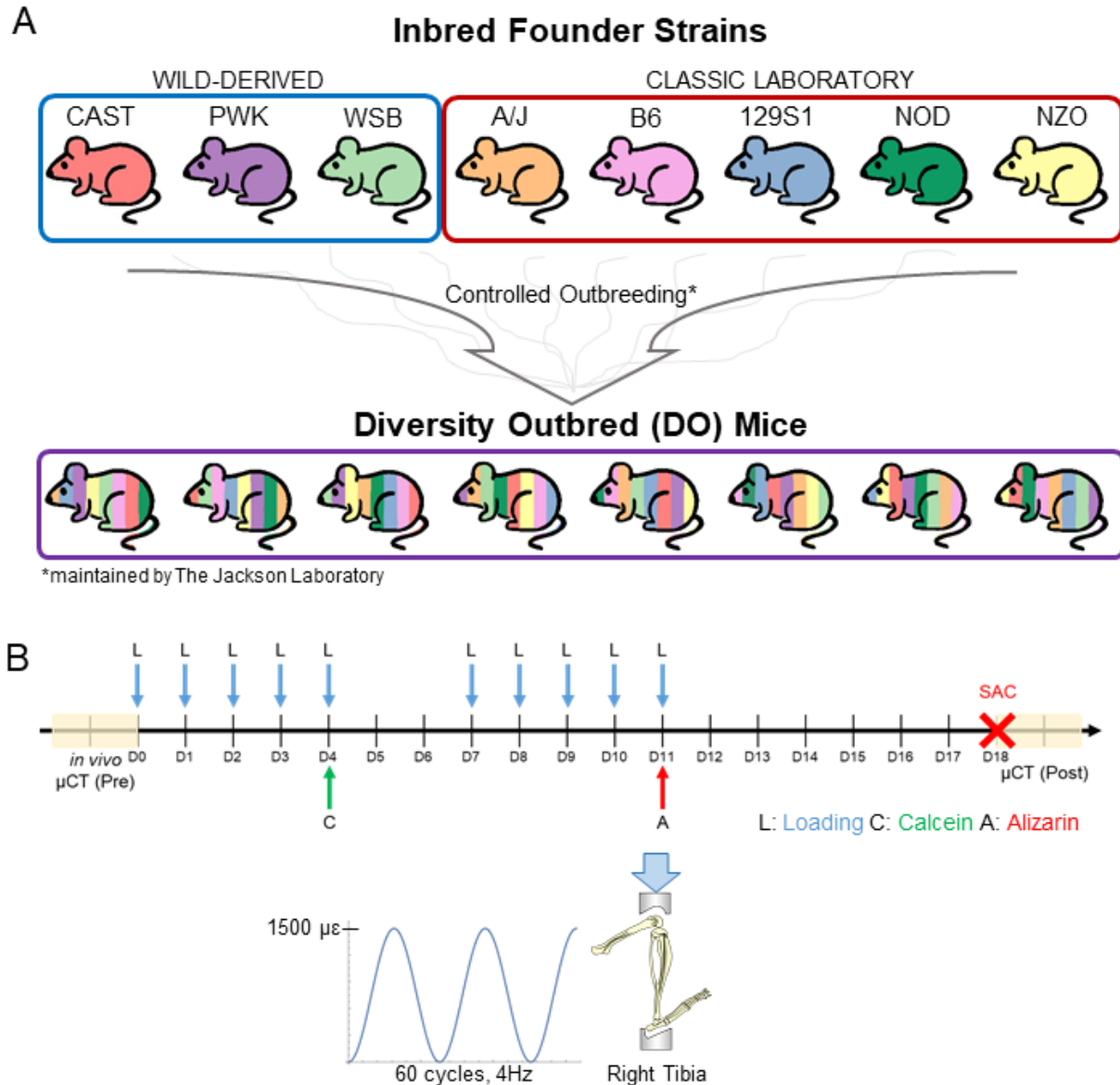


Figure 4.2: Overview of experimental groups and timeline.

A) Two mouse models of genetic diversity were used, eight inbred mouse strains and an outbred stock. The inbred strains were the founders used by The Jackson Laboratory to create the diversity outbred (DO) population. After controlled outbreeding of the founder lines, each DO mouse is genetically unique. Loading was performed on 5 mo-old female and male mice from the eight Inbred Founder strains and the DO mice from generations 46 and 47. B) The right tibia of all mice were loaded 5 days per week for 2 weeks. At the end of each week of lading mice were injected with calcein and alizarin. μ CT scans were taken before and after loading to track change in morphology.

4.3.2 Axial Tibial Loading

Mice were loaded in axial, tibial compression for two weeks to stimulate bone formation (Fig. 4.2 B). While under anesthesia (Isoflurane 2-4% vol/vol) the right tibia was placed in a custom-built holder and loaded to a strain of 1500 $\mu\epsilon$ (section 4.3.3 *Calculation of Necessary Force*) using a dynamic testing machine (ElectroPuls 1000, Instron, Norwood, MA) as previously described^{90,181}. The left tibia remained non-loaded as an internal, contralateral control. Mice were loaded using a haversine waveform for 60 cycles per day at 4 Hz, 5 days per week for 2 wks. Calcein green and alizarin red were injected (IP) at the end of each week, respectively, to allow for the visualization of newly mineralized bone. One week after the last bout of loading mice were euthanized using CO₂ and kept at 4° C until post-loading microCT scanning (Section 4.3.4 *MicroCT*).

4.3.3 Calculations of Necessary Force

All mice were strain matched to 1500 $\mu\epsilon$ on the antero-medial surface of the tibia 5 mm proximal to the distal tibiofibular junction (TFJ). To calculate the force necessary to engender 1500 $\mu\epsilon$, a calibration set of non-loaded Inbred Founder strains were strain gauged (using mice phenotyped in Chapter 3). Briefly, the antero-medial surface of the right tibia was exposed *in situ* and a uniaxial strain gauge was glued 5 mm proximal to the TFJ (Supp Fig 4.9 A). The tibia was loaded from 2N – 12N while force and mechanical strain were simultaneously recorded. From the force-strain linear regression, the force intercept at 1500 $\mu\epsilon$ was calculated per animal (Supp Fig 4.9 B). An average value per strain/sex group was calculated from n = 4-9 mice (Supp Fig 4.9 C). Force per 1500 $\mu\epsilon$ also serves as a proxy measurement for whole-bone, axial stiffness.

Because each DO mouse does not have a genetically identical duplicate, invasive strain gauging is not a feasible method to calculate the necessary loading force per animal. Therefore, we used the strain gauging and phenotyping data from our Inbred Founder mice (N = 130 total animals) to build a multi-variable linear regression to predict necessary loading force using non-invasively measured traits from μ CT. Starting with 11 traits, backwards elimination was used to remove non-significantly contributing variables, leaving five variables in the linear regression. The final equation used to estimate loading force was $Force = 14.98 - 5.38(T.Ar) + 24.1(Ct.Ar) - 0.07(Weight) - 13.68(AreaRatio) - 10.98(Eccentricity)$. This regression explains 57% of the variation in the population (Supp Fig 4.9 D). To validate the accuracy of this approach, strain gauging was performed on the left, non-loaded tibia of DO mice (n = 16-17 per sex) after sacrifice. On average, the error in loading input strain was 32 $\mu\epsilon$ (range -437 – +499 $\mu\epsilon$) (Supp Fig 4.10 A). Errors were randomly distributed across loading forces (Supp Fig 4.10 B).

4.3.4 MicroCT (μ CT)

The morphology of the tibia was evaluated before and after loading to track changes. One to two days prior to loading, the left and right tibia were μ CT scanned *in vivo* at 10.5 $\mu\text{m}/\text{pixel}$ resolution 5 mm proximal to the TFJ (vivaCT 40, Scanco Medical, Switzerland, -70kVP, 8W, 300ms integration time, 213 slices). The same region was scanned *in situ* one week after the last day of loading using the same settings (Fig 4.2 B). Loading-induced changes in morphology per animal were calculated as the change in the loaded bone over time minus the change in the non-loaded bone over time ($\Delta\Delta_{\mu\text{CT}} = (\text{Post}_{\text{loaded}} - \text{Pre}_{\text{loaded}}) - (\text{Post}_{\text{non-loaded}} - \text{Pre}_{\text{non-loaded}})$). To calculate loaded and resorbed volumes we performed time-lapse μ CT (3D Dynamic Histomorphometry) similarly to Birkhold et al¹⁸². Pre- and post-scans of the same limb were registered in 3D and resampled to the same coordinate system. Formed volumes were defined as voxels only present

in the post-scan. Resorbed volumes were defined as voxels only present in the pre-scan. The periosteal and endocortical surfaces were analyzed separately. Image-registered bones were compared to dynamic histomorphometry to validate the accuracy of image-registration (Supp Fig 4.11). Formed and resorbed volumes were normalized to the original bone cortical area. Relative values for all outcomes were calculated as loaded minus non-loaded.

4.3.5 Dynamic Histomorphometry

After the μ CT post-scan, the left and right tibias were dissected clean of muscle and stored in 70% ethanol until plastic embedding. Bones were dehydrated in ethanol and embedded in methyl methacrylate (MMA, Thermo Scientific AAA130300F, Thermo Fisher Scientific). Blocks were cut transversely (Leica SP1600 Microtome, Leica Microsystems, Inc., Buffalo Grove, IL) 5 mm proximal to the TFJ and three 100 μ m thick slices were taken. Sections were imaged on a confocal microscope (Leica TCS SPEII, 10x lens, 2048x2048, 400Hz, 1.5x zoom) with a pixel resolution of 358.25 nm. A maximum projection was created from a five slice, 20 μ m thick z-stack for final analysis. Images were blinded and fluorochrome-labeled surfaces were analyzed (Osteo II, Bioquant Image Analysis Corporation, Nashville, TN) separately on the periosteal and endocortical surfaces¹⁸³. In cases where no double label was visualized, a value of 0.3 μ m/day was assigned for the respective mineral apposition rate (MAR)^{184,185}. Relative values for all outcomes were calculated as loaded minus non-loaded.

4.3.6 Heritability Calculations

The broad-sense heritability (H^2) of all relative loading responses in the Inbred Founder mice was determined to assess the proportion of variance attributed to genetic differences, following the methodology described by Moran et al.¹⁷³. Heritability was calculated using the formula $H^2 = \sigma^2_{\text{strain}} / (\sigma^2_{\text{strain}} + \sigma^2_{\text{sex}} + \sigma^2_{\text{res}})$, where σ^2_{strain} denotes the variance between strains, σ^2_{sex} denotes the

variance between sexes, and σ^2_{res} denotes the residual variance. The variances were computed based on the sum of squares derived from a two-factor analysis of variance (ANOVA) defining strain and sex as the factors. Specifically, σ^2_{strain} was calculated as $SS_{\text{strain}}/n_{\text{avg}}$ (where n_{avg} corresponds to the average group size), σ^2_{sex} was determined as $SS_{\text{sex}}/df_{\text{sex}}$, (where σ^2_{res} corresponds to $SS_{\text{res}}/df_{\text{res}}$).

4.3.7 Correlations

To examine the relationship between bone response to loading and bone morphology, we performed several analyses. First, bivariate plots were generated to compare axial stiffness with relative periosteal bone formation rate per animal in both the Inbred Founder population and DO population. Second, a correlation matrix of Pearson's r coefficients was computed to assess the association between all initial μCT outcomes of the right tibia and the loading response outcomes per animal in both the Inbred Founder population and DO population. Third, a correlation matrix of Pearson's r coefficients was calculated to examine the correlation between all osteocyte lacunar traits and the loading responses per strain/sex group within the Inbred Founder population. The average lacunar trait values were collected from non-loaded mice (Chapter 3). Bivariate plots were also generated to visualize the relationship between lacunar volume density and lacunar aspect ratio with periosteal bone formation rate.

4.3.8 Statistical Analysis

Statistical analysis was conducted using GraphPad Prism (v9). Relative loading response outcomes from the eight Inbred Founders were analyzed using a two-factor analysis of variance (ANOVA) with mouse strain and sex as factors. Similarly, outcomes from the Inbred Founder population and the DO population were compared using a two-factor ANOVA with population and sex as factors. Post-hoc tests were conducted with Sidak correction. To evaluate the

significance of the loading response within a given strain/sex group, the value of the right tibia (loaded) was compared to the value of the left tibia (non-loaded) during post-hoc testing. The significance level was set at $p < 0.05$. Pearson's correlation coefficients were calculated using the *cor* function in R (v4.0.2), and the resulting correlations were visualized using the *corrplot* function.

4.4 Results

4.4.1 Changes in bone morphology due to loading vary with mouse strain and sex

To assess morphological changes in the cortical bone, we calculated the loading-induced change of standard transverse, cross-sectional μ CT parameters (Fig 4.3 A). Changes in bone area varied significantly with mouse strain in a sex-dependent manner (Fig 4.3 B). Ten of the sixteen strain/sex groups had a significant response to loading. Sex as a main effect was not significant, although significant sex differences were seen in CAST and PWK mice; CAST males responded more than CAST females, whereas PWK females responded more than PWK males. Inbred strain 129S1 had the largest increase in bone area in both sexes. Compared to the Inbred Founders, the DO population on average had a larger increase in bone area indicating a greater response to loading (Fig 4.3 C). There was no sex difference in either the Inbred Founder population or the DO population for any measured μ CT parameter. In the Inbred Founders, all other morphology traits varied significantly with strain in a sex-dependent manner, while sex as a main effect was not significant (Fig 4.3 D, Supp Fig 4.12). The DO population only had significant differences compared to the Inbred Founders in total area and polar moment of inertia (pMOI) changes (Supp Fig 4.12). There were no changes in TMD due to loading in any Inbred Founder strain or the DO population. In summary, we saw strain and sex-dependent variations in

cortical bone morphology in response to loading. The Diversity Outbred population exhibited a greater overall response compared to the Inbred Founders.

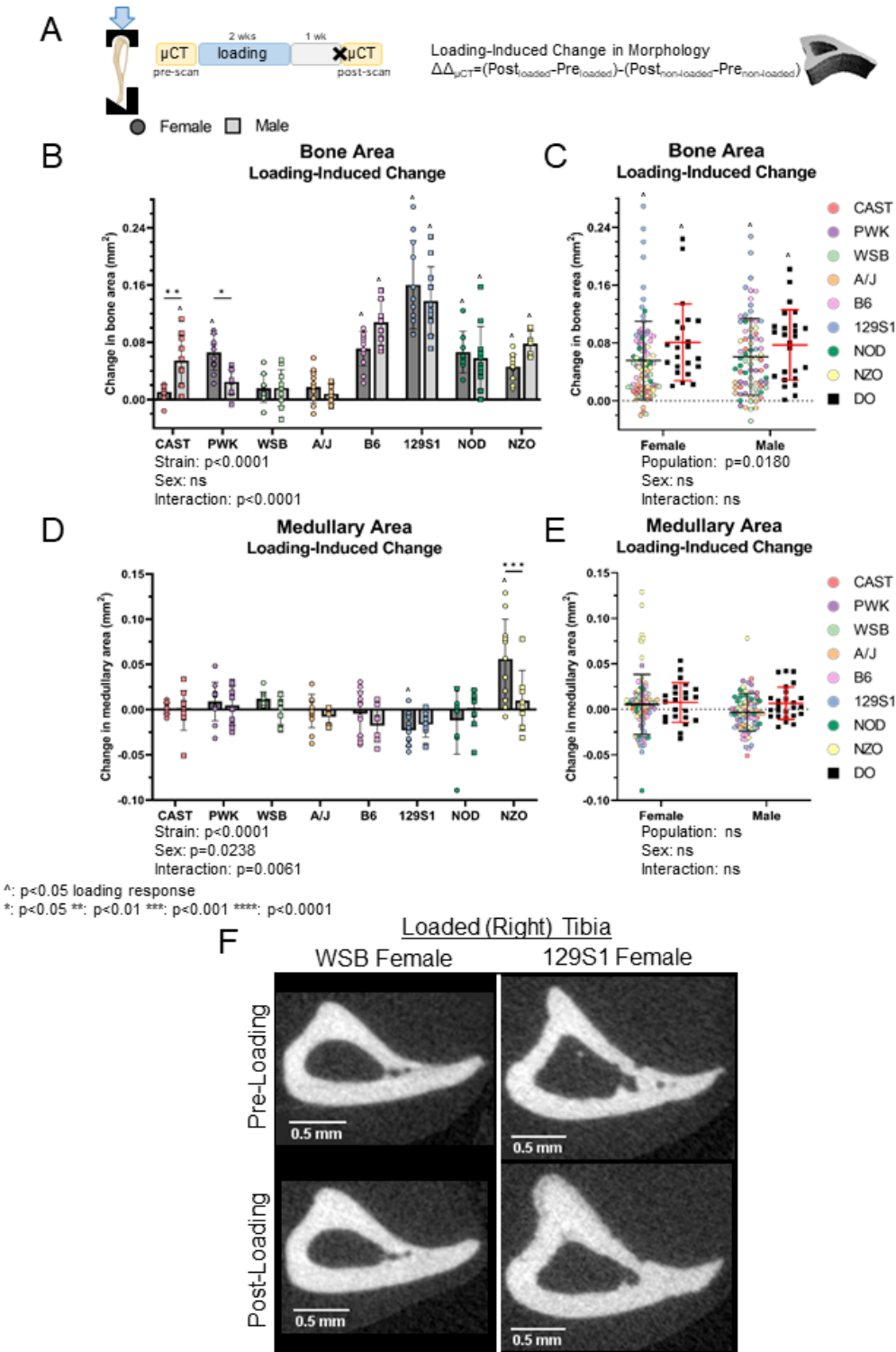


Figure 4.3: Changes in morphology between the pre-scan and post-scan.

A) Timeline of μ CT and loading. Pre-scans and post-scans were 18 days apart. B) Loading-induced change in bone area of the Inbred Founders have significant strain and strain-sex interaction terms (ANOVA). C) The DO mice have a larger average increase in bone area than the pooled Inbred Founders. D) Loading-induced change in medullary area of the Inbred Founders have a significant strain, sex, and strain-sex interaction term. Only NZO have a significantly different response between females and males. E) The DO mice respond to the same degree as the Inbred Founder population. F) Representative μ CT cross-sections from a lowly responding strain (WSB F) and a highly responding strain (129S1 F).

4.4.2 Bone formation increases and bone resorption decreases in response to loading vary with mouse strain and sex

To assess changes in bone formation and resorption on the periosteal and endocortical surfaces, we compared the post-scan to the pre-scan μ CT voxel by voxel (Fig 4.4 A). In response to loading, eleven of the sixteen strain/sex groups significantly increased bone formation on the periosteal surface (Fig 4.4 B). The magnitude of response varied significantly between strains in a sex-dependent manner. Only the PWK and 129S1 strains showed significant sex differences; the females had larger increases in formation than the males. Additionally, eight of the sixteen strain/sex groups significantly decreased bone resorption on the periosteal surface and no strains increased resorption (Fig 4.4 D). The magnitude of decrease in resorption varied between strains in a sex-dependent manner. Only CAST mice showed a significant sex difference with males having a larger decrease in resorption. Compared to the Inbred Founders, the DO mice on average had a larger increase in formation on the periosteal surface (Fig 4.4 C) but no difference in resorption (Fig 4.4 E). On the endocortical surface, bone formation increased, but to a much smaller degree than on the periosteal surface; the variation between strains remained (Supp Fig 4.13). NZO females increased bone resorption in response to loading on the endocortical surface, opposite what was seen on the periosteal surface. As populations, both the Inbred Founder and DO population had an average increase in resorption in response to loading on the endocortical surface. No differences were seen between the Inbred Founders and DO population for endocortical formation, but DO mice had significantly higher increases in endocortical resorption (Supp Fig 4.13). In summary, we saw strain and sex-dependent variations in bone formation and

resorption patterns in response to loading, with the Diversity Outbred population demonstrating a greater overall response compared to the Inbred Founders on the periosteal surface.

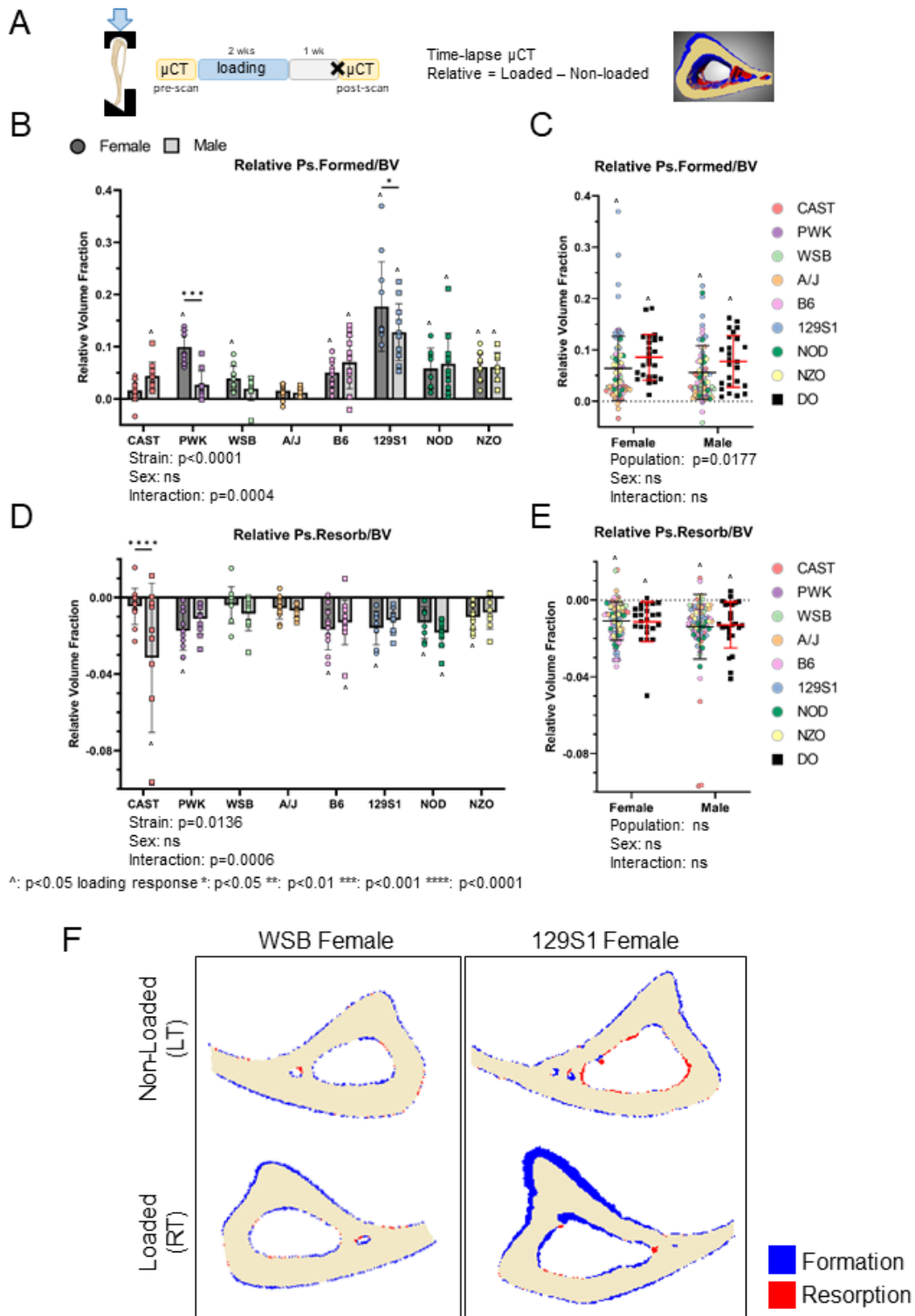


Figure 4.4: Bone formation and resorption on the periosteal surface measured from image-registered time-lapse μ CT.

A) Timeline of μ CT and loading. Pre-scans and post-scans were registered and rotated to a shared geometric space. B) Relative increase in periosteal formed volume fraction of the Inbred Founders have significant strain and strain-sex interaction terms. C) The DO mice have a larger average increase formed volume than the pooled Inbred Founders. D) Relative decrease in periosteal resorbed volume fraction of the Inbred Founders have significant strain and strain-sex interaction terms. E) The DO mice respond to the same degree as the Inbred Founder population. F) Representative cross-sections from a lowly responding strain (WSB) and a highly responding strain (129S1).

4.4.3 Increases in mineralizing surface and mineral apposition rate vary with mouse strain and sex

To assess bone formation/mineralization in response to loading, we quantified fluorochrome labels from dynamic histomorphology (Fig 4.5 A). On the periosteal surface, mineralized surface (MS/BS), mineral apposition rate (MAR), and bone formation rate (BFR/BS) all varied with mouse strain (Fig 4.5 B, Supp Fig 4.14). Mineralizing surface (an indicator of active osteoblast number) and mineral apposition rate (an indicator of osteoblast activity) also have a significant strain/sex interaction (Supp Fig 4.14). Inbred strain 129S1 had the largest increase in all dynamic histomorphology parameters. Ten of the sixteen strain/sex groups had significant increases in periosteal bone formation rate while five strain/sex groups had significant increases on the endocortical surface (Fig 4.5 B,D). For every mouse strain, the loading response on the endocortical surface had a lower magnitude than the periosteal surface. Fewer significant sex differences were seen within individual strains; only r.Ps.MS/BS was significantly different between PWK males and females, and r.Ec.MS/BS between NOD males and females. Compared to the Inbred Founders, the DO population had larger increases in periosteal bone formation rate but no difference in endocortical bone formation rate (Fig 4.5 C,E). This was driven by larger increases in mineralizing surface in the DO population (Supp Fig 4.14). In summary, we demonstrated strain-dependent variation in bone formation on both the endocortical and periosteal surfaces, with the Diversity Outbred population exhibiting greater increases in periosteal bone formation compared to the Inbred Founders.

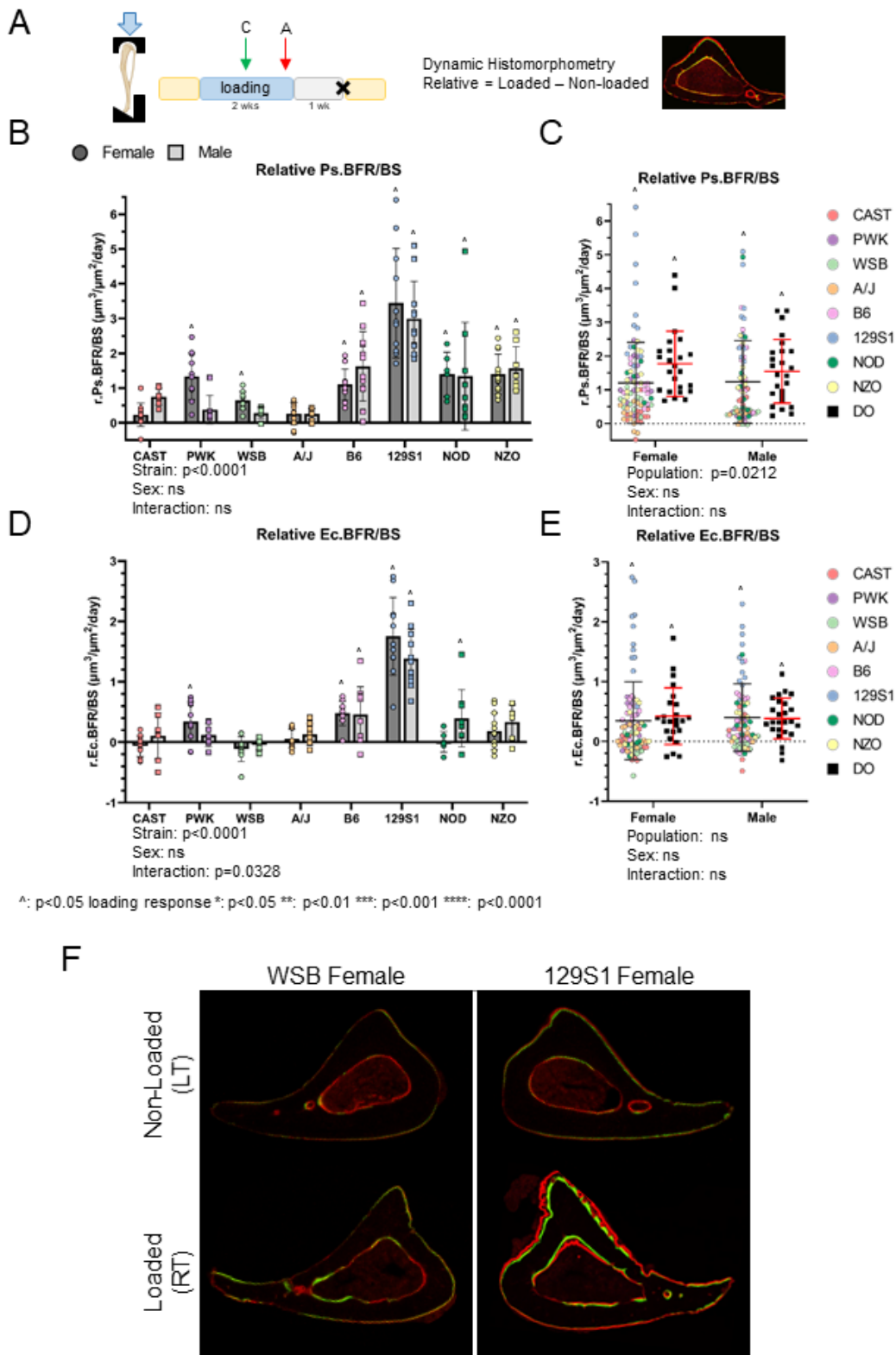


Figure 4.5: Bone formation rate on the periosteal and endocortical surfaces measured from dynamic histomorphometry. A) Timeline of loading and fluorochrome injections. Calcein and alizarin were given a week apart. B) Relative increase in periosteal bone formation rate of the Inbred Founders have significant strain term. C) The DO mice have a larger average increase in bone formation rate than the pooled Inbred Founders. D) Relative increase in endocortical bone formation rate of the

Inbred Founders have significant strain and strain-sex interaction terms. E) The DO mice respond to the same degree as the Inbred Founder population. F) Representative cross-sections from a lowly responding strain (WSB) and a highly responding strain (129S1).

4.4.4 Bone response to mechanical loading is highly heritable

Broad-sense heritability was calculated for each loading response variable measured in the Inbred Founder strains (Table 4.1). Endocortical bone formation rate had the highest heritability (97%) while endocortical mineralized surface had the lowest heritability (32%). All measurements of periosteal formation/expansion had heritability values over 79%.

Table 4.1: Heritability (H^2) of all relative outcomes (relative = loaded – nonloaded) measured in the Inbred Founders.

Trait	Heritability (H^2)
Ec.BFR/BS	0.970
Ct.Ar	0.953
Ps.MAR	0.950
Ct.Th	0.946
Ps.BFR/BS	0.943
Ec.MAR	0.936
Ec.Form/BV	0.921
pMOI	0.893
Ps.MS/BS	0.870
Ct.Ar/Tt.Ar	0.860
Tt.Ar	0.850
Ps.Formed/BV	0.792
Ma.Ar	0.546
TMD	0.459
Ec.Resorb/BV	0.436
Ps.Resorb/BV	0.355
Ec.MS/BS	0.317

μCT Morphology
 Timelapse μCT
 Dynamic Histomorphology

4.4.5 Stiffer bones respond more to mechanical loading

Correlation analyses were performed to examine whether relative periosteal bone formation rate was associated with measures of bone phenotype, in the Inbred Founder population and DO population separately. Relative periosteal bone formation rate was selected as a representative outcome for periosteal anabolic response. In both populations, relative bone formation rate was

positively and significantly correlated with axial stiffness (Fig 4.6). In the Inbred Founders (Fig 4.7 A), weak correlations were seen between bone morphology and loading response, except for loading induced-change in pMOI. Loading-induced change in pMOI was positively correlated with original cortical area, total area, medullary area, and pMOI. In the DO population (Fig 4.7 B), weakly positive correlations were seen between original cortical area and many loading outcomes. In summary, stiffer bones consistently responded more to mechanical loading, but few morphology μ CT outcomes correlated strongly with loading response.

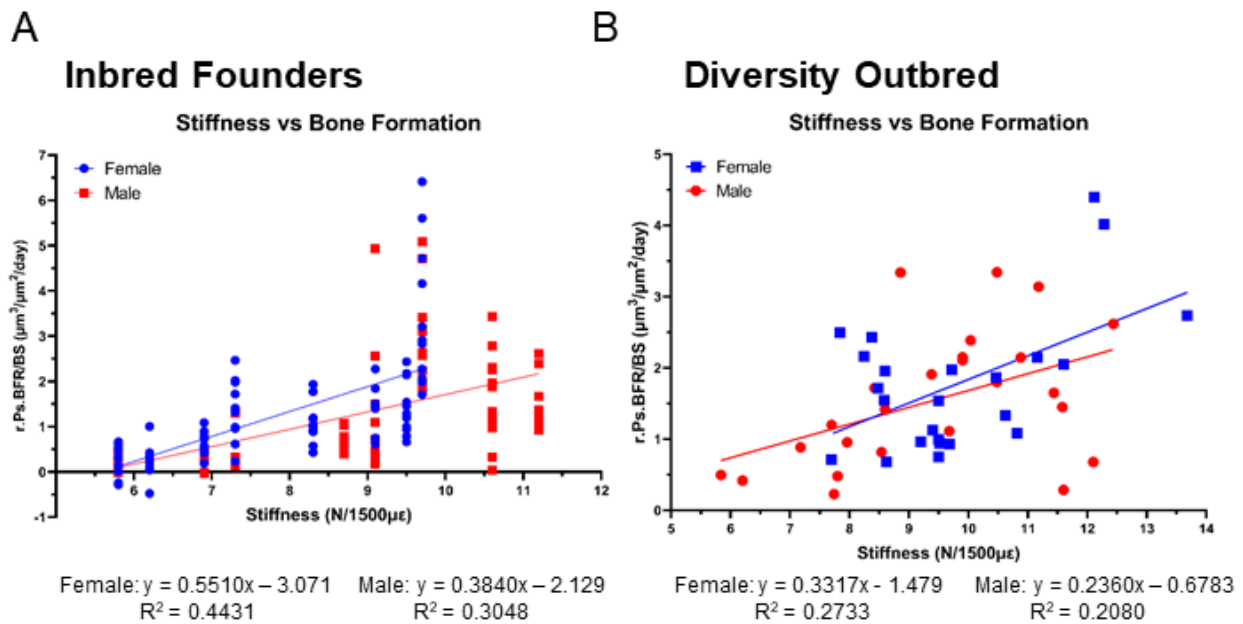
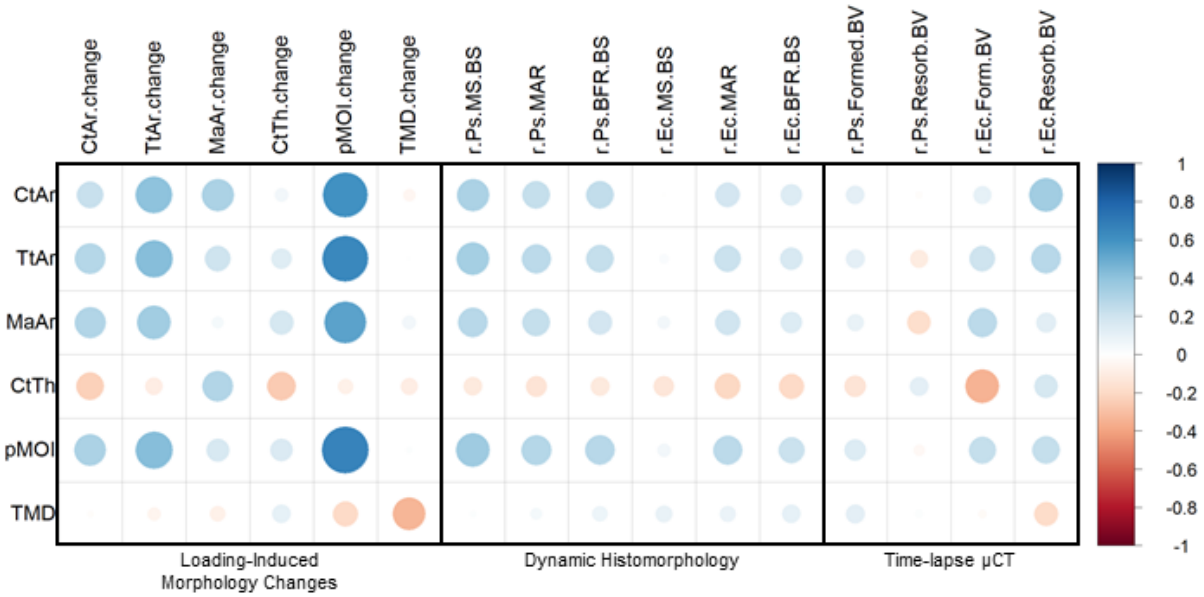


Figure 4.6: Correlation between bone axial stiffness and response to loading. A) Stiffness positively correlates with relative periosteal bone formation response in the Inbred Founder strains and B) DO mice. For all linear regressions, the slope is significantly greater than zero.

A

Inbred Founders



B

Diversity Outbred

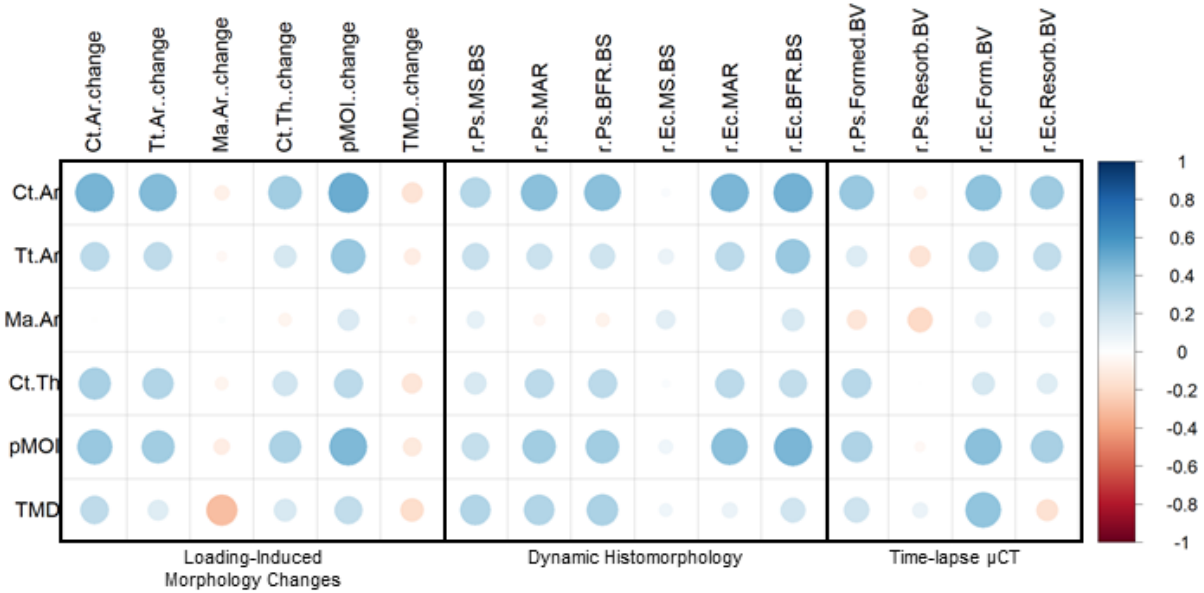


Figure 4.7: Correlation matrix of Pearson's coefficients between starting μ CT parameters (pre-loading) and all loading response outcomes.

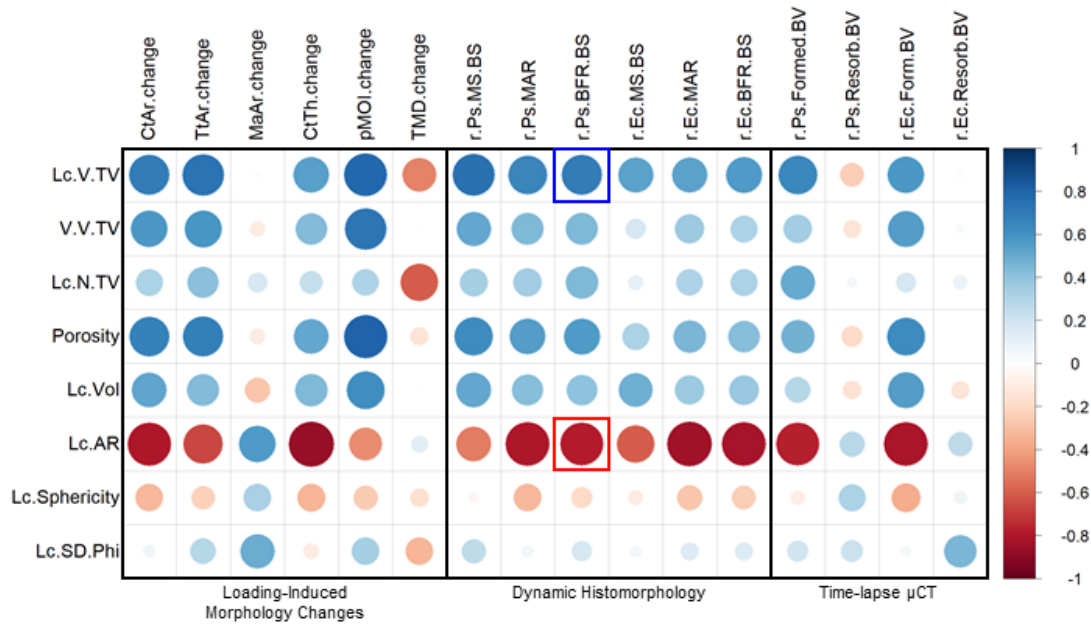
A) Correlations in the Inbred Founder strains show weak correlations, except for change in pMOI and pre-loading morphology.
 B) Correlations in the DO mice slightly stronger correlations are seen specifically with pre-loading cortical area and loading outcomes. Black boxes group the method of quantification for loading outcomes.

4.4.6 Mouse strains with more elongated lacunae respond more to mechanical loading

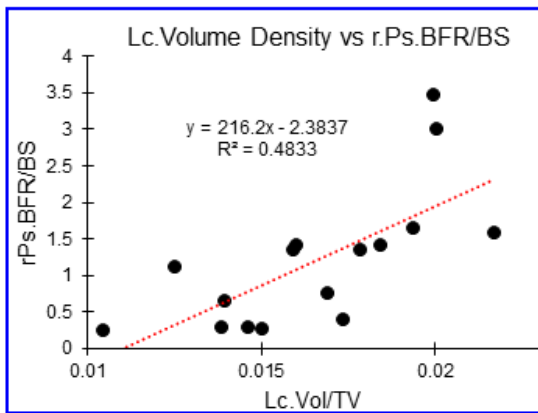
Because osteocytes are known to be a mechanosensitive and responsive cell in bone, we correlated bone response to loading with lacunar morphology traits. In our previous work (Chapter 3) lacunar traits were evaluated using x-ray microscopy in the eight Inbred Founder strains and we reported significant variation between strains. We correlated the average value per strain/sex group for all measured loading response traits to the average value per strain/sex group for all lacunar traits (Fig 4.8 A). Lacunar volume density (Lc.Vol/TV) positively correlated with many loading outcomes; strain/sex groups with greater lacunar volume fraction responded more to mechanical loading (Fig 4.8 B). Lacunar aspect ratio (Lc.AR) negatively correlated with many loading outcomes; strain/sex groups with more elongated lacunae responded more to mechanical loading (Fig 4.8 C).

A

Inbred Founders



B



C

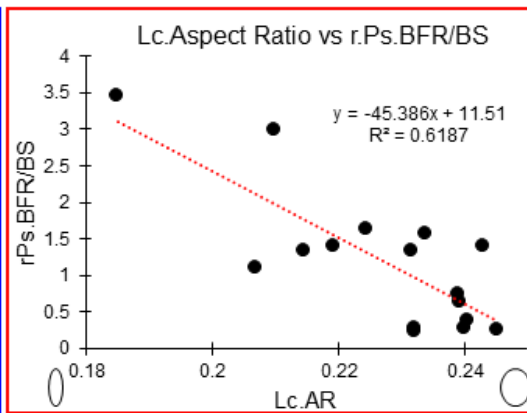


Figure 4.8: Correlation matrix of Pearson's coefficients for average lacunar traits and loading outcomes in the Inbred Founder strains.

B) The blue box highlights the strong, positive correlation between lacunar volume density and periosteal bone formation rate.
 C) The red box highlights the strong, negative correlation between lacunar aspect ratio and periosteal bone formation rate. A smaller aspect ratio represents a more elongated lacuna.

4.5 Discussion

In our study, we employed two models of genetic diversity to investigate the variability of anabolic response to mechanical loading depending on genetic background. Our findings revealed that the loading response exhibited significant variability across different mouse strains.

Notably, we observed moderate to high heritability in all measurements of loading response,

indicating a strong genetic component underlying bone's adaptive capacity. Within the inbred strains, 129S1 demonstrated the highest magnitude of response on both the periosteal and endocortical surfaces. Conversely, the A/J strain exhibited the lowest response, while the B6 strain displayed a moderate response. Moreover, our study revealed sex differences in the mechanoresponsive behavior of wild-derived strains, with CAST males and PWK females displaying heightened responsiveness compared to their opposite sex. Comparing the inbred and outbred populations, the DO population showed a more robust response to mechanical loading. Additionally, bone axial stiffness and lacunar traits correlate with the magnitude in loading outcomes. Overall, genetic background significantly contributes to cortical bone response to loading, which indicates genetic control of mechanoresponsiveness.

We tested three hypotheses using two models of genetic diversity. Our data supports our first hypothesis; the change due to loading for all traits measured, except TMD, varied significantly with mouse strain. (Changes to TMD with loading were not expected since the newly formed bone will have very similar density to the existing bone and the μ CT does not have the resolution to detect small differences if they exist.) Additionally, broad-sense heritability for all outcomes measuring periosteal formation was near or above 80%, matching the high heritability values reported by Kesavan et al¹²⁸. Among the mouse strains subjected to loading, only the B6 strain had previously been loaded, highlighting the novelty of our investigation in other strains. A recent study by Friedman et al. investigated the response to *unloading* in male Inbred Founder mice¹⁸⁶ using a single-limb casting model. In the cortical mid-diaphysis of the femur, they found B6 mice had the greatest loss of bone tissue, while we saw B6 had a moderate response to *loading*. They reported the largest effects of unloading in the trabecular region. The only two inbred strains without a significant decrease in epiphyseal BV/TV were A/J and 129S1. When

combined with our findings, it appears A/J mice are unresponsive to both loading and unloading interventions, whereas 129S1 are highly sensitive to loading, but not to unloading. Most previously published loading studies, including the unloading study of the Inbred Founder mice¹²¹, have not directly compared the outcomes between male and female mice. We found significant sex effect or a sex/strain interaction in 13 of the 16 measured trait changes. Notably, r.Ps.BFR/BS and r.Ec.MAR do not vary with sex. The sex/strain interaction highlights the complex interplay between genetic factors and sex. However, when all Inbred Founders are evaluated as a population, there is no systemic difference between how the two sexes respond to mechanical loading.

Contrary to our second hypothesis, our data indicate that the outbred mouse population (DO) have a heightened response to mechanical loading. We saw significantly higher increases in bone area, total area, pMOI, periosteal formed volume fraction, and periosteal bone formation rate in the DO population compared to the Inbred Founder population. While some Inbred Founder mice had zero or even negative relative values for these formation outcomes, all DO animals had positive increases. On the other hand, very few DO mice had larger increases in response to loading than the most response Inbred Founder (129S1). In partial contrast, results from 4-pt tibial loading of the second generation (F2) of a C3HxB6 intercross, Kesevan et al. showed the average response in F2 mice were in between the average of inbred C3H and B6, but the range did extend lower than C3H and higher than B6¹²⁸. While it is difficult to compare an intercross of two inbred strains to DO mice that have a combination of alleles from eight founders, results from both show that the loading response is highly variable and does not simply replicate the average response from the original founders. To our knowledge, this the first report of

mechanical loading of DO mice, and our results provide novel data that genetically diverse mice will exhibit a range of bone mechanoresponsiveness.

Supporting our third hypothesis, we saw many significant correlations with baseline phenotype and response to loading. Specifically, the correlation between bone axial stiffness and response to loading was maintained in both populations of genetic diversity investigated; stiffer bones responded more to mechanical loading. However, correlations between homeostatic, baseline morphology and the response to loading was slightly different between the two populations. In the Inbred Founders we saw strong correlations to change in pMOI, but this was diminished in the DO population. Baseline cortical thickness was weakly, negatively correlated to many loading outcomes in the Inbred Founders but weakly, positively correlated to many loading outcomes in the DO population. Weaker correlations may have been observed due to the smaller variation in both baseline morphology as well as the response to loading in the DO population compared to the Inbred Founder population. Correlations between lacunar morphology and loading response were only investigated in the Inbred Founder population. Overall, these correlations were much stronger than those seen for baseline morphology. Bones with greater lacunar volume fraction and more elongated lacunae respond more to mechanical loading. This contradicts the findings from Robling and Turner which correlated the osteocyte lacunar number density in B6, C3H, and DBA to their response to axial, ulnar mechanical loading. In the three inbred strains they loaded, they did not see a clear relationship between osteocyte density and mechanosensitivity¹⁰⁸. Differences in results are possibly due to differences in the bone evaluated, how the lacunae were analyzed, and how many mouse strains were evaluated. Using more inbred strains with a larger range of both lacunar density and loading response revealed a correlation not previously detected. These correlations at both the whole-bone and lacunar length

scales highlight the importance of considering not only the genetic background but also the underlying bone phenotype when assessing mechanoresponsiveness.

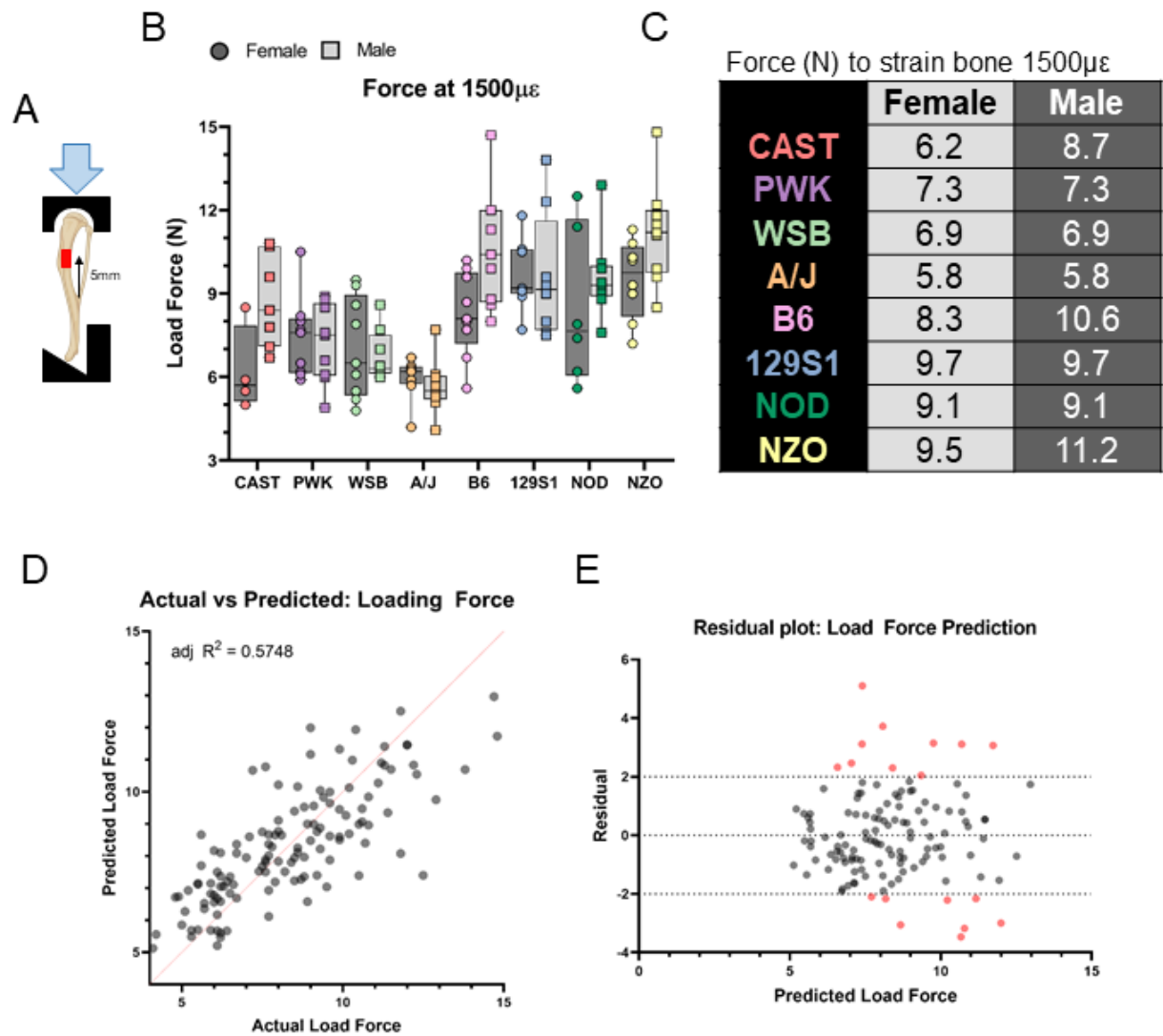
Image-registration has been used by other groups to quantify bone's response to mechanical loading, and they have shown it is sufficiently sensitive to detect decreases in mechanoresponsiveness with aging¹⁸². The current study supports the use of this technique to measure bone response across a wide range of values. When compared to the gold standard of dynamic histomorphology, we found an R^2 value close to 0.90 (Supp Fig 4.11). Additionally, this is the only method available to quantify resorption, which we find also varies with genetic background. Using a time-lapse μ CT technique instead of dynamic histomorphology, future studies would allow bones to go to a different destructive outcome such as gene expression, immunohistochemistry, mechanical loading, or high-resolution imaging. However, using μ CT to detect changes in bone does have limitations. Enough time must pass between the pre-scan and post-scan to allow enough change to occur to be above the resolution detection level of the μ CT scanner being used. In this study, 3 weeks separated the pre-scan and post-scan to allow for more change than the resolution of the μ CT scans (10.5 μ m/pixel).

While this work has many novel outcomes, there still exist some limitations. First, we observed (but did not quantify) large differences in baseline activity between the different mouse strains. The level of loading intensity and frequency at baseline could alter the response to our specific loading intervention. To attempt to control for this, all loading parameters reported were relative values isolating the response in the loaded limb compared to the non-loaded limb. Second, the estimation of loading force to achieve strain-matched loading for the DO has a large range of error. While the average accuracy of the model was 32 $\mu\epsilon$, the range was approximately +/- 500 $\mu\epsilon$. However, this error was randomly distributed across all loading forces (Supp Fig 4.10 A),

and we found no significant correlation of estimated strain produced by the loading force to response to loading (Supp Fig 4.10 B). Thus, while the error of the force estimation adds variability to the population it does not bias our results. Third, the values for the lacunar traits used in our correlation were not measured from the same animals that were loaded. The values were averages for each strain/sex group reported in Chapter 3. While we believe the values are representative since the mice within a strain/sex group are genetically identical, there could be differences due to batch effects and biologic variation. Future work is needed to investigate the lacunar morphology of loaded animals.

Taken together, our findings demonstrate the substantial impact of genetic background on the cortical bone response to mechanical loading, affirming the role of genetic control in determining mechanoresponsiveness. The response to mechanical loading, measured with three methods, significantly varied with inbred mouse strain. We have also provided a method to load genetically unique animals without the need of strain gauging allowing for future use of the DO mice to study bone mechanobiology. Using this method, we loaded a cohort of 50 DO mice and were able to show an enhanced response to loading in the outbred population compared to the average of the Inbred Founders. This work provides the groundwork and rationale to perform genome wide association studies (GWAS) and quantitative trait loci (QTL) analysis to identify candidate genes regulating the response to loading. Uncovering novel genes can provide new targets for therapeutics to not just halt the bone loss associated with osteoporosis but also increase bone mass, therefore decreasing fracture risk.

4.6 Supplemental Information

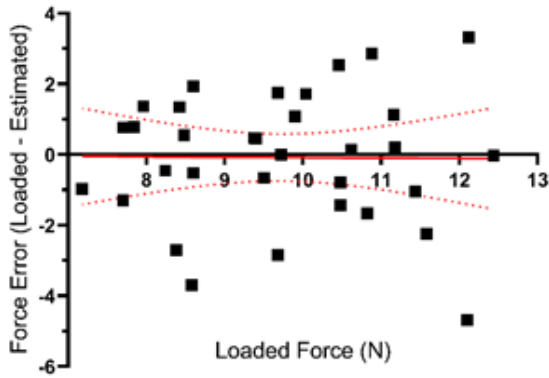


$$Force = 14.98 - 5.38(T. Ar) + 24.1(Ct. Ar) - 0.07(Weight) - 13.68(AreaRatio) - 10.98(Eccentricity)$$

Supplemental Figure 4.9: Strain gauge data from the Inbred Founder strains.

A) A strain gauge was glued 5 mm proximal to the distal tibiofibular junction (TFJ) while load was applied. B) The necessary force to engender 1500 $\mu\epsilon$ was calculated for non-loaded Inbred Founder strain mice. These mice were phenotyped in Chapter 3. C) The average force per strain/sex group that was used to load animals in this study. D) Results from the multi-variable linear regression showing the predicted loading force from the model compared to the actual load force calculated from strain gauging. E) Residuals are mainly between -2N and +2N.

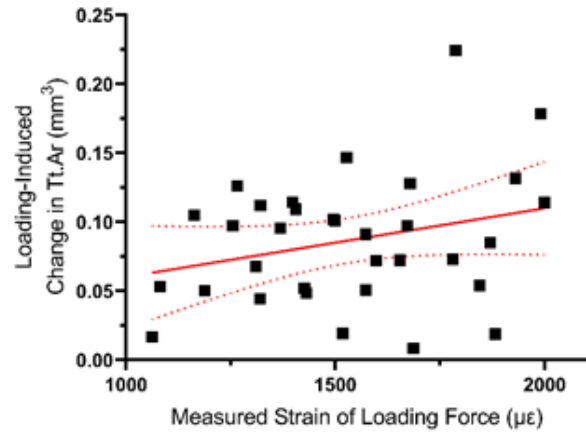
A



$$Y = -0.01146 * X + 0.03167$$

Slope not significantly different from zero

B



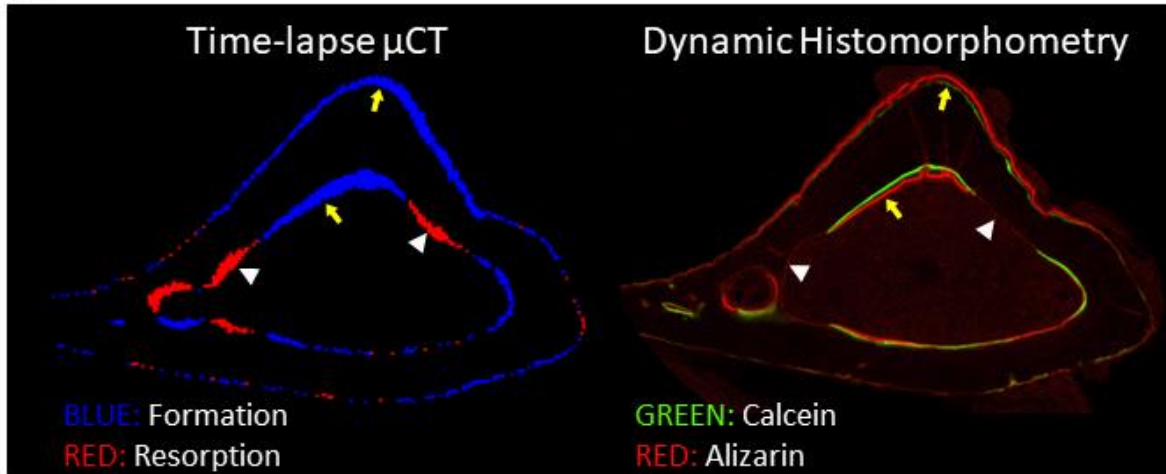
$$Y = 4.983e-005 * X + 0.01031$$

Slope not significantly different from zero

Supplemental Figure 4.10: Force estimation error in the DO mice.

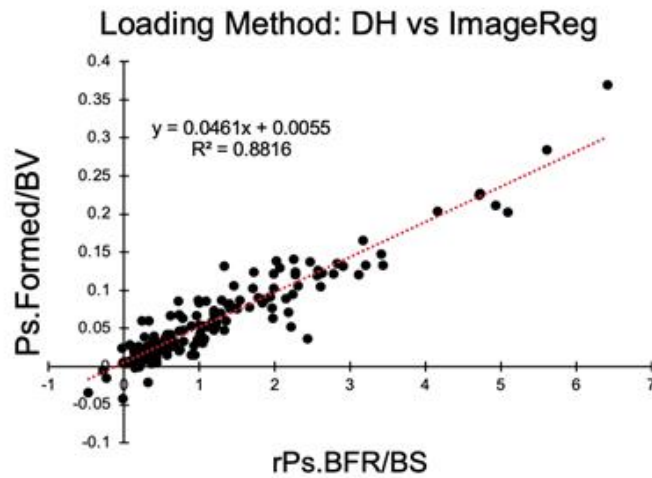
A) The error in loading force calculated from strain gauging DO mice after loading are evenly distributed across loading forces. The regression slope is not different from zero. B) Correlation of the strain DO mice were loaded to with loading-induced change in total area. The slope is not different from zero indicating there is no relationship between the error in loading force and bone formation.

A



Yellow arrow: region of **formation** from μ CT corresponds to **double** fluorochrome labeling
White arrowhead: region of **resorption** from μ CT corresponds to **no** fluorochrome labeling

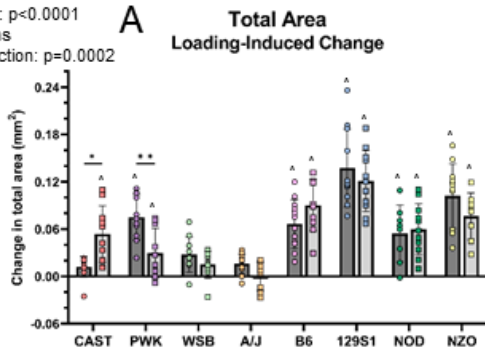
B



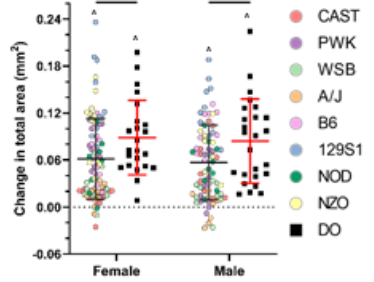
Supplemental Figure 4.11: Validation of image-registered time-lapse μ CT.

A) Cross-section of the same bone from image registration and dynamic histomorphometry show formation in the same regions (yellow arrow). Regions of bone resorption (white arrowhead) can only be measured from image-registered time-lapse μ CT. The regions of resorption correspond to regions with no fluorochrome label. B) Correlation between loading response measured from the gold-standard dynamic histomorphology (relative periosteal bone formation rate) and the newer image registration (periosteal formed volume fraction).

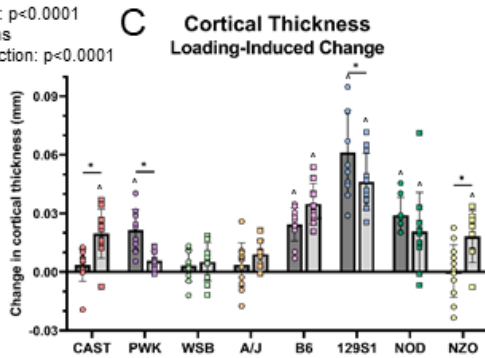
Strain: $p < 0.0001$
 Sex: ns
 Interaction: $p = 0.0002$



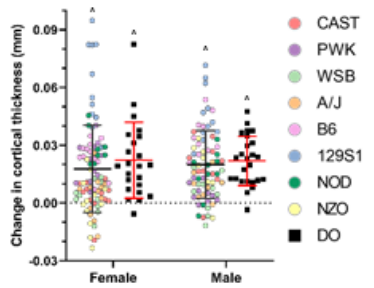
Population: $p = 0.0010$
 Sex: ns
 Interaction: ns



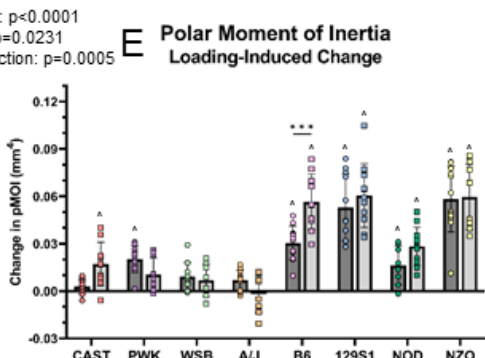
Strain: $p < 0.0001$
 Sex: ns
 Interaction: $p < 0.0001$



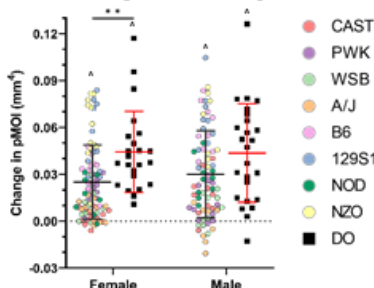
Population: ns
 Sex: ns
 Interaction: ns



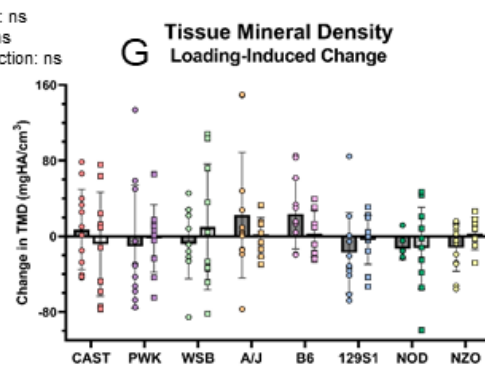
Strain: $p < 0.0001$
 Sex: $p = 0.0231$
 Interaction: $p = 0.0005$



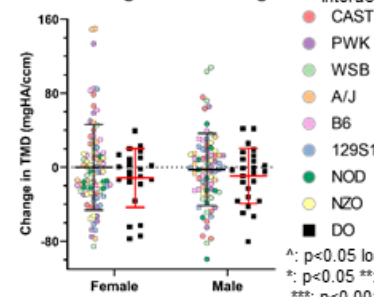
Population: $p = 0.0002$
 Sex: ns
 Interaction: ns



Strain: ns
 Sex: ns
 Interaction: ns

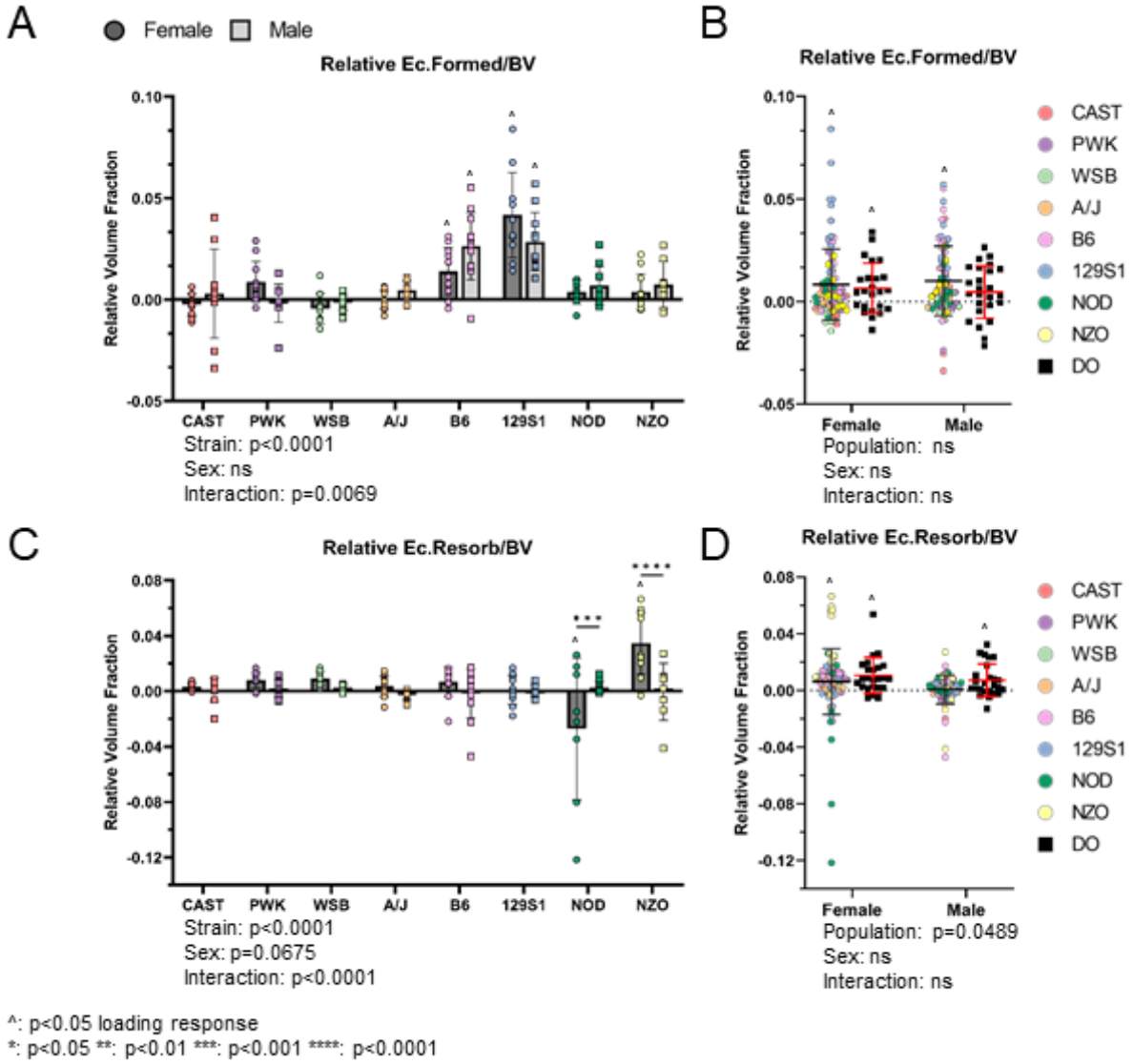


Population: ns
 Sex: ns
 Interaction: ns

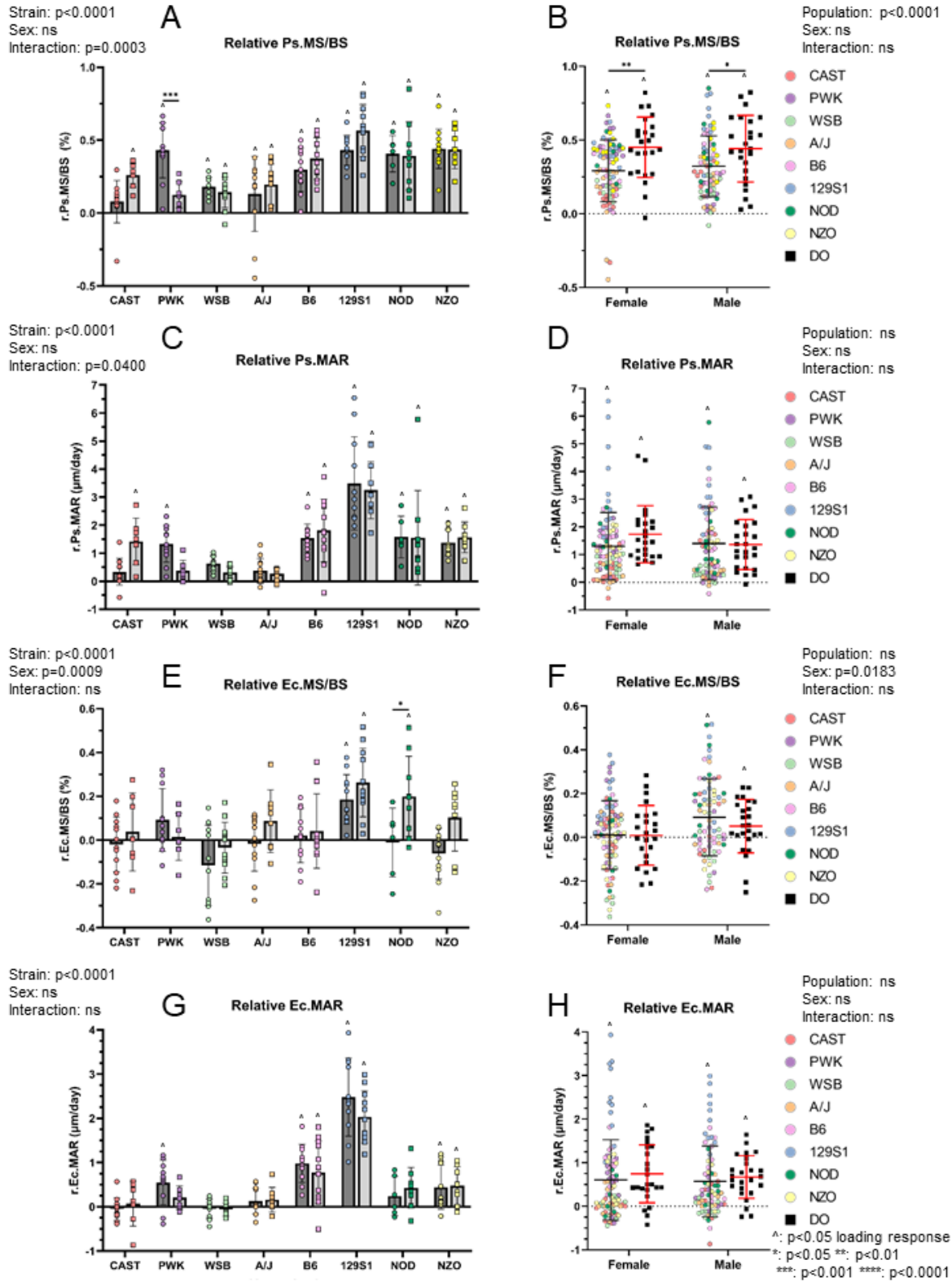


^: $p < 0.05$ loading response
 *: $p < 0.05$ **: $p < 0.01$
 : $p < 0.001$ *: $p < 0.0001$

Supplemental Figure 4.12: Loading-induced changes in bone morphology not shown in Fig 4.3.



Supplemental Figure 4.13: Relative bone response on the endocortical surface measured from image-registered time-lapse μ CT.



Supplemental Figure 4.14: Relative dynamic histomorphometry outcomes not reported in Fig 4.5. Mineralized surface (MS/BS) (A, B, E, F) measured the number of osteoblasts. Mineral apposition rate (MAR) (C, D, G, H) measures the work per osteoblast.

Chapter 5: Conclusions and Future Directions

5.1 Conclusions

Bone is a complex and dynamic organ that responds to the mechanical demands placed on it, yet the health, strength, and ability to remodel declines with age. Osteoporosis is a large and growing public health burden and understanding how bone is maintained in the adult skeleton can provide insight in how to increase bone health in the aged skeleton. My goal in this dissertation was to understand the role of genetic diversity on bone traits and its ability to remodel. First, I investigated the effect of genetic diversity on bone traits across length scales by quantifying bone phenotypes in eight Inbred Founder mouse strains and Diversity Outbred mice. Next, I investigated the effect of genetic diversity on the response of bone to mechanical stimulation by loading the tibia of the same two mouse populations that I phenotyped. Finally, I correlated the phenotype data to the loading response to investigate what traits are highly correlated to mechanoresponsiveness.

Cortical bone traits, from the whole-bone down to the mineral composition, vary with genetic background and have non-zero heritability. However, the relationships between bone traits within a single animal are maintained in three different populations that were investigated providing support that these relationships are conserved for all strains of *Mus musculus*. This was highlighted by the almost identical linear regression between bone area and ultimate force in the Inbred Founder population and the DO population. The most variability between mouse strains was seen in morphology and mechanical properties while less variability was seen for material properties and bone composition. The bone that is created by each mouse is relatively similar, yet how the bone is distributed throughout the skeleton highly varies. While the mice spanned

large ranges in body mass and skeletal size (BMC), the differences in cortical bone traits were retained after adjustment for body mass implying there are genes that independently control bone traits and body size. The genetically unique outbred mice (DO) appeared healthier compared to the Inbred Founders, being larger, heavier, and protected from hyperglycemia. These outbred mice (DO) have cortical bones that do not resemble a single Inbred Founder strain, but instead demonstrate intermediate phenotypes that eliminate extreme values. Overall, genetic background significantly contributes to cortical bone phenotype implying genetic control of bone traits across length scales.

The ability of bone to remodel in response to mechanical stimulation also highly varies with genetic background and is highly variable. All measures of periosteal bone formation showed heritability values near or above 80%. Inbred strain 129S1 had the highest response to loading while strain WSB had a significant, but low response to loading. Inbred strain A/J appears unresponsive to mechanical stimulus, either loading or unloading¹²¹. In addition to variability with mouse strain, we also discovered a complex interplay between sex and genetic background. While there were differences in the response to loading between male and female mice in certain Inbred Founder strains, there were no systemic differences between male and female mice when all Inbred Founder mice were evaluated as a population or in the Diversity Outbred mice. Taken together, our findings demonstrate the substantial impact of genetic background on the cortical bone response to mechanical loading, affirming the role of genetic control in determining mechanoresponsiveness.

There were many significant correlations between bone phenotype and bone ability to respond to loading. Specifically, stiffer bones responded more to mechanical loading. This was conserved in both the Inbred Founder mice and Diversity Outbred mice. Additionally, lacunar-level traits and

morphology highly correlated with response to loading. Bones with a higher lacunar volume fraction, but less so a higher lacunar number fraction, responded more to an equal mechanical stimulus. Bones with more elongated lacunae (smaller aspect ratio) also responded more to an equal mechanical stimulus. These correlations highlight the importance of considering not only the genetic background but also the underlying bone phenotype when assessing mechanoresponsiveness.

This work shows the response to mechanical loading is highly heritable implicating a large role of genetics in mechanosensitivity of osteocytes. My working model is that genetics drives intrinsic mechanosensitivity of osteocytes and this drives bone morphology to maintain an equilibrium strain state. Based off the mechanostat theory^{88,187}, the equilibrium strain state of bone should be at the mechano-threshold of loading or unloading response. If homeostatic strain were above the mechano-threshold, bone would constantly be forming, and the reverse would occur if the homeostatic strain were below the mechano-threshold. More mechanosensitive osteocytes have a lower strain threshold to initiate an anabolic response. Therefore, under daily loading and homeostasis, the bone must be kept at a low strain level. To do this, we propose the bone becomes stiffer to maintain a low strain state. Conversely, lowly sensitive bones have a higher strain threshold and can afford to have less stiff bones to maintain a high strain state at equilibrium (Fig 5.1). This is supported by our data since we see more stiff bones are more responsive to loading. At the lacunar level, osteocytes can reduce the strain state around them by creating more elongated ellipsoidal shapes. The long axis of the osteocyte lacunae is typically in the direction of loading. Therefore, a more elongated lacunae will amplify the strain less than a more circular lacunar pore^{174,188} (Fig 5.1). This is supported by our data since we see more elongated lacunae respond more to mechanical loading. Additionally, this model is supported by

what is seen with aging in bone. During aging the mechanosensitivity of bone declines as well as the overall stiffness and elongation of lacunae³⁹. Using a *Dmp1Cre Piezo1^{fl/fl}* mouse model Li et al showed a decrease in mechanosensation and response to loading paired with a reduction of bone stiffness when the mechanically sensitive Piezo1 channels were knocked out in mature osteoblasts and osteocytes¹⁸⁹. While these changes were not due to an increase in osteocyte death, the lacunae were not thoroughly evaluated. More work is needed to investigate the lacunar morphology to see if upon reduction of mechanosensation in osteocytes the lacunae adapt to a less elongated state.

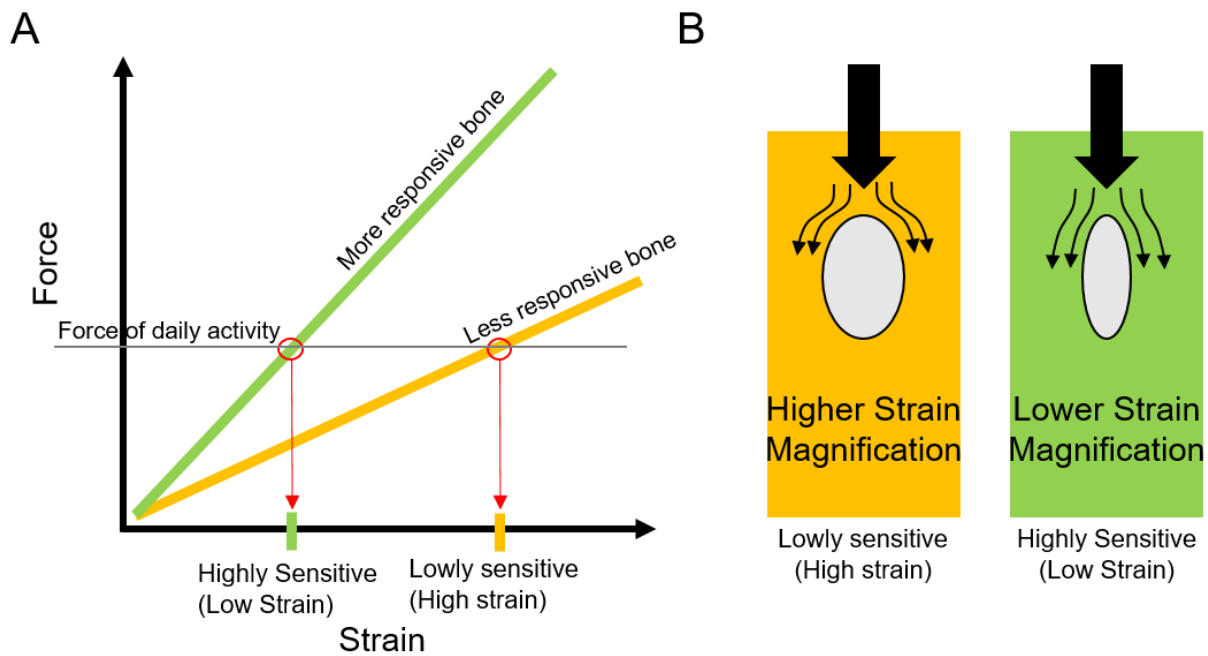


Figure 5.1: Working model that osteocyte mechanosensitivity drives the morphology of cortical bone. Bones with more sensitive osteocytes will develop stiffer bones with more elongated lacunae to maintain a low strain state.

5.2 Future Directions

The work in this thesis supports the use of these mouse models to further investigate the effects of genetic variability in bone research. Now that we know how the response to loading differs between the eight Inbred Founder strains, future studies can focus on the mechanistic reasons why. Investigating the gene expression responses of the Inbred Founders can provide insight into

what pathways are activated and if they differ with genetic variability. Comparing similarly responding strains, you can investigate if the activation of different genes and biological pathways lead to the same amount of bone or if the upregulated pathways are conserved. This will provide insight into whether there are multiple pathways to make bone that could potentially be therapeutically activated. Comparing high and low responding strains, you can investigate if the magnitude of gene regulation scales with eventual bone formation. Genes differentially expressed early (Day 1) after loading represent the mechanosensation (sensing mechanical stimulus) response while genes differentially expressed later (Day 5) after loading represent the mechanotransduction (relaying message to form bone) response⁸³. Comparing these two time points, you can investigate if both mechanosensation and mechanotransduction are different between the different mouse strains.

The work in this thesis is also the first instance where genetically unique mice have been mechanically loaded. Traditionally, a genetically identical calibration set of mice is needed for strain gauging to determine a loading force to engender equal strain. The generation of the multi-variable linear regression used in this thesis to estimate loading force lays the groundwork to use the Diversity Outbred (DO) mice in large-scale genetic studies including genome-wide association studies (GWAS) and quantitative trait loci (QTL) analysis. These studies require the use of hundreds of animals but allow for specific regions of the genome to be identified as potentially causing the phenotype of interest. Future studies can identify and validate candidate genes that are responsible for an increased or decreased response to loading. These genes could then be targets for new therapeutic drugs to increase bone formation alone or in conjunction with loading.

The work in this thesis provides support that genetic diversity highly affects both bone phenotype and its ability to remodel in response to mechanically loading. It is the first study to investigate the lacunar morphology across genetically different mice and to show these lacunar differences are correlated to loading response. This is also the first study to mechanically load genetically unique (DO) mice laying the groundwork for genetic studies to discover novel genes regulating the magnitude of bone response to mechanical loading. Uncovering novel genes can provide new targets for therapeutics to increase bone mass providing a new treatment strategy for osteoporosis.

References

1. Wright, N. C. *et al.* The recent prevalence of osteoporosis and low bone mass in the United States based on bone mineral density at the femoral neck or lumbar spine. *J Bone Miner Res* **29**, 2520–6 (2014).
2. Singer, A. *et al.* Burden of Illness for Osteoporotic Fractures Compared With Other Serious Diseases Among Postmenopausal Women in the United States. *Mayo Clin Proc* **90**, 53–62 (2015).
3. Beamer, W. G., Donahue, L. R., Rosen, I. C. J. & Baylink, D. J. *Genetic Variability in Adult Bone Density Among Inbred Strains of Mice*. *Bone* vol. 18 (1996).
4. Turner, C. H. *et al.* Genetic Regulation of Cortical and Trabecular Bone Strength and Microstructure in Inbred Strains of Mice. *Journal of Bone and Mineral Research* **15**, 1126–1131 (2000).
5. Brent Richards, J., Zheng, H.-F. & Spector, T. D. Genetics of osteoporosis from genome-wide association studies: advances and challenges. (2012) doi:10.1038/nrg3228.
6. Tam, V. *et al.* Benefits and limitations of genome-wide association studies. *Nat Rev Genet* **20**, 467–484 (2019).
7. Sabik, O. L., Medrano, J. F. & Farber, C. R. Genetic Dissection of a QTL Affecting Bone Geometry. (2017) doi:10.1534/g3.116.037424.
8. Mitlak, B. H., Burr, D. B. & Allen, M. R. *Pharmaceutical Treatments of Osteoporosis. Basic and Applied Bone Biology* (Elsevier Inc., 2013). doi:10.1016/B978-0-12-416015-6.00017-4.
9. Matsumoto, T. & Fukumoto, S. Recent advances in the management of osteoporosis. *F1000Research* vol. 6 Preprint at <https://doi.org/10.12688/f1000research.10682.1> (2017).
10. Schilcher, J., Koeppen, V., Aspenberg, P. & Michaëlsson, K. Risk of atypical femoral fracture during and after bisphosphonate use: Full report of a nationwide study. *Acta Orthop* **86**, 100–107 (2015).
11. Anagnostis, P. *et al.* New therapeutic targets for osteoporosis. (2018) doi:10.1016/j.maturitas.2018.11.010.
12. Romosozumab: Drug information. https://www.uptodate.com/contents/romosozumab-drug-information?search=Romosozumab&topicRef=2064&source=see_link.

13. Parathyroid hormone/parathyroid hormone-related protein analog for osteoporosis. <https://www.uptodate.com/contents/parathyroid-hormone-parathyroid-hormone-related-protein-analog-for-osteoporosis#H934952735>.
14. Mohamed, A. M. F. S. An overview of bone cells and their regulating factors of differentiation. *Malaysian Journal of Medical Sciences* **15**, 4–12 (2008).
15. Anderson, H. C. Vesicles associated with calcification in the matrix of epiphyseal cartilage. *J Cell Biol* **41**, 59–72 (1969).
16. Friedenstein, A. J. Precursor Cells of Mechanocytes. *Int Rev Cytol* **47**, 327–359 (1976).
17. Stein, G. S. & Lian, J. B. Molecular Mechanisms Mediating Proliferation/Differentiation Interrelationships During Progressive Development of the Osteoblast Phenotype. *Endocr Rev* **14**, 424–442 (1993).
18. Walker, D. G. Osteopetrosis Cured by Temporary Parabiosis. *Science (1979)* **180**, 875 (1973).
19. Sims, N. A. & Martin, T. J. Osteoclasts Provide Coupling Signals to Osteoblast Lineage Cells through Multiple Mechanisms. *Annu Rev Physiol* **82**, 507–529 (2020).
20. Bonewald, L. F. Mechanosensation and Transduction in Osteocytes. *Bonekey Osteovision* **3**, 7 (2006).
21. Carter, Y. *et al.* Variation in osteocyte lacunar morphology and density in the human femur - a synchrotron radiation micro-CT study. *Bone* **52**, 126–132 (2013).
22. Robling, A. G., Daly, R., Fuchs, R. K. & Burr, D. B. *Mechanical Adaptation. Basic and Applied Bone Biology* (2019). doi:10.1016/B978-0-12-813259-3.00011-7.
23. Klein-Nulend, J., Van Oers, R. F. M., Bakker, A. D. & Bacabac, R. G. Bone cell mechanosensitivity, estrogen deficiency, and osteoporosis. *J Biomech* **48**, 855–865 (2015).
24. Klein-Nulend, J., Bakker, A. D., Bacabac, R. G., Vatsa, A. & Weinbaum, S. Mechanosensation and transduction in osteocytes. *Bone* **54**, 182–190 (2013).
25. Bonewald, L. F. Osteocyte mechanosensation and transduction. *Mechanosensing Biology* **9784431897**, 141–155 (2011).
26. Prideaux, M., Findlay, D. M. & Atkins, G. J. Osteocytes: The master cells in bone remodelling. *Curr Opin Pharmacol* **28**, 24–30 (2016).
27. Bonewald, L. F. The Amazing Osteocyte. doi:10.1002/jbmr.320.

28. Burger, E. H. & Klein-Nulend, J. Mechanotransduction in bone - Role of the lacuno-canalicular network. *FASEB Journal* **13**, (1999).
29. Kamel-Elsayed, S. A., Tiede-Lewis, L. M., Lu, Y., Veno, P. A. & Dallas, S. L. Novel approaches for two and three dimensional multiplexed imaging of osteocytes. *Original Full Length Article* (2015) doi:10.1016/j.bone.2015.02.011.
30. Schneider, P., Meier, M., Wepf, R. & Müller, R. Towards quantitative 3D imaging of the osteocyte lacuno-canalicular network. (2010) doi:10.1016/j.bone.2010.07.026.
31. Varga, P. *et al.* Synchrotron X-ray phase nano-tomography-based analysis of the lacunar–canalicular network morphology and its relation to the strains experienced by osteocytes in situ as predicted by case-specific finite element analysis. *Biomech Model Mechanobiol* **14**, 267–282 (2015).
32. Ganesh, T., Laughrey, L. E., Niroobakhsh, M. & Lara-Castillo, N. Multiscale finite element modeling of mechanical strains and fluid flow in osteocyte lacunocanalicular system. *Bone* 115328 (2020) doi:10.1016/j.bone.2020.115328.
33. Fritton, S. P. & Weinbaum, S. Fluid and Solute Transport in Bone: Flow-Induced Mechanotransduction. *Annu Rev Fluid Mech* **41**, 347–374 (2009).
34. CURREY, J. D. Stress Concentrations in Bone. *J Cell Sci* **s3-103**, (1962).
35. Han, Y., Cowin, S. C., Schaffler, M. B. & Weinbaum, S. Mechanotransduction and strain amplification in osteocyte cell processes. *Proc Natl Acad Sci U S A* **101**, 16689–94 (2004).
36. Zaman, G. *et al.* Mechanical strain stimulates nitric oxide production by rapid activation of endothelial nitric oxide synthase in osteocytes. *Journal of Bone and Mineral Research* **14**, 1123–1131 (1999).
37. Bacabac, R. G. *et al.* Round versus flat: Bone cell morphology, elasticity, and mechanosensing. *J Biomech* **41**, 1590–1598 (2008).
38. Donahue, H. J., Friendman, M. J. & Genetos, D. Osteocyte Mechanobiology in Aging and Disease. in *Mechanobiology* 1–21 (Elsevier, 2020). doi:10.1016/B978-0-12-817931-4.00001-7.
39. Hemmatian, H., Bakker, A. D., Klein-Nulend, J. & van Lenthe, G. H. Aging, Osteocytes, and Mechanotransduction. *Curr Osteoporos Rep* **15**, 401–411 (2017).
40. Tomlinson, R. E. & Silva, M. J. Skeletal Blood Flow in Bone Repair and Maintenance. *Bone Res* **1**, 311 (2013).

41. McCarthy, I. The physiology of bone blood flow: A review. *Journal of Bone and Joint Surgery* **88**, 4–9 (2006).
42. However, I. Flow to Canine Muscle , Hind-Limb Skin. (1969).
43. Hendriks, M. & Ramasamy, S. K. Blood Vessels and Vascular Niches in Bone Development and Physiological Remodeling. *Front Cell Dev Biol* **8**, 1–13 (2020).
44. Gross, P. M., Marcus, M. L. & Heistad, D. D. Measurement of blood flow to bone and marrow in experimental animals by means of the microsphere technique. *J Bone Joint Surg Am* **63**, 1028–1031 (1981).
45. Knothe Tate, M. L., Adamson, J. R., Tami, A. E. & Bauer, T. W. The osteocyte. *International Journal of Biochemistry and Cell Biology* vol. 36 1–8 Preprint at [https://doi.org/10.1016/S1357-2725\(03\)00241-3](https://doi.org/10.1016/S1357-2725(03)00241-3) (2004).
46. Dallas, S. L., Prideaux, M. & Bonewald, L. F. The Osteocyte: An Endocrine Cell. .. and More. (2013) doi:10.1210/er.2012-1026.
47. Office of the Surgeon General (US). Bone health and osteoporosis: a report of the Surgeon General. *US Health and Human Services* 437 (2004).
48. Burr, D. B. *Bone Morphology and Organization. Basic and Applied Bone Biology* (Elsevier Inc., 2019). doi:10.1016/b978-0-12-813259-3.00001-4.
49. Oftadeh, R., Perez-Viloria, M., Villa-Camacho, J. C., Vaziri, A. & Nazarian, A. Biomechanics and Mechanobiology of Trabecular Bone: A Review. *J Biomech Eng* **137**, 1–15 (2015).
50. Bjornerem, A. *et al.* Menopause-Related Appendicular Bone Loss is Mainly Cortical and Results in Increased Cortical Porosity. *Journal of Bone and Mineral Research* **33**, 598–605 (2017).
51. Dwek, J. R. The periosteum: what is it, where is it, and what mimics it in its absence? *Skeletal Radiol* **39**, 319 (2010).
52. Nahian, A. & Chauhan, P. R. Histology, Periosteum And Endosteum. *StatPearls* (2022).
53. Öhman-Mägi, C., Holub, O., Wu, D., Hall, R. M. & Persson, C. Density and mechanical properties of vertebral trabecular bone-A review. *JOR Spine* **4**, e1176 (2021).
54. D’Amelio, P. *et al.* Bone mineral density and Singh index predict bone mechanical properties of human femur. *Connect Tissue Res* **49**, 99–104 (2008).
55. Dalén, N., Hellström, L. G. & Jacobson, B. Bone mineral content and mechanical strength of the femoral neck. *Acta Orthop Scand* **47**, 503–508 (1976).

56. Ammann, P. & Rizzoli, R. Bone strength and its determinants. *Osteoporosis International* 2003 14:3 **14**, 13–18 (2003).
57. Ammann, P., Rizzoli, R., Meyer, J. M. & Bonjour, J. P. Bone density and shape as determinants of bone strength in IGF-I and/or pamidronate-treated ovariectomized rats. *Osteoporos Int* **6**, 219–227 (1996).
58. Lu, J., Shin, Y., Yen, M. S. & Sun, S. S. Peak Bone Mass and Patterns of Change in Total Bone Mineral Density and Bone Mineral Contents From Childhood Into Young Adulthood. *Journal of Clinical Densitometry* **19**, 180–191 (2016).
59. Ammann, P. & Rizzoli, R. Bone strength and its determinants. *Osteoporos Int* **14 Suppl 3**, 13–18 (2003).
60. Turner, C. H. & Burr, D. B. Basic biomechanical measurements of bone: A tutorial. *Bone* **14**, 595–608 (1993).
61. Arcan, M., Hashin, Z. & Voloshin, A. A method to produce uniform plane-stress states with applications to fiber-reinforced materials - A specially designed specimen yields material properties under pure shear or uniform plane-stress conditions. *Exp Mech* **18**, 141–146 (1978).
62. Iosipescu, N. New Accurate Procedure for Single Shear Testing of Metals. *J Mater* **1**, 145–164 (1967).
63. Walrath, D. E. & Adams, D. F. The Iosipescu shear test as applied to composite materials. *Exp Mech* **23**, 105–110 (1983).
64. Harrigan, T. P., Jasty, M., Mann, R. W. & Harris, W. H. Limitations of the continuum assumption in cancellous bone. *J Biomech* **21**, 269–275 (1988).
65. Forwood, M. R. & Parker, A. W. Effects of exercise on bone growth mechanical and physical properties studied in the rat. *Clinical Biomechanics* **2**, 185–190 (1987).
66. Einhorn, T. A. *et al.* Incorporation of sodium fluoride into cortical bone does not impair the mechanical properties of the appendicular skeleton in rats. *Calcif Tissue Int* **51**, 127–131 (1992).
67. Wallace, J. M. *Skeletal Hard Tissue Biomechanics. Basic and Applied Bone Biology* (Elsevier Inc., 2013). doi:10.1016/B978-0-12-416015-6.00006-X.
68. Jepsen, K. J., Silva, M. J., Vashishth, D., Guo, X. E. & Van Der Meulen, M. C. H. Establishing biomechanical mechanisms in mouse models: Practical guidelines for systematically evaluating phenotypic changes in the diaphyses of long bones. *Journal of Bone and Mineral Research* **30**, 951–966 (2015).

69. Julius Wolff. *The Law of Bone Remodelling*. (1986).
70. Frost, H. M. Wolff's Law and bone's structural adaptations to mechanical usage: an overview for clinicians. *Angle Orthod* **64**, 175–188 (1994).
71. Lanyon, L. E., Goodship, A. E., Pye, C. J. & MacFie, J. H. Mechanically adaptive bone remodelling. *J Biomech* **15**, 141–154 (1982).
72. Rowe, P., Koller, A. & Sharma, S. Physiology, Bone Remodeling. *StatPearls* (2023).
73. Rubin, C. T. & Lanyon, L. E. *Regulation of Bone Formation by Applied Dynamic Loads**.
74. LANYON, L. E. Control of Bone Architecture by Functional Load Bearing. *Journal of Bone and Mineral Research* **7**, S369–S375 (1992).
75. McBride, S. H. & Silva, M. J. Adaptive and injury response of bone to mechanical loading. *Bonekey Rep* **1**, (2012).
76. Turner, C. H. *Three Rules for Bone Adaptation to Mechanical Stimuli*. (1998).
77. Robling, A. G., Fuchs, R. K. & Burr, D. B. Mechanical Adaptation. *Basic and Applied Bone Biology* 175–204 (2013) doi:10.1016/B978-0-12-416015-6.00009-5.
78. Burr, D. B., Robling, A. G. & Turner, C. H. Effects of biomechanical stress on bones in animals. *Bone* **30**, 781–786 (2002).
79. Meakin, L. B., Price, J. S. & Lanyon, L. E. The contribution of experimental in vivo models to understanding the mechanisms of adaptation to mechanical loading in bone. *Frontiers in Endocrinology* vol. 5 Preprint at <https://doi.org/10.3389/fendo.2014.00154> (2014).
80. Patel, T. K., Brodt, M. D. & Silva, M. J. Experimental and finite element analysis of strains induced by axial tibial compression in young-adult and old female C57Bl/6 mice. (2013) doi:10.1016/j.jbiomech.2013.10.052.
81. Holguin, N., Brodt, M. D. & Silva, M. J. Activation of Wnt Signaling by Mechanical Loading Is Impaired in the Bone of Old Mice. *Journal of Bone and Mineral Research* **31**, 2215–2226 (2016).
82. Holguin, N., Brodt, M. D., Sanchez, M. E. & Silva, M. J. Aging diminishes lamellar and woven bone formation induced by tibial compression in adult C57BL/6. *Bone* **65**, 83–91 (2014).
83. Chermiside-Scabbo, C. J. *et al.* Old Mice Have Less Transcriptional Activation but Similar Periosteal Cell Proliferation Compared to Young-Adult Mice in Response to

- In Vivo* Mechanical Loading. *Journal of Bone and Mineral Research* jbmr.4031 (2020)
doi:10.1002/jbmr.4031.
84. Bellido, T. Osteocyte-Driven Bone Remodeling. *Calcif Tissue Int* **94**, 25–34 (2014).
 85. Baylink, D. J. & Wergedal, J. E. Bone formation by osteocytes. *Am J Physiol* **221**, 669–678 (1971).
 86. Robling, A. G. & Bonewald, L. F. The Osteocyte: New Insights. *Annu Rev Physiol* **82**, 485–506 (2020).
 87. Frost, H. M. Bone “Mass” and the Mechanostat”- A Proposal. *Anat Rec* **219**, (1987).
 88. Frost, H. M. Bone’s Mechanostat: A 2003 Update. *Anatomical Record - Part A Discoveries in Molecular, Cellular, and Evolutionary Biology* **275**, 1081–1101 (2003).
 89. Tyrovola, J. B. & Odont, X. X. The ‘mechanostat Theory’ of Frost and the OPG/RANKL/RANK System. *J Cell Biochem* **116**, 2724–2729 (2015).
 90. Main, R. P. *et al.* The murine axial compression tibial loading model to study bone mechanobiology: Implementing the model and reporting results. *Journal of Orthopaedic Research* jor.24466 (2019) doi:10.1002/jor.24466.
 91. Yang, H. *et al.* Characterization of cancellous and cortical bone strain in the in vivo mouse tibial loading model using microCT-based finite element analysis. *Bone* **66**, 131–139 (2014).
 92. Sun, D., Brodt, M. D., Zannit, H. M., Holguin, N. & Silva, M. J. Evaluation of loading parameters for murine axial tibial loading: Stimulating cortical bone formation while reducing loading duration. *Journal of Orthopaedic Research* **36**, 682–691 (2018).
 93. De Souza, R. L. *et al.* Non-invasive axial loading of mouse tibiae increases cortical bone formation and modifies trabecular organization: A new model to study cortical and cancellous compartments in a single loaded element. (2005)
doi:10.1016/j.bone.2005.07.022.
 94. Fritton, J. C., Myers, E. R., Wright, T. M. & Van Der Meulen, M. C. H. Loading induces site-specific increases in mineral content assessed by microcomputed tomography of the mouse tibia. doi:10.1016/j.bone.2005.02.013.
 95. Heřt, J., Lišková, M. & Landa, J. Reaction of bone to mechanical stimuli. 1. Continuous and intermittent loading of tibia in rabbit. *Folia Morphol (Warsz)* (1971).
 96. O’Connor, J. A., Lanyon, L. E. & MacFie, H. The influence of strain rate on adaptive bone remodelling. *J Biomech* **15**, 767–781 (1982).

97. Turner, C. H., Akhter, M. P., Raab, D. M., Kimmel, D. B. & Recker, R. R. A noninvasive, in vivo model for studying strain adaptive bone modeling. *Bone* **12**, 73–79 (1991).
98. Gross, T. S., Srinivasan, S., Liu, C. C., Clemens, T. L. & Bain, S. D. Noninvasive loading of the murine tibia: An in vivo model for the study of mechanotransduction. *Journal of Bone and Mineral Research* **17**, 493–501 (2002).
99. Torrance, A. G., Mosley, J. R., Suswillo, R. F. L. & Lanyon, L. E. Noninvasive loading of the rat ulna in vivo induces a strain-related modeling response uncomplicated by trauma or periosteal pressure. *Calcif Tissue Int* **54**, 241–247 (1994).
100. Lee, K. C. L., Maxwell, A. & Lanyon, L. E. Validation of a technique for studying functional adaptation of the mouse ulna in response to mechanical loading. *Bone* **31**, 407–412 (2002).
101. Fritton, J. C., Myers, E. R., Wright, T. M. & Van Der Meulen, M. C. H. H. Loading induces site-specific increases in mineral content assessed by microcomputed tomography of the mouse tibia. *Bone* **36**, 1030–1038 (2005).
102. De Souza, R. L. *et al.* Non-invasive axial loading of mouse tibiae increases cortical bone formation and modifies trabecular organization: a new model to study cortical and cancellous compartments in a single loaded element. *Bone* **37**, 810–818 (2005).
103. Main, R. P. *et al.* The murine axial compression tibial loading model to study bone mechanobiology: Implementing the model and reporting results. *Journal of Orthopaedic Research* **38**, jor.24466 (2019).
104. Robling, A. G. *et al.* Mechanical Adaptation. *Basic and Applied Bone Biology* 175–204 (2013) doi:10.1016/B978-0-12-416015-6.00009-5.
105. Holguin, N., Brodt, M. D., Sanchez, M. E., Kotiya, A. A. & Silva, M. J. Adaptation of Tibial Structure and Strength to Axial Compression Depends on Loading-History in Both C57BL/6 and BALB/C Mice. doi:10.1007/s00223-013-9744-4.
106. Brodt, M. D. & Silva, M. J. Aged mice have enhanced endocortical response and normal periosteal response compared with young-adult mice following 1 week of axial tibial compression. *Journal of Bone and Mineral Research* **25**, 2006–2015 (2010).
107. Silva, M. J. *et al.* Tibial loading increases osteogenic gene expression and cortical bone volume in mature and middle-aged mice. *PLoS One* **7**, (2012).
108. Robling, A. G. & Turner, C. H. Mechanotransduction in bone: Genetic effects on mechanosensitivity in mice. *Bone* **31**, 562–569 (2002).

109. Akhter, M. P., Cullen, D. M., Pedersen, E. A., Kimmel, D. B. & Recker, R. R. Bone response to in vivo mechanical loading in two breeds of mice. *Calcif Tissue Int* **63**, 442–449 (1998).
110. García-García, M. J. A History of Mouse Genetics: From Fancy Mice to Mutations in Every Gene. *Adv Exp Med Biol* **1236**, 1–38 (2020).
111. Russell, E. S. Origins and History of Mouse Inbred Strains: Contributions of Clarence Cook Little. *The Jackson Laboratory* Preprint at <http://www.informatics.jax.org/morsebook/chapters/russell.shtml>.
112. Yang, H. *et al.* Subspecific origin and haplotype diversity in the laboratory mouse HHS Public Access Author manuscript. *Nat Genet* **43**, 648–655.
113. Petkov, P. M. *et al.* An Efficient SNP System for Mouse Genome Scanning and Elucidating Strain Relationships. **223**, 1806–1811 (2004).
114. Keane, T. M. *et al.* Mouse genomic variation and its effect on phenotypes and gene regulation. *Nature* **477**, 289–294 (2011).
115. Churchill, G. A., Gatti, D. M., Munger, S. C. & Svenson, K. L. The Diversity Outbred Mouse Population. doi:10.1007/s00335-012-9414-2.
116. Svenson, K. L. *et al.* High-resolution genetic mapping using the mouse Diversity Outbred population. *Genetics* **190**, 437–447 (2012).
117. Olson, E. & Graham, D. *Animal Models in Pharmacogenomics. Handbook of Pharmacogenomics and Stratified Medicine* (Elsevier Inc., 2014). doi:10.1016/B978-0-12-386882-4.00005-0.
118. Olson, E. & Graham, D. *Animal Models in Pharmacogenomics. Handbook of Pharmacogenomics and Stratified Medicine* (Elsevier Inc., 2014). doi:10.1016/B978-0-12-386882-4.00005-0.
119. Jorde, L. B. *Genetic Variation and Human Evolution*.
120. Levy, R., Mott, R. F., Iraqi, F. A. & Gabet, Y. Collaborative cross mice in a genetic association study reveal new candidate genes for bone microarchitecture. *BMC Genomics* **16**, 1013 (2015).
121. Friedman, M. A. *et al.* Genetic variability affects the skeletal response to immobilization in founder strains of the diversity outbred mouse population. *Bone Rep* **15**, 101140 (2021).
122. Al-Barghouthi, B. *et al.* Systems genetics analyses in Diversity Outbred mice inform human bone mineral density GWAS and identify Qsox1 as a novel determinant of bone strength. (2020) doi:10.1101/2020.06.24.169839.

123. Mayhew, A. J. & Meyre, D. Assessing the Heritability of Complex Traits in Humans: Methodological Challenges and Opportunities. *Curr Genomics* **18**, 332 (2017).
124. Marini, F., Masi, L., Marcucci, G., Cianferotti, L. & Brandi, M. L. Genetics of osteoporosis. *Multidisciplinary Approach to Osteoporosis: From Assessment to Treatment* **23**, 25–44 (2018).
125. Min, J., Chiu, D. T. & Wang, Y. Variation in the Heritability of Body Mass Index Based on Diverse Twin Studies: A Systematic Review. *Obes Rev* **14**, 871 (2013).
126. Karasik, D. *et al.* Heritability and Genetic Correlations for Bone Microarchitecture: The Framingham Study Families. *Journal of Bone and Mineral Research* **32**, 106–114 (2017).
127. Genetics for all. *Nat Genet* **51**, 579 (2019).
128. Kesavan, C. *et al.* Identification of genetic loci that regulate bone adaptive response to mechanical loading in C57BL/6J and C3H/HeJ mice intercross. *Bone* **39**, 634–643 (2006).
129. Kesavan, C., Baylink, D. J., Kapoor, S. & Mohan, S. Novel loci regulating bone anabolic response to loading: Expression QTL analysis in C57BL/6JXC3H/HeJ mice cross. *Bone* **41**, 223–230 (2007).
130. Robling, A. G., Li, J., Shultz, K. L., Beamer, W. G. & Turner, C. H. Evidence for a skeletal mechanosensitivity gene on mouse chromosome 4. *The FASEB journal : official publication of the Federation of American Societies for Experimental Biology* **17**, 324–326 (2003).
131. Robling, A. G., Warden, S. J., Shultz, K. L., Beamer, W. G. & Turner, C. H. Genetic Effects on Bone Mechanotransduction in Congenic Mice Harboring Bone Size and Strength Quantitative Trait Loci. *Journal of Bone and Mineral Research* **22**, 984–991 (2007).
132. Srivastava, A. K. *et al.* Identification of Novel Genetic Loci for Bone Size and Mechanosensitivity in an ENU Mutant Exhibiting Decreased Bone Size. *Journal of Bone and Mineral Research* **20**, 1041–1050 (2005).
133. Burstein, A. H. & Frankel, V. H. A standard test for laboratory animal bone. *J Biomech* **4**, 155–158 (1971).
134. Pelker, R. R., Friedlaender, G. E., Markham, T. C., Panjabi, M. M. & Moen, C. J. Effects of freezing and freeze-drying on the biomechanical properties of rat bone. *Journal of Orthopaedic Research* **1**, 405–411 (1983).

135. Lang, D. H. *et al.* Quantitative Trait Loci Analysis of Structural and Material Skeletal Phenotypes in C57BL/6J and DBA/2 Second-Generation and Recombinant Inbred Mice. *Journal of Bone and Mineral Research* **20**, 88–99 (2005).
136. Bonadio, J. *et al.* A murine skeletal adaptation that significantly increases cortical bone mechanical properties. Implications for human skeletal fragility. *J Clin Invest* **92**, 1697–1705 (1993).
137. Mikić, B., Van Der Meulen, M. C. H., Kingsley, D. M. & Carter, D. R. Long bone geometry and strength in adult BMP-5 deficient mice. *Bone* **16**, 445–454 (1995).
138. Mikić, B., Van Der Meulen, M. C. H., Kingsley, D. M. & Carter, D. R. Mechanical and geometric changes in the growing femora of BMP-5 deficient mice. *Bone* **18**, 601–607 (1996).
139. Brent, M. B., Stoltenborg, F. E., Brüel, A. & Thomsen, J. S. Teriparatide and Abaloparatide Have a Similar Effect on Bone in Mice. *Front Endocrinol (Lausanne)* **12**, 1–9 (2021).
140. Berman, A. G., Clauser, C. A., Wunderlin, C., Hammond, M. A. & Wallace, J. M. Structural and mechanical improvements to bone are strain dependent with axial compression of the tibia in female C57BL/6 mice. *PLoS One* **10**, 1–16 (2015).
141. Brodt, M. D., Ellis, C. B. & Silva, M. J. Growing C57Bl/6 Mice Increase Whole Bone Mechanical Properties by Increasing Geometric and Material Properties. *Journal of Bone and Mineral Research* **14**, 2159–2166 (1999).
142. Jepsen, K. J., Silva, M. J., Vashishth, D., Guo, X. E. & Van Der Meulen, M. C. H. Establishing biomechanical mechanisms in mouse models: Practical guidelines for systematically evaluating phenotypic changes in the diaphyses of long bones. *Journal of Bone and Mineral Research* **30**, 951–966 (2015).
143. Lanyon, L. E., Goodship, A. E., Pye, C. J. & MacFie, J. H. Mechanically adaptive bone remodelling. *J Biomech* **15**, 141–154 (1982).
144. Goodship, A. E., Lanyon, L. E. & McFie, H. Functional Adaptation of Bone to Increased Stress. *J Bone Joint Surg* **61-A**, 539–546 (1979).
145. Jepsen, K. J., Akkus, O., Majeska, R. J. & Nadeau, J. H. Hierarchical relationship between bone traits and mechanical properties in inbred mice. *Mammalian Genome* **14**, 97–104 (2003).
146. Gardinier, J. D., Al-Omaishi, S., Morris, M. D. & Kohn, D. H. PTH signaling mediates perilacunar remodeling during exercise. *Matrix Biology* **52–54**, 162–175 (2016).

147. Jepsen, K. J., Pennington, D. E., Lee, Y.-L., Warman, M. & Nadeau, J. Bone Brittleness Varies with Genetic Background in A/J and C57BL/6J Inbred Mice. *Journal of Bone and Mineral Research* **16**, 1854–1862 (2001).
148. Jepsen, K. J., Akkus, O. J., Majeska, R. J. & Nadeau, J. H. Hierarchical relationship between bone traits and mechanical properties in inbred mice. *Mammalian Genome* **14**:2 **14**, 97–104 (2003).
149. Voide, R., Lenthe, G. H. van & Müller, R. Bone Morphometry Strongly Predicts Cortical Bone Stiffness and Strength, but Not Toughness, in Inbred Mouse Models of High and Low Bone Mass. *Journal of Bone and Mineral Research* **23**, 1194–1203 (2008).
150. Cole, J. H. & Meulen, M. C. H. van der. Whole Bone Mechanics and Bone Quality. *Clin Orthop Relat Res* **469**, 2139 (2011).
151. Turner, C. H. *et al.* Congenic mice reveal sex-specific genetic regulation of femoral structure and strength. *Calcif Tissue Int* **73**, 297–303 (2003).
152. Silva, M. J. *et al.* Effects of High-Fat Diet and Body Mass on Bone Morphology and Mechanical Properties in 1100 Advanced Intercross Mice. *Journal of Bone and Mineral Research* **34**, 711–725 (2019).
153. Coulombe, J. C., Mullen, Z. K., Lynch, M. E., Stodieck, L. S. & Ferguson, V. L. Application of machine learning classifiers for microcomputed tomography data assessment of mouse bone microarchitecture. *MethodsX* **8**, 101497 (2021).
154. Coulombe, J. C. *et al.* Microgravity-induced alterations of mouse bones are compartment- and site-specific and vary with age. *Bone* **151**, 116021 (2021).
155. Schriefer, J. L. *et al.* A comparison of mechanical properties derived from multiple skeletal sites in mice. *J Biomech* **38**, 467–475 (2005).
156. van Lenthe, G. H., Voide, R., Boyd, S. K. & Müller, R. Tissue modulus calculated from beam theory is biased by bone size and geometry: Implications for the use of three-point bending tests to determine bone tissue modulus. *Bone* **43**, 717–723 (2008).
157. Silva, M. J., Brodt, M. D., Fan, Z. & Rho, J. Y. Nanoindentation and whole-bone bending estimates of material properties in bones from the senescence accelerated mouse SAMP6. *J Biomech* **37**, 1639–1646 (2004).
158. Patton, D. M. *et al.* The relationship between whole bone stiffness and strength is age and sex dependent. *J Biomech* **83**, 125–133 (2019).
159. Riggs BL & Melton LJ III. The worldwide problem of osteoporosis: insights afforded by epidemiology. *Bone* **17**, 505S-511S (1995).

160. Johnell, O. & Kanis, J. A. An estimate of the worldwide prevalence and disability associated with osteoporotic fractures. *Osteoporosis International* **17**, 1726–1733 (2006).
161. Richards, B. J., Zheng, H.-F. & Spector, T. D. Genetics of osteoporosis from genome-wide association studies: advances and challenges. (2012) doi:10.1038/nrg3228.
162. Turner, C. H. *et al.* Genetic regulation of cortical and trabecular bone strength and microstructure in inbred strains of mice. *Journal of Bone and Mineral Research* **15**, 1126–1131 (2000).
163. Ammann, P. & Rizzoli, R. Bone strength and its determinants. *Osteoporosis International* **2003 14:3 14**, 13–18 (2003).
164. Churchill, G. A., Gatti, D. M., Munger, S. C. & Svenson, K. L. The Diversity Outbred Mouse Population. doi:10.1007/s00335-012-9414-2.
165. Svenson, K. L. *et al.* High-resolution genetic mapping using the mouse Diversity Outbred population. *Genetics* **190**, 437–447 (2012).
166. Olson, E. & Graham, D. *Animal Models in Pharmacogenomics. Handbook of Pharmacogenomics and Stratified Medicine* (Elsevier Inc., 2014). doi:10.1016/B978-0-12-386882-4.00005-0.
167. Bouxsein, M. L. *et al.* Guidelines for assessment of bone microstructure in rodents using micro-computed tomography. *Journal of Bone and Mineral Research* **25**, 1468–1486 (2010).
168. Jepsen, K. J., Silva, M. J., Vashishth, D., Guo, X. E. & Van Der Meulen, M. C. H. Establishing biomechanical mechanisms in mouse models: Practical guidelines for systematically evaluating phenotypic changes in the diaphyses of long bones. *Journal of Bone and Mineral Research* **30**, 951–966 (2015).
169. Kegelman, C. D. *et al.* YAP and TAZ mediate osteocyte perilacunar/canalicular remodeling. *Journal of Bone and Mineral Research* **35**, 196–210 (2020).
170. Makowski, A. J., Patil, C. A., Mahadevan-Jansen, A. & Nyman, J. S. Polarization control of Raman spectroscopy optimizes the assessment of bone tissue. *J Biomed Opt* **18**, 055005 (2013).
171. Akkus, O., Adar, F. & Schaffler, M. B. Age-related changes in physicochemical properties of mineral crystals are related to impaired mechanical function of cortical bone. *Bone* **34**, 443–453 (2004).
172. Heveran, C. M. *et al.* Chronic kidney disease and aging differentially diminish bone material and microarchitecture in C57Bl/6 mice. *Bone* **127**, 91–103 (2019).

173. Moran, M. M. *et al.* Intramembranous bone regeneration differs among common inbred mouse strains following marrow ablation. *Journal of Orthopaedic Research* **33**, 1374–1381 (2015).
174. Nicolella, D. P., Moravits, D. E., Gale, A. M., Bonewald, L. F. & Lankford, J. Osteocyte lacunae tissue strain in cortical bone. *J Biomech* **39**, 1735–1743 (2006).
175. Morris, M. D. & Mandair, G. S. Raman assessment of bone quality. *Clin Orthop Relat Res* **469**, 2160–2169 (2011).
176. Jepsen, K. J., Akkus, O. J., Majeska, R. J. & Nadeau, J. H. Hierarchical relationship between bone traits and mechanical properties in inbred mice. *Mammalian Genome* **14**, 97–104 (2003).
177. Jepsen, K. J. *et al.* Genetic randomization reveals functional relationships among morphologic and tissue-quality traits that contribute to bone strength and fragility. *Mamm Genome* **18**, 492–507 (2007).
178. Turner, C. H. *et al.* Variation in Bone Biomechanical Properties, Microstructure, and Density in BXH Recombinant Inbred. *Journal of Bone and Mineral Research* **16**, 206–213 (2001).
179. Migotsky, N., Brodt, M. D., Cheverud, J. M. & Silva, M. J. Cortical bone relationships are maintained regardless of sex and diet in a large population of LGXSM advanced intercross mice. *Bone Rep* **17**, 101615 (2022).
180. Svenson, K. L. *et al.* High-Resolution Genetic Mapping Using the Mouse Diversity Outbred Population. (2012) doi:10.1534/genetics.111.132597.
181. Sun, D., Brodt, M. D., Zannit, H. M., Holguin, N. & Silva, M. J. Evaluation of loading parameters for murine axial tibial loading: Stimulating cortical bone formation while reducing loading duration. *Journal of Orthopaedic Research* **36**, 682–691 (2018).
182. Birkhold, A. I. *et al.* Mineralizing surface is the main target of mechanical stimulation independent of age: 3D dynamic in vivo morphometry. *Bone* **66**, 15–25 (2014).
183. Brodt, M. D. & Silva, M. J. Aged mice have enhanced endocortical response and normal periosteal response compared with young-adult mice following 1 week of axial tibial compression. *Journal of Bone and Mineral Research* **25**, 2006–2015 (2010).
184. Allen, M. R. & Burr, D. B. Techniques in Histomorphometry. *Basic and Applied Bone Biology* 131–148 (2013) doi:10.1016/B978-0-12-416015-6.00007-1.

185. Dempster, D. W. *et al.* Standardized nomenclature, symbols, and units for bone histomorphometry: A 2012 update of the report of the ASBMR Histomorphometry Nomenclature Committee. *Journal of Bone and Mineral Research* **28**, 2–17 (2013).
186. Friedman, M. A. *et al.* Genetic variability affects the skeletal response to immobilization in founder strains of the diversity outbred mouse population. *Bone Rep* **15**, 101140 (2021).
187. Frost, H. M. Bone “mass” and the “mechanostat”: A proposal. *Anat Rec* **219**, 1–9 (1987).
188. Stern, A. R. & Nicoletta, D. P. Measurement and estimation of osteocyte mechanical strain. *Bone* **54**, 191–195 (2013).
189. Li, X. *et al.* Stimulation of *piezo1* by mechanical signals promotes bone anabolism. *Elife* **8**, 1–22 (2019).